



VCU

Virginia Commonwealth University
VCU Scholars Compass

Theses and Dissertations

Graduate School

2015

Conduction states of the human dopamine transporter

Krasnodara Cameron

Follow this and additional works at: <https://scholarscompass.vcu.edu/etd>



Part of the [Medical Physiology Commons](#)

© The Author

Downloaded from

<https://scholarscompass.vcu.edu/etd/3676>

This Dissertation is brought to you for free and open access by the Graduate School at VCU Scholars Compass. It has been accepted for inclusion in Theses and Dissertations by an authorized administrator of VCU Scholars Compass. For more information, please contact libcompass@vcu.edu.

Krasnodara N. Cameron. 2015

All Rights Reserved

CONDUCTION STATES OF THE HUMAN DOPAMINE TRANSPORTER

A dissertation submitted in partial fulfillment of the requirements for the degree of
Doctor of Philosophy at Virginia Commonwealth University School of Medicine.

by

Krasnodara Nikolaeva Cameron
BS, Virginia Union University, 2005

Director: LOUIS J DE FELICE, PH.D.
Professor of Physiology and Biophysics

Virginia Commonwealth University
Richmond, Virginia
February, 2015

Acknowledgement

First, I would like to thank my mentor Dr. Louis De Felice for his incredible continuous support. He is not only an amazing scientist who helped me acquire a lot of important research and career skills, but also an outstanding listener and problem solver who guided me through all types of challenging situations with much care. Thank you for being the number one mentor!

Next, I would like to thank Dr. Jose Miguel Eltit for the endless hours of technical training, discussions, and support. Your role was integral in my successful program completion.

To my committee members, Dr. Glennon, Dr. Logothetis, Dr. Negus, and Dr. Ramsey, thank you for your continuous guidance. Having you on my committee enriched tremendously my experience here at VCU.

I would like to thank all the De Felice lab members, Ernesto Solis Jr., Tyler Steele, and Iwona Ruchala, and all of Physiology and Biophysics students, faculty and staff for the continuous support, advice, and friendship.

There are a few inspirational women in my life that I would like to acknowledge and thank. First my mother (Yanka) and grandmother (Yordanka) who are amazing, strong, and loving women that have raised me to be strong, loving, and hard-working just like them. Next, I want to thank Dr. Islam for her outstanding mentorship during my undergraduate years. She showed me that being a successful scientist and a loving and devoted mother is something attainable. Last, but

not least, I want to thank Dr. Gentile for the outstanding scientific and personal training during my post-bac years. Seeing you, brilliant, confident, creative, and greatly competitive women scientist, inspire me to strive for the best and to believe in myself.

Finally, I would like to thank my family and friends: my husband (Allen), my children (Santino, Niccolo, Nila, and Shaquel), my mother (Yanka), father (Nikolai), grand-mother (Yordanka), sister (Stanislava), nephew (Nikolai), and niece (Plamena), my in-law family members, and my dear friends Petya, Pooja, and Hema. Thank you all for the constant love, support, and encouragement. You brought balance, love and many blessings to my daily life. I also want to acknowledge three amazing women that are not here to share with me this joyous moment; however, they have been great supporters of my higher education pursuit for the time we were together: my best friend Danielle Watson-Greene, my host-mother Susan Stone, and my mother-in-law Linda Lambert. You will be forever in my heart.

Table of Contents

Acknowledgement	ii
List of Figures	viii
Abstract	xiv
Chapter 1 BACKGROUND.....	1
1.1. Introduction of DAT	1
1.2. DAT function	5
1.3. DAT regulation	8
1.4. DAT-associated currents.....	9
1.5. DAT substrate type psychostimulants- STPs.....	12
1.5.1. Amphetamine and methamphetamine.....	13
1.5.2. Synthetic cathinones	14

1.6. DAT reuptake inhibitors	16
1.7. DA transients in the action of abused drugs	18
1.8. Ca ²⁺ channels and excitability	20
1.9. The objective of the present study	21
Chapter 2 MATERIALS AND METHODS	22
2.1. Expression of hDAT in <i>Xenopus</i> oocytes	22
2.2. Two-electrode voltage clamp.....	22
2.3. Solutions for <i>Xenopus</i> oocytes.....	23
2.4. Materials	23
2.5. Culture of HEK 293 cells.....	23
2.6. Generation of Flp-In Trex cells expressing hDAT	24
2.7. Whole cell patch clamp and electrophysiological recordings.....	24
2.8. Experimental solutions.....	25
2.9. APP ⁺ uptake assay	25
2.10. Ca ²⁺ current-voltage dependence determination.....	26
2.11. Intracellular Ca ²⁺ determination	26
2.12. Immunofluorescence.....	27

2.13. Western Blot	27
2.14. Maintaining LUHMES.....	27
2.15. Quantitative PCR	28
2.16. Statistics	28
Chapter 3 RESULTS.....	29
3.1. Conduction states in hDAT.....	29
3.1.1. Structures	29
3.1.2. Dopamine, STPs, and reuptake inhibitors differentially affect hDAT	31
3.1.3. The potency and efficacy of I_{STP} at hDAT varies	33
3.1.4. Difference in efficacy but not potency of MDPV and COC to inhibit constitutive hDAT current	35
3.2. Action of reuptake inhibitors at hDAT	37
3.2.1. Reuptake inhibitors block different levels of hDAT's constitutive leak current	37
3.2.2. MDPV has the electrophysiological signature of a tight binding reuptake inhibitor	38
3.2.3. Time course of COC and MDPV block in oocytes.....	40
3.2.4. MDPV reversibility in mammalian expression system	43
3.2.5. Action of <i>bath salts</i> mixture	45
3.3. STP-induced persistent current at hDAT.....	47

3.3.1. I_{PC} is dependent on intracellular STP concentration	47
3.3.2. I_{PC} does not depend on the lipophylicity of STPs	49
3.3.3. I_{PC} is induced by a unique conductance state of hDAT	51
3.3.4. I_{PC} causes a dysfunctional DAT state	53
3.3.5. DAT's dysfunctional state can be reversed using reuptake inhibitor	55
3.4. hDAT expression in mammalian cells	57
3.4.1. hDAT currents in HEK 293 cells	59
3.4.2. Potency of S- and R- AMPH differs in mammalian cells	61
3.4.3. hDAT-induced currents are electrically coupled to voltage-gated Ca^{2+} channels	63
3.5. hDAT current effect in neurons	71
3.5.1. LUHMES selection	71
3.5.2. Differentiation changes	72
3.5.3. STP effect on LUHMES excitability	78
Chapter 4 DISCUSSION	81
Curriculum Vitae	100

List of Figures

Figure 1: Dopaminergic synapse	2
Figure 2: Dopaminergic pathways and their involvement in diseased states.	4
Figure 3: Alternating access and channel modes of transport	7
Figure 4: hDAT currents.....	11
Figure 5: Chemical structures of DA and STPs.....	30
Figure 6: DA, STP, and reuptake inhibitor-induced currents at hDAT	32
Figure 7: Dose-response curves of STPs.	34
Figure 8: COC and MDPV dose-response curves.	36
Figure 9: COC and MDPV blockade.....	39
Figure 10: MDPV and COC blockade reversibility.....	42
Figure 11: MDPV long action in hDAT expressing HEK 293 cells	44
Figure 12: Bath salts currents	46
Figure 13: I_{PC} is time and concentration dependent and is induced by internal STP	48

Figure 14: I_{PC} vs. lipophilicity..	50
Figure 15: Current-voltage relationship of I_{DA} , I_{STP} , and I_{PC}	52
Figure 16: S-METH induced dysfunctional hDAT	54
Figure 17: COC recovers hDAT from substrate-insensitive state.	56
Figure 18: Expression of hDAT in Flp-In T-Rex mammalian cells	58
Figure 19: Persistent current in hDAT transfected HEK cells.....	60
Figure 20: Dose-response curves for DA and AMPH enantiomers in mammalian cells	62
Figure 21: Voltage dependence of Cav1.3, Cav1.2, and Cav2.2.....	64
Figure 22. S-AMPH- and DA-induced hDAT currents activate Cav1.2 and Cav1.3, but not Cav2.2..	66
Figure 23: hDAT blockade prevents L-type Ca^{2+} channel activation in Flp _{hDAT} cells.	68
Figure 24: S-AMPH is more potent in producing Ca^{2+} signals, hDAT currents, and hDAT-Cav coupling	70
Figure 25: Conversion of LUHMES from proliferating to post-mitotic neurons.....	72
Figure 26: hDAT expression in Lund derived human mesencephalic cells (LUHMES).	74
Figure 27: Quantitative PCR analysis of dopaminergic and neuronal mRNA in LUHMES and LUHMES _{hDAT}	77

Figure 28: Excitability of LUHMES..... 80

Figure 29: Time courses (\pm)-MDPV effects on full ICSS frequency– rate curves..... 86

Abbreviation	Full Name
5-HT.	serotonin
AAM.	alternating access model
ADHD.	attention deficit hyperactivity disorder
AMPH.	amphetamine
AP.	action potential
bFGF.	basic fibroblast growth factor
Ca ²⁺	calcium
CATH.	cathinone
Ca _v	voltage-gated calcium channel
Cl ⁻	chloride
CNS.	central nervous system
COC.	cocaine
DA.	dopamine
DAT.	dopamine transporter
dDAT.	<i>Drosophila</i> dopamine transporter
DMEM.	Dulbecco's Modified Eagle Medium
DMSO.	dimethyl sulfoxide
EC ₅₀	half maximal concentration, potency
ER.	endoplasmic reticulum
FBS.	fetal bovine serum
GAPDH.	Glyceraldehyde 3-phosphate dehydrogenase

GDNF.....	glial cell-line-derived neurotrophic factor
GIRK.....	G protein-coupled inwardly-rectifying potassium channel
GPCR.....	G protein coupled receptor
hDAT.....	human dopamine transporter
hSERT.....	human serotonin transporter
HEK 293.....	human embryonic kidney (parental) cells
HEPES.....	(4-(2-hydroxyethyl)-1-piperazine-ethanesulfonic acid
ICSS.....	intracranial self-stimulation
I _{DA}	dopamine-induced current
I _L	constitutive leak current
I _{PC}	persistent current
I _{STP}	substrate type psychostimulant-induced current
I (V).....	current – voltage
K ⁺	potassium
LUHMES.....	Lund derived human mesencephalic neuronal cell line
MCAT.....	methcathinone
MDMA.....	3,4-methylenedioxy-N-methylamphetamine
MDPV.....	3,4-methylenedioxy pyrovalerone
MEPH.....	mephedrone
METH.....	methamphetamine
Na ⁺	sodium
NAcc.....	nucleus accumbens

Nav.....	voltage gated sodium channel
NE.....	norepinephrine
NET.....	norepinephrine transporter
NMDG.	N-methyl-D-glucamine
pCA.....	para-chloroamphetamine
PFC.	prefrontal cortex
PKC.	protein kinase C
PTSD.	post traumatic stress disorder
SEM.....	standard error of the mean
SN.	substantia nigra
STP.	substrate type psychostimulant
TEVC.	two-electrode voltage clamp
TH.	tyrosine hydroxylase
TTX.	tetrodotoxin
VMAT2	vesicular monoamine transporter type 2
V_{max}	maximal current response, efficacy
VTA	ventral tegmental area

ABSTRACT

CONDUCTION STATES OF THE HUMAN DOPAMINE TRANSPORTER

By Krasnodara Nikolaeva Cameron, Ph.D.

A dissertation submitted in partial fulfillment of the requirements for the degree of Doctor of Philosophy at Virginia Commonwealth University School of Medicine.

Virginia Commonwealth University, 2015

Dissertation Director: Louis J De Felice, Ph.D.
Professor of Physiology and Biophysics

Under normal conditions, a natural rewarding experience causes depolarization of midbrain dopaminergic neurons and exocytotic dopamine (DA) release into the synaptic cleft. A tonic increase of dopamine (DA) in the nucleus accumbens is required for associating everyday events and behaviors with rewards. The increase in synaptic DA activates presynaptic and postsynaptic dopamine receptors and results in reward-directed associative learning behaviors. The dopamine transporter (DAT) clears DA from the synaptic cleft by transporting it back into the presynaptic terminal, thus terminating DA signal transduction. However, many addictive exogenous compounds such as amphetamine (AMPH) and cocaine (COC) directly interact with DAT and produce a much greater phasic augmentation of synaptic DA levels. The dysregulation of dopaminergic homeostasis has been established as the primary source of numerous neurological disorders including Parkinson's disease and drug addiction. DAT's activity is also associated with ionic current that can be measured by voltage clamp techniques. Psychostimulants like AMPH and

COC directly interact with DAT altering its ionic currents. The classical view of psychostimulant action suggests that these drugs can be discriminated based on their effects on DAT activity. Reuptake inhibitors like COC decrease constitutive leak currents through DAT and prevent DA transport and thus raise its synaptic concentration. Substrates like AMPH enter the presynaptic terminal via DAT and thus compete with DA uptake. Under voltage clamp conditions, the transport of substrate alongside Na^+ and other ions give rise to a net inward depolarizing current. The resulting increase of extracellular DA levels is thus due to competition for transport, reverse transport, and exocytotic DA release due to DAT-induced depolarization.

Focusing our attention on electrophysiological techniques, we show that certain functional substrate-type psychostimulants (STPs), but not COC or DA itself, can produce a novel type of DAT-associated persistent current (I_{PC}) in addition to an initial peak current (I_{STP}). The persistent current is distinct from the transport-associated current elicited by DA (I_{DA}) and the constitutive leak current (I_L) through DAT. Unlike I_{DA} and I_L , the newly-identified STP-dependent persistent current, I_{PC} , lasts for many minutes after external substrate removal in the oocyte expression system. In transiently transfected HEK 293 cells we also see a persistent current that is described kinetically. HEK 293 cells have faster on and off kinetics ($\tau_{1/2}$) than their counterparts in oocytes for both DA and S-AMPH induced currents; however, the persistence ratio of S-AMPH to DA induced off kinetics was comparable in both oocyte and mammalian expression systems. Finally, we demonstrate drug-induced DAT currents can activate voltage-gated calcium channels (C_{av}) associated with dopaminergic excitability mammalian expression system. The electrical coupling between hDAT and C_{av} was further investigated in a human midbrain dopaminergic cell line. Understanding how STPs interact with DAT to produce novel conductance states may facilitate the development of unique therapeutic strategies to treat psychostimulant abuse.

Chapter 1 BACKGROUND

1.1. Introduction of DAT

The neurotransmitter DA regulates cognition, voluntary movement, motivation, and reward [7, 9]. As illustrated in Figure 1, DA is synthesized in the cell bodies of dopaminergic neurons located in the substantia nigra (SN) and the ventral tegmental area (VTA) of the brain. Upon depolarization of the presynaptic terminal, voltage-gated calcium channels (Ca_v s) activate and allow calcium (Ca^{2+}) to enter and to interact with proteins required for vesicular fusion and exocytotic DA release. DA signaling is a balance of neurotransmitter release during tonic and phasic activity of dopaminergic neurons and its clearance from the cleft. The primary mechanism of clearance is reuptake through the dopamine transporter (DAT, *SLC6A*), and to a lesser extent degradation by enzymes and diffusion away from the synapse [9]. The plasma membrane protein DAT regulates DA signal transduction and homeostasis by transporting the released synaptic neurotransmitter into the presynaptic neuron using Na^+ and Cl^- electrochemical gradients [10, 11]. Within dopaminergic neurons in the central nervous system (CNS) another transporter, the vesicular monoamine transporter 2 (VMAT2), uses a proton gradient to recycle and concentrate cytosolic DA back in synaptic vesicles for subsequent release [12]. DATs are strategically located

in the soma, dendrites, and perisynaptic areas of dopaminergic neurons [13]. Their proper function and location are crucial for dopaminergic signaling.

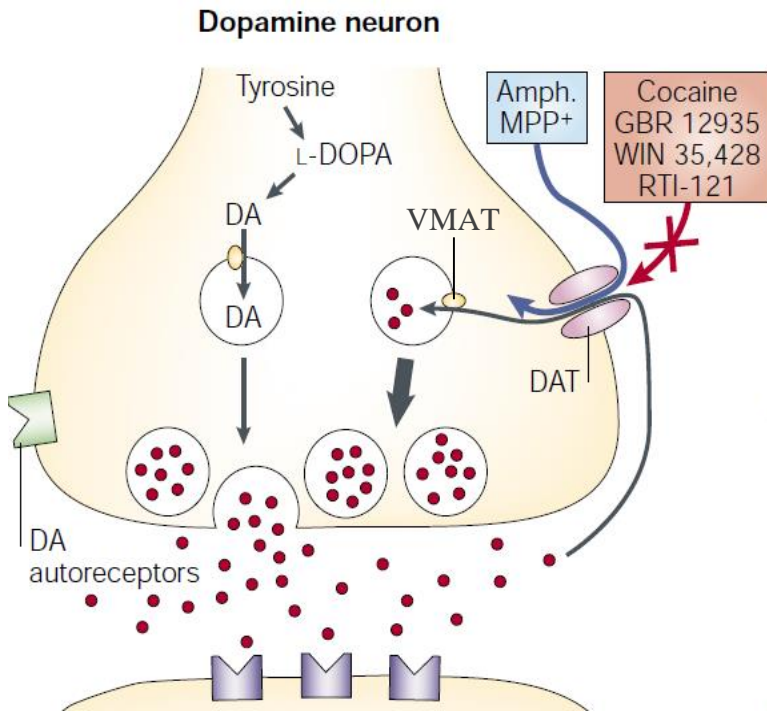


Figure 1: Dopaminergic synapse DAT is located at the perisynaptic area of dopaminergic terminal. It transports released synaptic DA back in the presynaptic cell to be repackaged in vesicles for subsequent release. AMPH and COC interact directly with DAT. AMPH acts as substrate and is transported, while COC binds the transporter and arrests its function. Figure adapted from [7].

Dysfunction in transporter activity or expression levels that affect DA concentration in different locations of the brain may lead to neurological, psychiatric, and neuroendocrine disorders. Figure 2 lists some of the disorders associated with either increased or decreased DA levels in the different dopaminergic pathways [8]. For example, augmentation of DA in the prefrontal cortex (PFC) is linked to attention deficit hyperactivity disorder (ADHD) and schizophrenia, while decreased DA levels in the striatum are associated with Parkinson's and Huntington's disease. Increased levels of DA in the nucleus accumbens (NAcc) has been implicated in drug addiction. Albeit through different mechanisms, all classes of abused drugs increase extracellular levels of DA particularly in NAcc [14]. The released DA activate DA receptors which signal higher brain regions, e.g., the prefrontal cortex, to translate motivational input into behavioral output [15]. The importance of DAT in the psychostimulant dependence is confirmed in animals with disrupted mesolimbic dopaminergic system (via knock-outs or lesions) or dopamine receptor antagonists, where abuse related effects of psychostimulants can be eliminated [16-18]. Moreover, in DAT knock-in mice enhanced psychostimulant reinforcement is observed [19, 20].

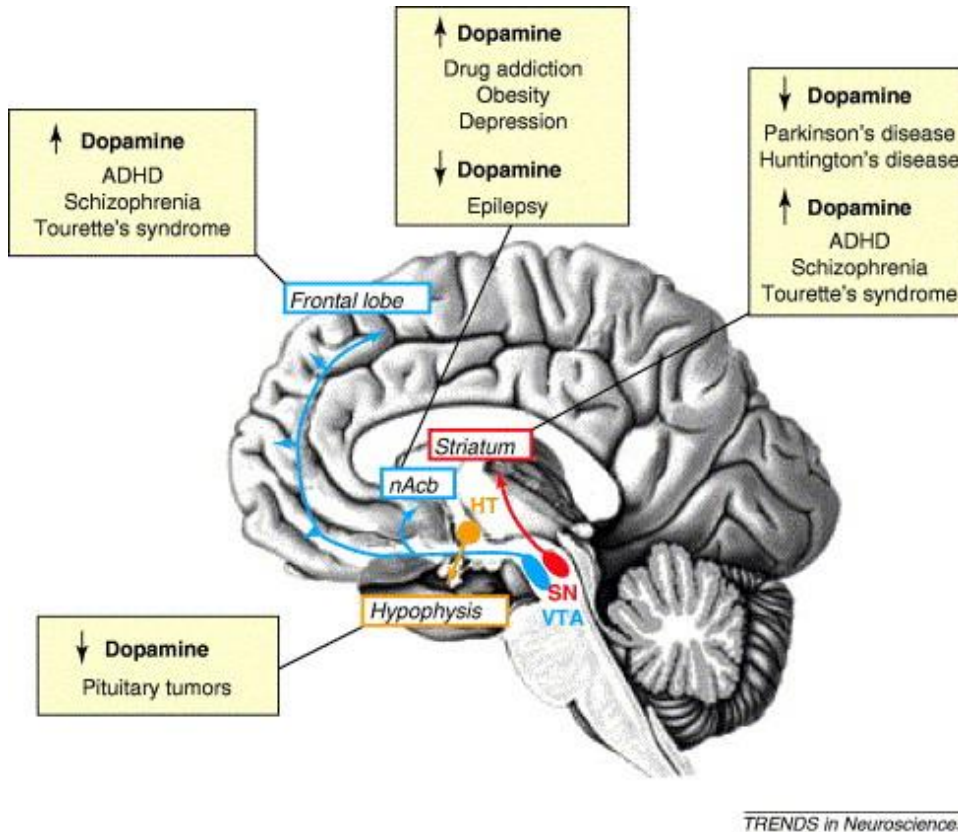


Figure 2: Dopaminergic pathways and their involvement in diseased states There are four major dopaminergic pathways that are involved in numerous neurological psychiatric, and neuroendocrine diseased. The mesocortical pathway (blue) originates from the ventral tegmental area (VTA) and projects to the prefrontal cortex (PFC). The mesolimbic pathway (blue) connects VTA to the nucleus accumbens (nAcb). The nigrostriatal pathway (red) projects from the substantia nigra to the striatum. Lastly, the tuberoinfundibular pathway (orange) connects the hypothalamus to the pituitary gland. Disorders associated with each pathway are listed in the text boxes linked to them. Figure adapted from [8].

1.2. DAT function

DAT is the primary mediator of synaptic DA clearance. The transport process is Na^+ and Cl^- dependent and it is driven by Na^+ electrochemical gradient. Transporter function is classically described as following the alternating access model (AAM) originally defined in 1966 by Jardetzky for ATPase pumps and since adopted for co-transporters [21]. Flux studies revealed Michaelis-Menten type relationship between transport and concentration of DA, Na^+ , and Cl^- [10]. Independent studies from Krueger and Schenk's laboratory found Na^+ concentration dependence on uptake was sigmoidal while Cl^- concentration dependence was rectangular hyperbola, hence assigning a transport stoichiometry of $1\text{DA} : 2\text{Na}^+ : 1\text{Cl}^-$ per transport cycle [10, 21, 22]. Using radiolabeled ligand uptake and irreversible binding assays, transporter turnover rate was calculated to be one full cycle every two seconds; therefore, using the proposed stoichiometry and because DA is a monovalent cation at physiological pH, one positive charge enters the cell every second through DAT [10]. Thus, the transporter is predicted to be electrogenic and the current generated by 1 million transporters acting simultaneously would be 0.16 pA. Nevertheless, numerous reports exist of the dopamine transporter eliciting much larger currents, well beyond the prediction of AAM [1, 6, 21, 23]. In addition, Sonders et. al. report a variable number of charges moving through DAT at different membrane potentials, thus contradicting the fixed stoichiometry model and proposing transport-uncoupled DAT current [23]. The unaccounted for DAT currents in addition to the fast reuptake of DA required at the synapse suggest for an alternative and/or combined ion channel/transporter mechanism of action. Figure 3 depicts a DAT model that has both alternating access mode (outward open, occluded, inward facing) and ion channel mode of transport [4]. DAT-generated currents through the ion channel mode are sufficient to affect membrane potential and excitability [24, 25]. Because a number of psychostimulants interact with DAT to produce or alter

its ionic currents [1, 2, 6, 26]. The mechanisms by which STPs control DAT activity and modulate membrane potential is of particular interest.

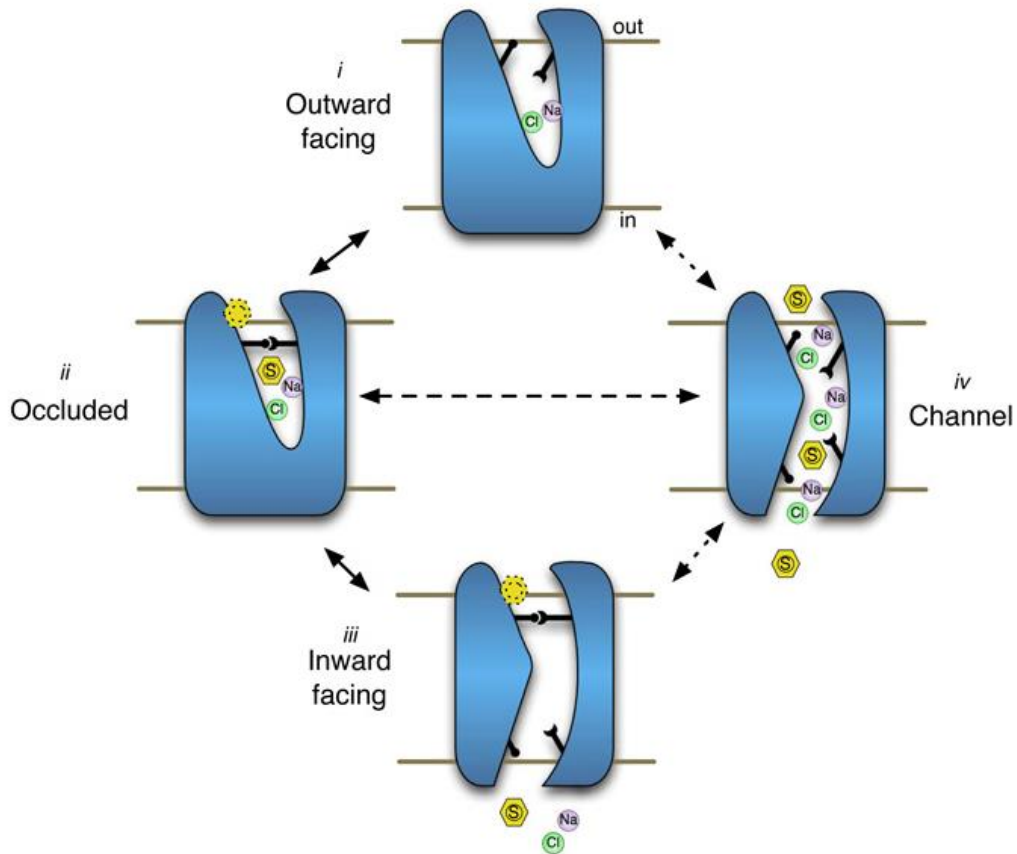


Figure 3: Alternating access and channel modes of transport Substrate, Na^+ , and Cl^- bind to outward facing transporter (i) outer gate closing (black bars) brings DAT to occluded state (ii) which then transitions to the inward facing conformation (iii) releasing substrate and ions to cytosol. The empty transporter then returns to the outward facing conformation (i). The transporter may undergo another transition (dashed lines) to a channel state (iv) where both gates are open simultaneously and currents are observed following rush of ions down their electrochemical gradients. Figure adapted from [4].

1.3. DAT regulation

DAT activity is contingent upon its presence at the cell membrane. DAT is synthesized in the endoplasmic reticulum (ER), transported to the Golgi for N-glycosylation at the 2nd extracellular loop and trafficked to the plasma membrane [27]. Different signaling pathways have shown effect on transporter cell surface expression both constitutively and upon stimulation [28, 29]. DAT has several consensus sites for posttranslational modifications at its cytosolic amino (N) and carboxyl (C) terminus. On the N terminus a cluster of serine residues are involved in PKC phosphorylation, which is important in DA efflux. Deletions and mutations of these residues on DAT results in reduced phosphorylation and internalization of the protein upon PKC activation [30, 31]. There is evidence for Ca²⁺/Calmodulin-dependent protein kinase II interactions with the C-terminus of DAT that regulate DA efflux [32, 33]. Residues 587-596 in DAT's carboxyl terminus play a role in its constitutive protein internalization [34]. More recent studies show that DAT is regulated by PIP2 suggesting the importance of membrane lipid composition in transporter function [35]. DAT substrates like AMPH and METH cause DAT down-regulation, while DAT reuptake inhibitors or blockers cause transporter up-regulation as determined by immunofluorescence confocal microscopy in mammalian expression system [36, 37]. The reduction and rise of DAT at the plasma membrane can be further monitored using voltage clamp techniques where current amplitude and kinetics can be measured for functional transporters [2, 38]. Moreover, DAT regulation by psychostimulants was confirmed by postmortem binding studies in cocaine overdose victims, showing higher number DAT binding sites [39, 40]. The numerous DAT regulation mechanisms contribute to an already complex picture of DAT function and are an active area of research aiming at understanding drug dependence.

1.4. DAT-associated currents

DAT uses Na^+ and Cl^- electrochemical gradients for the uphill DA transport. At physiological pH, DA carries one positive charge (the $-\text{NH}$ group has a $\text{pK}_a \sim 10$, www.drugbank.ca). Using voltage clamp techniques one can monitor the ionic currents generated by the charged species moving through DAT. Various studies show DAT has an inherent leak current (I_L) [1, 2, 6] that is present in the absence of substrates. This current, I_L , is observed upon insertion of the protein in the cell membrane. I_L is composed of monovalent cations and is revealed upon application of DAT inhibitors [23]. Figure 4 shows DA and other substrate, like AMPH, induce relatively large inward drug-induced currents (I_{DA} and I_{STP}) representing a net positive charge entering the cell at potentials near rest. All DAT currents (I_L , I_{DA} , and I_{STP}) can be identified using DAT reuptake inhibitors like cocaine (COC). COC's block of inward I_L or I_{DA} appears as an outward deflection of the current trace under voltage clamp conditions, demonstrating the inhibition of the inward constitutive leak through the transporter [1, 6, 23]. Recently, we described a new long lasting conduction state of DAT. Following S-AMPH exposure and subsequent removal, DAT continues to elicit an inward current that persists for many minutes in *Xenopus* oocyte expression system. We termed this depolarizing current induced by previous exposure to S-AMPH the persistent current (I_{PC}) [1, 2, 6]. This current appears to be caused by an internal S-AMPH and hDAT interaction [2]. We have built a functional model of hDAT with two binding sites for STPs: an extracellular site that opens the transporter-channel, and an intracellular site that holds the transporter open after external S-AMPH is removed and is responsible for the persistent current; this mechanism is referred to as a molecular stent [2]. The location of interaction site(s) is an ongoing project in our laboratory utilizing the structure of the *Drosophila* DA transporter, dDAT [41] to build and test an hDAT homology model. The data we have gathered strongly

supports the idea that hDAT currents play a significant role in neuronal excitability and consequently in transmitter release.

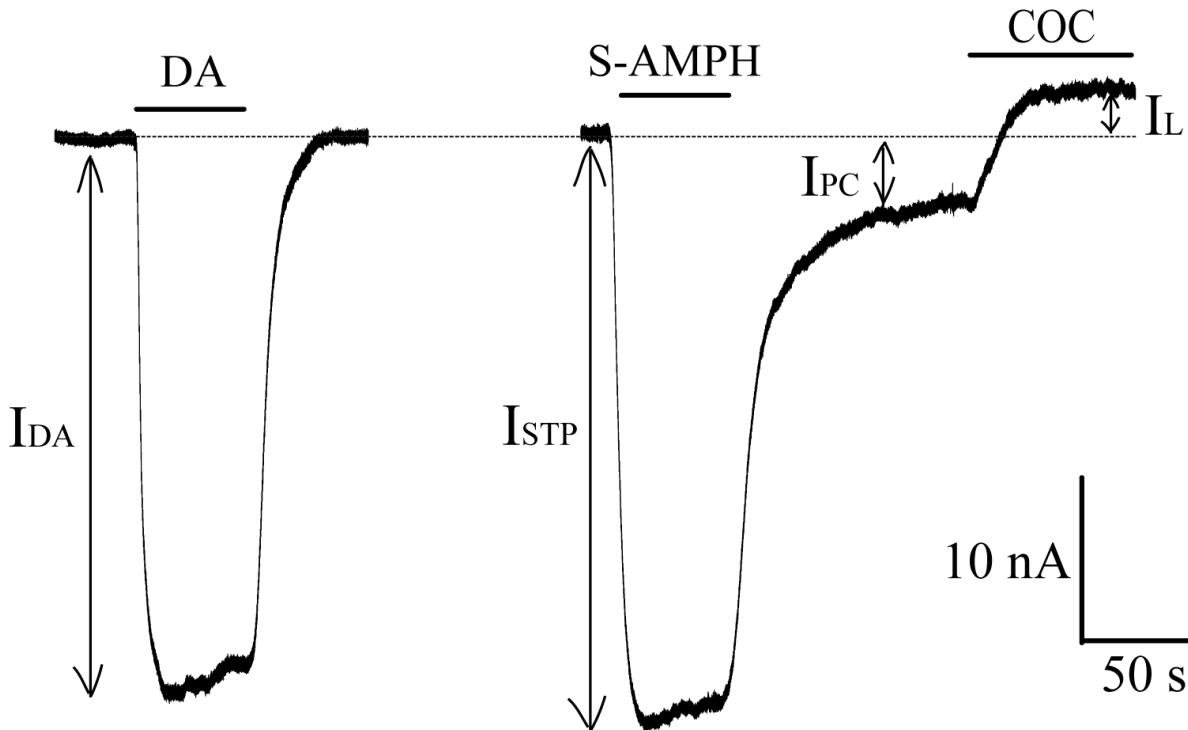


Figure 4: hDAT currents hDAT expressing *Xenopus* oocytes voltage clamped to -60 mV. All drug applications are of 10 μ M concentration. DA perfused outside for 60 s (horizontal bar above trace) induces inward depolarizing current (I_{DA}) that returns swiftly to baseline upon removal. 60 s application of S-AMPH produces similar size peak current (I_{STP}); however, after washout, the current establishes a new baseline below the original value, called persistent current (I_{PC}). This I_{PC} is hDAT-mediated since it is blocked by addition of COC. In addition, COC reduces/eliminates the constitutive leak current (I_L) associated with hDAT insertion in the cell membrane, which appears as an outward deflection in the current trace.

1.5. DAT substrate type psychostimulants- STPs

Psychostimulants cause hyperactivity, euphoria, and cardiovascular effects [42, 43]. The elevation of mood and the subsequent drug seeking behavior associated with psychostimulants are mediated by increased levels of DA in the nucleus accumbens (mesolimbic reward circuits) that stimulate dopamine receptors [44, 45]. A number of psychostimulants such as amphetamine (AMPH) and methamphetamine (METH), abbreviated as STPs (substrate type psychostimulants), are DAT substrates [1, 6, 46]. These compounds mimic the action of the endogenous neurotransmitter DA and are transported into the presynaptic cell via DAT, producing an inward depolarizing current at the resting membrane potential [1, 2, 6, 47]. DAT substrates, including DA itself, cause DA release [48-52]. This substrate-induced release is partially attenuated by the presence of voltage-gated sodium channel blockers like tetrodotoxin (TTX); it is also partially affected by external Ca^{2+} manipulation, but pretreatment with gamma-butyrolactone (an inhibitor of dopaminergic cell firing) fails to alter DA release [48, 52, 53]. There are several proposed mechanisms for the STP-induced DA release: 1) exocytotic DA release [2, 24, 44, 54], 2) facilitated exchange [55], 3) weak base DA depletion from synaptic vesicles [56, 57], and 4) reverse transport [58]. These mechanisms are not mutually exclusive, and abundant experimental evidence exists for each one. Ingram et al. and Saha et al. show that in midbrain dopaminergic neurons, AMPH-induced depolarizing currents increase cell excitability and thereby exocytotic DA release [24, 59]. Likewise, in 2011 Ramsson et al. demonstrated action potential-dependent dopaminergic neurotransmission by AMPH in anesthetized rats [44], while Daberkow et al. showed equivalent results in ambulatory rats [54]. Meanwhile, in a study by Jones et al., it is pointed out that in DAT homozygous knock-out mice, DAT's presence is essential for substrate-induced DA efflux into the extracellular space [18]; in the DAT $-/-$ mice study, AMPH decreases

stimulation-dependent DA release, which is an exocytotic process. On the other hand, after increase of cytoplasmic DA, there is no increase of extracellular dopamine, implying the necessity of AMPH-bound DAT for reverse transport of neurotransmitters [18]. Furthermore, Sulzer et al. found AMPH reduces DA quantal size due to redistribution of DA in the cytosol [57]. Thus evidence exists for both exocytotic and reverse transport as mechanisms for substrate-induced DA release.

Although the dopaminergic system is established as the site of action of psychostimulants, it is well known that many compounds also affect the serotonergic system which is important modulator of behavioral effects. Thus, psychostimulants can produce both DA-mediated, abuse-related effects and 5-HT-mediated, abuse limiting effects [3, 60]. Furthermore, studies show that releasers that are equipotent at DAT and SERT have minimal abuse liability and suppress drug-seeking behavior, especially promising appears the 30-fold selectivity of DA vs. 5-HT release [46, 61].

1.5.1. Amphetamine and methamphetamine

Amphetamine and methamphetamine (METH) are homologues of phenethylamine and are the parent compounds of a wide range of psychoactive derivatives. These stimulants increase locomotion and focus, and decrease appetite and food intake [62-64]. Both AMPH and METH have strong reinforcing properties evidenced in self-administration animal studies [65, 66] and high abuse liability assessed by intracranial self-stimulation (ICSS) [60]. Their primary effect is through DAT, demonstrated in DAT knock-out or knock-down mice who exhibit reduced or no sensitivity to the psychostimulants [16, 18, 67-70]. Using *in vitro* synaptosomal release studies, both compounds are shown to release all monoamines; however, they exhibit much greater potency

for DA and NE than 5-HT [46]. AMPH and METH appear to be substrate to hDAT as they induce inward current through the transporter at physiological potential. In addition, the S- enantiomers, S-AMPH and S-METH, produce an inward persistent current at hDAT after their wash out [2, 6]. AMPH's and METH's intake can result in schizophrenia-like symptoms and fatal toxicity [71]. Paradoxically, AMPH appears useful in the treatment of conditions such as attention-deficit hyperactivity disorder (ADHD), narcolepsy, and obesity [72-74].

1.5.2. Synthetic cathinones

The beta-keto amphetamine, cathinone (CATH), is the primary active ingredient of the khat plant (*Catha edulis*) found in East Africa and the Arabian Peninsula [75]. Fresh leaves of this shrub contain CATH, which is often referred to as a “natural amphetamine” since it possesses amphetamine-like psychostimulant properties. The synthetic cathinones appear under numerous names (*bath salts*, plant food, insect repellent, and brand names such as red dove, zoom, ivory wave, vanilla sky etc) [76, 77]. Similar to AMPH, cathinone derivatives have psychoactive effects due to their action at the monoamine systems [75, 78-80]. In drug discrimination studies, CATH and N-methylated cathinone, methcathinone (MCAT), substitute for AMPH and METH and exhibit greater potency than METH or AMPH, with MCAT being more potent than CATH [79]. MCAT releases DA similar to AMPH and facilitates intracranial self-stimulation studies (ICSS) which shows its high abuse liability [3, 81]. A para-methylated MCAT, mephedrone (MEPH), is another cathinone derivative that has gained popularity in recent years in Europe and USA [78, 82, 83]. *In vitro* synaptosomal uptake inhibition studies and *in vivo* microdialysis and intracranial self-stimulation (ICSS) studies in rat brain reveals a mixed effect at both serotonergic and dopaminergic systems [3, 84]. Electrophysiological assays additionally imply that MCAT and

MEPH are substrates for DAT as they induce inward currents at physiological potentials under voltage clamp conditions [1, 6]. Similar to S-AMPH, the two cathinones S-MCAT and MEPH elicit persistent current, I_{PC} , at hDAT which we hypothesize alters subsequent DA exposure at DAT and neuronal excitability [1, 2, 6].

1.6. DAT reuptake inhibitors

Cocaine (COC) is a naturally occurring alkaloid from the *Erythroxylon coca* plant abused for many years due to its psychostimulant effects [85]. Cocaine has several different target proteins in the brain such as DAT, SERT, norepinephrine transporter (NET), sodium channels and perhaps others [17, 86]. For many years the mechanism for its strong reinforcing effects was unknown. In the 1987 publication of Ritz et al., cocaine was identified to exhibit its action mainly through binding to DAT and inhibition of DA uptake in rat striatal tissue [17]. In behavioral animal studies, lesions in the mesolimbic dopaminergic projection inhibited self-administration of cocaine in rats [17]. Similar to STPs, such as AMPH, COC increases DA extracellular levels. Unlike STPs, however, COC is not transported into the cell but rather exerts its actions through a blockade of the transport pathway within DAT. This “cork in a bottle” mode of action results not only in uptake inhibition and increased DA synaptic levels but also in reduction/elimination of ionic fluxes through the transporter [1, 6, 23]. Current recordings in voltage clamped *Xenopus* oocytes reveal COC blocks I_L , which is present in DAT in the absence of substrate. Furthermore, COC also inhibits I_{DA} , I_{STP} , and I_{PC} [1, 6, 23]. COC’s block of inward constitutive leak and substrate-induced peak currents, as mentioned previously, appears as an outward deflection of the current trace under voltage clamp conditions.

Physiological and anatomical changes ensue upon repeated cocaine exposure. Chronic cocaine administration in rats causes an increase in dendrite branching and spine density in the nucleus accumbens [62, 87]. Furthermore, prolonged exposure to cocaine in animals (rats, rhesus monkeys etc.) shows increased H^3DA uptake but unchanged K_m indicative of DAT insertion in the plasmalemmal membrane from the endosomal recycling pool, a finding substantiated in

postmortem human cocaine addict subjects [39, 88]. Uptake inhibitor induced up-regulation is opposite to the effect observed with substrates, which result in DAT down-regulation.

A synthetic cathinone, 3,4-methylenedioxypyrovalerone (MDPV) has gained tremendous popularity and is now a Schedule I drug as of October 2011 [89]. It is a central stimulant that, unlike CATH or MCAT, increases DA by acting as a reuptake inhibitor similar to COC [1, 6, 90]. Fatal overdoses of MDPV and its dominance in the seized *bath salts* mixtures have brought attention to its exact mechanism of action [91].

1.7. DA transients in the action of abused drugs

Electrophysiological studies of excitability in dopamine neurons show a unique action potential (AP) waveform: a long AP duration and a pronounced after AP hyperpolarization [92]. These neurons have a tonic (pace-making) activity (2-10 Hz) and a phasic or burst activity (15-30 Hz) [92]. The tonic activity gives rise to background levels of DA in the 5-20 nM range, while the bursting events raise extracellular levels of neurotransmitter to the low micromolar range [93]. When association between cues and reinforcers is established (both natural and drug related reinforcers) the cues stimulate burst firing and phasic DA release. The burst firing and transient extracellular DA augmentations require activation of high-voltage activated Ca^{2+} channels which in turn leads to calcium-activated potassium channel opening to end the bursting activity [94]. These DA transients are observed in expectation of natural rewarding experience or upon unexpected reward delivery and are associated with goal-directed behaviors. In addition, after reward delivery, there is a second effect that depends on the reward prediction error [95]. If the reward prediction error is positive, the expected reward is smaller than the obtained (better than expected), an additional increase of firing above the tonic level is observed. Negative reward prediction error, the expected reward is greater than what is obtained (worse than expected), causes a transient pause or silencing below the tonic level in neuronal firing results [96]. This reward prediction error is used to modulate reward expectations and it plays a role in the synaptic rearrangement to strengthen or weaken glutamatergic and GABAergic synapses onto dopaminergic neurons.

Using *in vivo* microdialysis, increases in extracellular DA levels due to phasic/burst firing are measured and compared to the tonic basal levels. Studies employing this technique reveal the action of abused psychostimulants to cause dramatic augmentations in DA in the NAcc, much

greater than natural rewards (food, sex). The exaggerated rise of DA is absent when drugs with no abuse liability are administered to the tested subjects. Often there is a cross talk between psychostimulants and several different cellular targets. For example, METH can release both DA and 5-HT; however, the selectivity for one neurotransmitter over the other is of great importance. Monoamine releasers with greater selectivity for DA over 5-HT produce more abuse-related behaviors, hence, the and the ratio of extracellular concentration of DA/5-HT is established as a good indicator for abuse liability [46, 97-99]

1.8. Ca²⁺ channels and excitability

Voltage-gated ion channels play a major role in many excitable cells: they do not only affect the membrane potential of the cell but also trigger a number of other effects such as neurotransmitter release, gene expression, certain kinases activation etc. [100]. The L-type Ca²⁺ channels (Cav1) are important modulators of signal transduction and excitability in excitable cells [94, 101, 102]. Their current is distinguished by large single channel conductance (compared to the other types of Cav_s), high voltage of activation, and slow voltage inactivation hence it is long lasting [103]. They are localized primarily in the cell bodies and dendrites of neurons as compared to Cav2 (N, P, Q-types) which are located in synaptic densities and involved in vesicular fusion [104]. The N-type of Cav_s (Cav2.2) have an intermediate rate of inactivation compared to other Cav types, however the voltage dependence and current can be highly variable depending on the subunit composition and neuronal identity [103, 105]. While Cav2.2 are reported to directly interact with SNARE proteins and entry of Ca²⁺ through the channels triggers vesicular fusion, Cav1.3 is implicated in pace-maker neurons, including some dopaminergic neurons and neuroendocrine cells like adrenal chromaffin cells [106, 107]. Since L-type Ca²⁺ channels (Cav1.2 and Cav1.3) are co-expressed with monoamine transporters in several types of excitable cells [94, 108], determining a functional interaction between these two classes of proteins could constitute an additional molecular mechanism of STP action. Previous studies using HEK 293 coexpression of L-type Ca²⁺ channel Cav1.3 or N-type Ca²⁺ channel Cav2.2 and hSERT show there is electrical coupling between the Cav1.3 and hSERT which was not observed with Cav2.2 and hSERT under the same conditions [109].

1.9. The objective of the present study

The overall goal of our studies was to elucidate the biophysics of reuptake inhibitors and STPs as they modulate the function of DAT and to uncover their physiological relevance in neuronal excitability. We specifically focused on two crucial elements of STP mechanisms: 1) characterizing the biophysical properties of I_{STP} and I_{PC} , and 2) measuring the effect of I_{STP} and I_{PC} on excitability in dopaminergic neurons. We hypothesized that the long-lasting I_{PC} will cause a moderate but persistent depolarization in DA neurons that will prolong neuronal depolarization and increase both excitability and vesicular DA release, thereby raising synaptic DA concentration and increasing reward-directed behavior.

Chapter 2 MATERIALS AND METHODS

2.1. Expression of hDAT in *Xenopus* oocytes

Oocytes were harvested and prepared from adult female *Xenopus laevis* following standard procedures [110]. Stages V–VI oocytes were selected for cRNA injection within 24 h of isolation. cRNA was transcribed in the pOTV oocyte transcription vector (gift of Mark Sonders, Columbia University) using Ambion mMessage Machine T7 kit (Ambion Inc., Austin, TX, USA). Each oocyte was injected with 40 nL of 1 $\mu\text{g}/\mu\text{L}$ hDAT cRNA (final amount 40 ng) (Nanoject AutoOocyteInjector, Drummond Scientific Co., Broomall, PA, USA) and incubated at 18°C for 6–10 days in Ringers solution supplemented with NaPyruvate (550 $\mu\text{g mL}^{-1}$), streptomycin (100 $\mu\text{g mL}^{-1}$), tetracycline (50 $\mu\text{g mL}^{-1}$) and 5% dialyzed horse serum.

2.2. Two-electrode voltage clamp

Electrodes had resistances from 1 to 3 M Ω . *Xenopus* oocytes expressing hDAT were voltage clamped to –60 mV (unless otherwise noted), and buffer was gently perfused until a stable baseline was obtained, then the experimental substrates were perfused until stable currents were obtained, or for time periods indicated. The voltage clamp apparatus used for these experiments was a Gene Clamp 500 Amplifier and a 16 bit A/D converter (Digidata 1320A, Axon Instruments). Data were sampled at 5 kHz and digitally stored for off line analysis using Clampfit 10.2 software and 1-kHz filtering. Inward and outward drug-induced currents were compared with holding

currents required for voltage clamp at -60 mV in the absence of drugs. Currents varied in size; however, oocytes with -20 to -60 mV resting potentials and 10 μ M DA responses of 20 nA to 100 nA were selected for the analysis. To measure drug-induced I(V) curves, we first generated an I(V) curve for buffer without drug, which we then subtract from I(V)s for buffer with drug. Buffer subtracted I(V) curves for 10 mM DA, MEPH-peak, MDPV and COC were generated under voltage clamp between -100 and $+20$ mV. To normalize I(V) curves, we set the 10 μ M DA-induced current to 100 at -100 mV in each oocyte [1, 2].

2.3. Solutions for *Xenopus* oocytes

Extracellular (in mM): 120 NaCl, 7.5 HEPES, 5.4 K Gluconate, 1.2 Ca Gluconate, pH adjusted to 7.4 with NaOH. Intracellular electrode: 3 M KCl. The speed of solution exchange was 4 mL min^{-1} . No drug used in this study had any effect in non-injected oocytes (data not shown). See also Rodriguez-Menchaca et al [2].

2.4. Materials

Mephedrone and 3,4-methylenedioxypropylvalerone (MDPV) were prepared as their hydrochloride salts and purified to homogeneity. S(+)-Methamphetamine and S(-)-methcathinone, as their hydrochloride salts, were available from a previous investigation and were purified to homogeneity. Cocaine hydrochloride was obtained from the NIDA drug supply program.

2.5. Culture of HEK 293 cells

Transiently expressed hDAT HEK 293 cells (HEK_{hDAT} cells) were prepared in Dulbecco's modified Eagle's medium (DMEM) supplemented with 10% fetal bovine serum (FBS), 2 mM L-glutamine, penicillin (100 units/ml), and streptomycin (100 g/ml) [111]. Wild type hDAT cDNA

subcloned in pIRES2 DsRED-Express2 (Clontech) were used to transfect HEK 293 cells via lipofectamine 2000 (GIBCO BRL). Cells were grown for 48-72 h before measurements. Since expression plasmid codifies the red fluorescent protein (DsRED) the transfected cells were identifiable at the red channel: excitation 550/15 nm and emission 620/60 nm.

2.6. Generation of Flp-In Trex cells expressing hDAT

The generation of the hDAT stable inducible cell line (Flp_{hDAT}) was done using the Flp-InTm T-RexTM 293 system (Invitrogen). The hDAT cDNA (accession number: NM_001044) was subcloned into pcDNA5/FRT/TO plasmid and the targeted recombination and cell selection were performed as described previously [112]. Flp-hDAT cells were grown in Dulbecco's modified Eagle medium supplemented with 10% fetal bovine serum. hDAT expression was induced with doxycycline (1µg/ml) at least 3 days before each experiment. The Ca²⁺ channels used in this study were Cav2.2 (α1B, Addgene #26570), Cav1.3 (α1D, Addgene # 26571), Cav1.2 (α1C accession number: NM_001136522), β₃ (Addgene #26574) and α₂δ₁ (Addgene #26575). All plasmids were kindly provided by Dr. Diane Lipscombe (Department of Neuroscience, Brown University, Providence, Rhode Island, USA) except Cav1.2 that was kindly provided by Dr. Manfred Grabner (Department of Medical Genetics, Molecular, and Clinical Pharmacology, Innsbruck Medical University, Innsbruck, Austria). The Cav1.2 cDNA was subcloned into pcDNA6 expression plasmid thus all α₁ subunits are expressed under the same background vector. In addition EGFP expression plasmid was used as transfection marker. The cells were co-transfected with the DNA ratio α₁:β₃:α₂δ₁:EGFP=1:1:1:0.2 using Fugene 6 (Promega) as transfection reagent.

2.7. Whole cell patch clamp and electrophysiological recordings

Cells were cultured on 12 mm round glass coverslips (Fisher Brand) for 1-2 days before measuring currents. Coverslip was placed on a stage of Olympus IX50 inverted microscope for whole cell recording configuration. Patch pipettes with resistance ranging from 3 -6 M Ω made from borosilicate glass capillary tubing and coated with Sylgard (Dow Chemicals) were filled with 133 K Gluconate, 5.9 NaCl, 1 CaCl₂, 0.7 MgCl₂, 10 EGTA, 10 HEPES, pH adjusted to 7.2 with KOH. The cells were continuously superfused with external solution containing 130 NaCl, 4 KCl, 2 CaCl₂, 1 MgCl₂, 10 HEPES, 10 Glucose, pH adjusted to 7.4 with NaOH. Patch clamp recording at T=35°C (AutoMate Scientific) were performed using an Axopatch 200A amplifier (Molecular Devices) and currents were acquired using Clampex 8.2 software (Molecular Devices). The voltage was clamped at -60 mV unless otherwise noted and drugs were applied for 5 s at various concentrations following a 30 μ M DA pre-pulse. Current traces were acquired at 1 kHz. Holding currents for all traces were subtracted and DA pre-pulse was normalized to 1 for cell to cell comparison.

2.8. Experimental solutions

Extracellular (in mM): 130 NaCl, 4 KCl, 2 CaCl₂, 1 MgCl₂, 10 HEPES, 10 Glucose, pH adjusted to 7.4 with NaOH. Intracellular electrode: 133 K Gluconate, 5.9 NaCl, 1 CaCl₂, 0.7 MgCl₂, 10 EGTA, 10 HEPES, pH adjusted to 7.2 with KOH.

For Ca²⁺-free imaging recording we used the following extracellular solution (in mM): 130 NaCl, 4 KCl, 2 MgCl₂, 10 HEPES, 10 Glucose, 2 EGTA, pH adjusted to 7.4 with NaOH.

2.9. APP⁺ uptake assay

4-(4-(Dimethylamino)phenyl)-1-methylpyridinium (APP⁺), a fluorescent substrate of hDAT, was used to monitor hDAT activity by fluorescence microscopy as previously described [111]. Cells grown on 96 well imaging plates were placed on the stage of the fluorescence microscope describe above. The wavelengths used to detect the APP⁺ signal were 460/10 nm for excitation and 535/50 nm for emission.

2.10. Ca²⁺ current-voltage dependence determination

The Ca²⁺ currents were determined in HEK 293T cells transfected with Cav1.2, Cav1.3 or Cav2.2 as described previously [112]. The external solution used was (in mM): 155 tetraethylammonium (TEA)-Cl, 5 CaCl₂, 10 Hepes, pH 7.4 with TEA-OH. The internal solution composition was (in mM): 130 CsCl, 10 Cs-EGTA, 1 CaCl₂, 4 MgATP and 10 HEPES, pH adjusted to 7.3 with CsOH. The effective serial resistance was corrected to 80% using the built-in circuit of the Axopatch 200B amplifier. The leak current was subtracted using a -P/6 protocol. The microelectrodes were made from 8520 glass capillary (Warner Instruments, #64-0817), fire polished, and Sylgard coated. The electrodes tip resistance was ~2.5 MΩ when filled with the internal solution.

2.11. Intracellular Ca²⁺ determination

The intracellular Ca²⁺ determinations were done using the Ca²⁺ sensitive dye Fura-2AM and visualized in an epifluorescence microscope following the procedure and using the equipment described previously [112]. The measurements were done at constant perfusion at 35°C. The Fura-2 signal was acquired switching the excitation wavelength between 340/10 to 380/10 nm using a monochromator as described previously [112], dichroic mirror 490LP and an emission filter

510/40 nm. The acquisition frequency was 1Hz. All images were background subtracted and the Ca^{2+} signals are shown as $F_{340/380}/F_0$. In the case of dose-response experiments the test values were normalized by the mean of the maximal value of control DA pre-pulse.

2.12. Immunofluorescence

Sample fixation and labeling was performed as described earlier [113]. The primary antibodies used were rat monoclonal anti-DAT (Santa Cruz Biotechnology, Cat# sc-32258) with secondary antibody used Alexa Fluor 555 goat anti-rat IgG (Invitrogen, Cat# A21434) and primary rabbit polyclonal anti-Pan Nav (Alomone Labs, Cat# ASC-003) with secondary antibody Alexa Fluor 488 goat anti-rabbit IgG (Invitrogen, Cat# A11008). The nuclei were stained with DAPI. The specimens were visualized either in a Zeiss 710 confocal microscope.

2.13. Western Blot

Total protein extracts were run in SDS-PAGE in duplicates. One gel was stained with Coomassie blue staining for total protein visualization and the other was electrically transferred to a PVDF membrane. To detect hDAT expression, the membrane was incubated in anti-hDAT monoclonal rat antibody and then exposed to secondary antibody conjugated with horseradish peroxidase. The hDAT band was visualized by chemiluminescence using RapidStep ECL Reagent (Calbiochem) and the images were acquired in a digital imaging system (FluorChem E, Protein Simple, Santa Clara, CA).

2.14. Maintaining LUHMES

Nunclon (Nunc, Roskilde, Denmark) plastic cell culture flasks and multi-well plates were pre-coated with poly-ornithine 50 $\mu\text{g}/\text{mL}$ overnight. After H_2O wash and dry, 1 $\mu\text{g}/\text{mL}$ fibronectin was applied for 3 hrs. (Sigma-Aldrich, St. Louis, MO, USA). After removal of the coating solution, culture flasks were washed once with H_2O and air-dried before cell seeding. Proliferation medium consisted of Advanced Dulbecco's modified Eagle's medium/F12 supplemented with 1% N-2 supplement (Invitrogen, Karlsruhe, Germany) and 40 ng/mL recombinant basic fibroblast growth factor (bFGF) (R&D Systems, Minneapolis, MN, USA). For differentiation, we used F12, 1% N-2 supplement, 1 mM dibutyryl cAMP (Sigma-Aldrich), 1 $\mu\text{g}/\text{mL}$ tetracycline (Sigma-Aldrich) and 2 ng/mL recombinant human GDNF (R&D Systems) [114].

2.15. Quantitative PCR

Total RNA was prepared with TRIzol (Invitrogen), and 1 μg RNA was reverse-transcribed with a High Capacity cDNA Archive kit (Applied Biosystems). The abundance of mRNA levels was assessed with premixed primer-probe sets and TaqMan Universal PCR Master Mix (Applied Biosystems). The cDNA for the target genes was left undiluted while the gene encoding GAPDH was diluted 10x and then was amplified with an ABI 7900HT cycler. Gene expression was normalized to that of the gene encoding GAPDH [115].

2.16. Statistics

Summary TEVC and patch clamp data are reported as mean \pm SEM; n denotes the number of cells and each cell tests one condition. Mean currents are expressed as test current normalized to DA pre-pulse to account for differences in hDAT expression level. Statistical analysis was executed using Origin 8 and Prism 5 (GraphPad).

Chapter 3 RESULTS

3.1. Conduction states in hDAT

3.1.1. Structures

Figure 5 shows the chemical structures of DA, as well as S-, and R- stereoisomers of AMPH, S-METH, S-CATH, S-MCAT, MEPH, MDPV, and COC. The top row compares the structures of the most commonly used psychostimulants for the treatment of ADHD and narcolepsy. It also illustrates the spatial orientation differences in the enantiomers of AMPH as well as S-METH. The bottom row shows the chemical structures of synthetic analogues of the naturally occurring cathinone: MCAT, MEPH, and MDPV. All of these compounds are analogous to AMPH or METH with the addition of a β -keto group. The cathinone analogues are components of *bath salts* which is common drug mixture with extensive web-based marketing [77, 116]. It is noteworthy that drugs found on the clandestine market are racemic mixtures comprised of equal amounts of their S- and R-enantiomers. On the other hand, pharmaceutical compounds are composed of specific ratios of enantiomers as in Adderall which is composed of 75% S- and 25% R-AMPH and is used to treat ADHD and narcolepsy [51, 117].

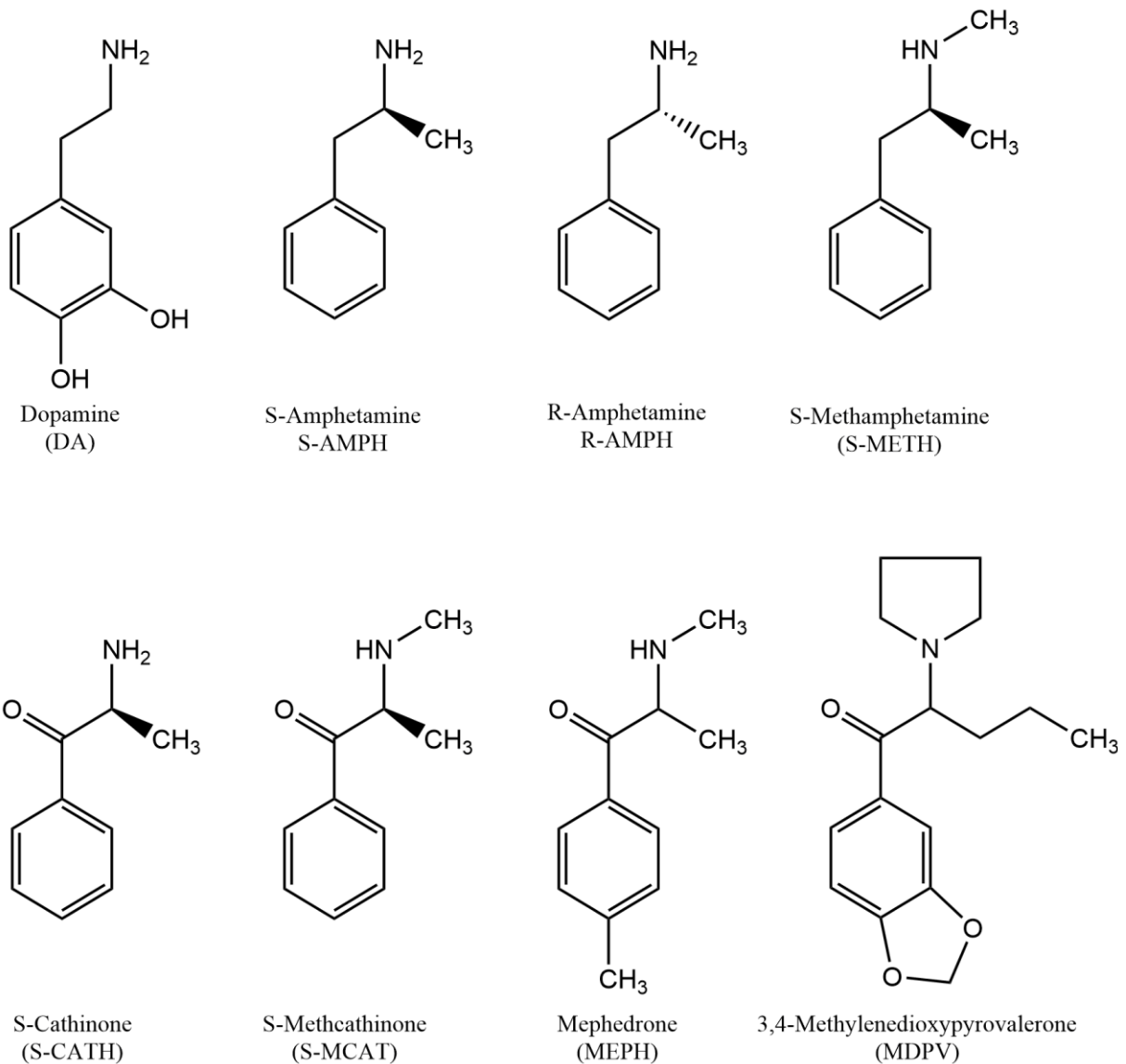


Figure 5: Chemical structures of DA and STPs Top row shows structural similarities among DA and the S- and R- isomers of AMPH and METH. Bottom row compares chemical structures of S-CATH and the cathinone analogues S-MCAT, MEPH, and MDPV which are common ingredients of *bath salts*.

3.1.2. Dopamine, STPs, and reuptake inhibitors differentially affect hDAT

Figure 6 displays currents elicited by the compounds illustrated in Fig 5. *Xenopus* oocytes expressing hDAT were exposed to substrates and reuptake inhibitors (10 μ M, a saturating concentration, -60 mV) for 1 min. Room temperature perfusion of DA stimulated an inward current (I_{DA}) that rapidly decayed to the original baseline upon wash out. Under the same conditions, all STPs S-AMPH, R-AMPH, S-METH, S-MCAT, and MEPH induced a qualitatively similar inward peak current (I_{STP}). Intriguingly, a persistent current was observed for minutes after STP removal (I_{PC}) in all S-isomers (S-AMPH, S-METH, S-MCAT) and the racemic MEPH. The I_{PC}/I_{STP} ratio varies widely among compounds. All traces of STPs are normalized to $I_{STP}=1$ for visual comparison. The reuptake inhibitors COC and MDPV evoked outward currents which are actually the inhibition of an inward constitutive leak current (I_L) through hDAT [1, 6, 23]. MDPV produced a larger outward current deflection as compared to COC, indicating that COC does not fully inhibit the leak through hDAT. Figure 7 is illustrative of the response of STPs used in this study.

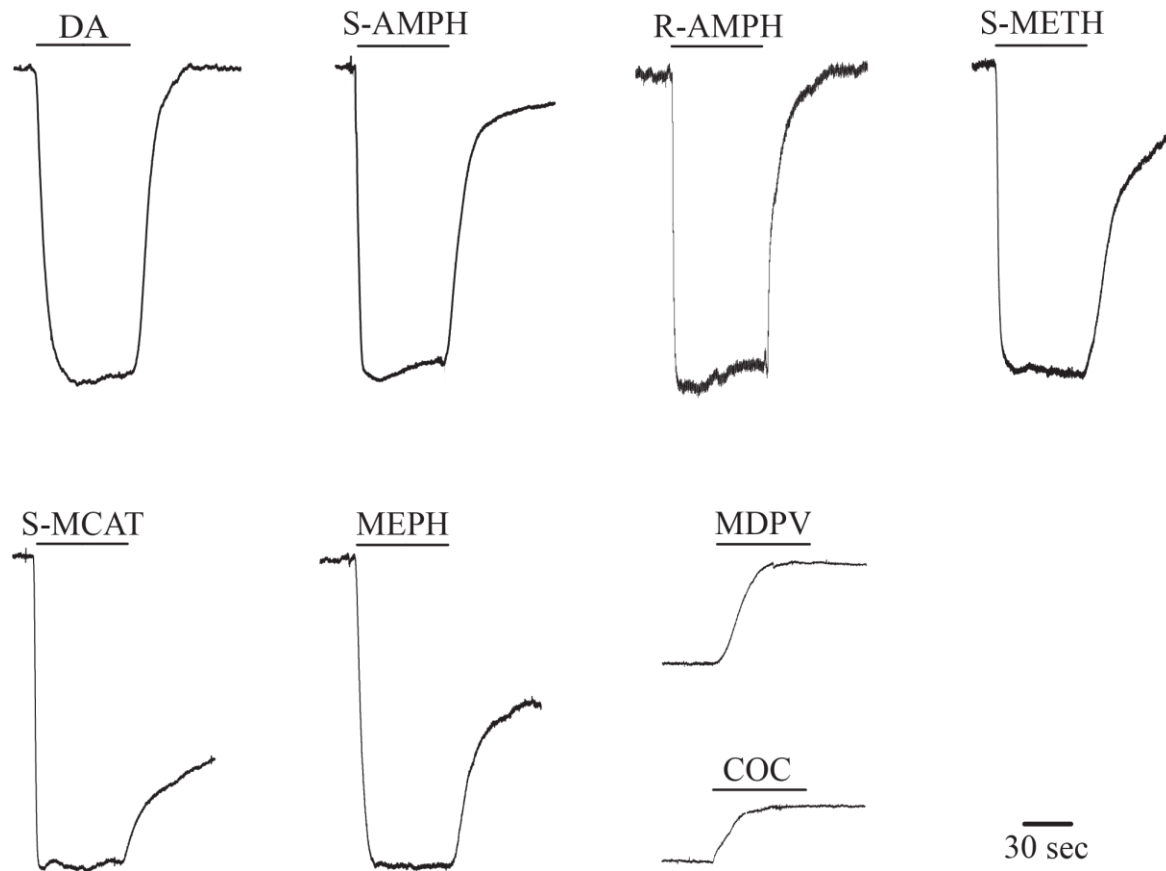


Figure 6: DA, STP, and reuptake inhibitor-induced currents at hDAT Sample currents generated in hDAT by 60 s. application of 10 μ M dopamine (DA), S-amphetamine (S-AMPH), R-amphetamine (R-AMPH), S-methamphetamine (S-METH), S-methcathinone (S-MCAT), mephedrone (MEPH), cocaine (COC), and 3,4-methylenedioxyrovalerone (MDPV) at -60 mV. All STP traces are normalized to the same peak size for comparison. COC and MDPV of oocytes with similar DA pre-pulse were used to illustrate the different levels of inhibition of the two compounds.

3.1.3. The potency and efficacy of I_{STP} at hDAT varies

In order to study STP's ability to induce hDAT currents we conducted dose-response studies (Figure 7). hDAT-expressing oocytes were exposed to 10 μ M DA pre-pulse followed by various drug concentrations at -60 mV. In Figure 7, summary of drug-induced responses are represented as a percentile of 10 μ M DA pre-pulse (DA= 100%). All examined STPs were in their more potent S-stereoisomer form with the exception of MEPH (the racemate was used, as in clandestine samples) [80, 118]. Dose response curves were fit to Hill 1 equation using Origin 8:

$$y = START + (END - START) \frac{x^n}{k^n + x^n}$$

where x is the concentration of the tested compound, Y is the response measured, START is min response and END is the maximal response, k is the concentration that yield half-maximal response, and n is the Hill slope parameter.

The order of potency (EC_{50}) was S-MCAT ($0.23 \pm 0.03 \mu$ M, $n=5$) > S-METH ($0.64 \pm 0.15 \mu$ M, $n \geq 5$) > MEPH ($0.84 \pm 0.14 \mu$ M, $n=5$) > S-AMPH ($1.21 \pm 0.15 \mu$ M, $n \geq 5$, data not shown). In terms of efficacy, S-AMPH ($118 \pm 7\%$, $n \geq 5$, data not shown) and S-METH ($107 \pm 6\%$, $n \geq 5$) produced the greatest inward current followed by S-MCAT ($57 \pm 1\%$, $n=5$) and MEPH ($41 \pm 1\%$, $n=5$). An important note here in comparing these values is that MEPH used was a racemic mixture (50% S- and 50% R- enantiomer), therefore the values for EC_{50} and V_{max} obtained from this studies are likely right and down shifted respectively. Here we did not explore STP's ability to induce I_{PC} : that will be investigated in later section.

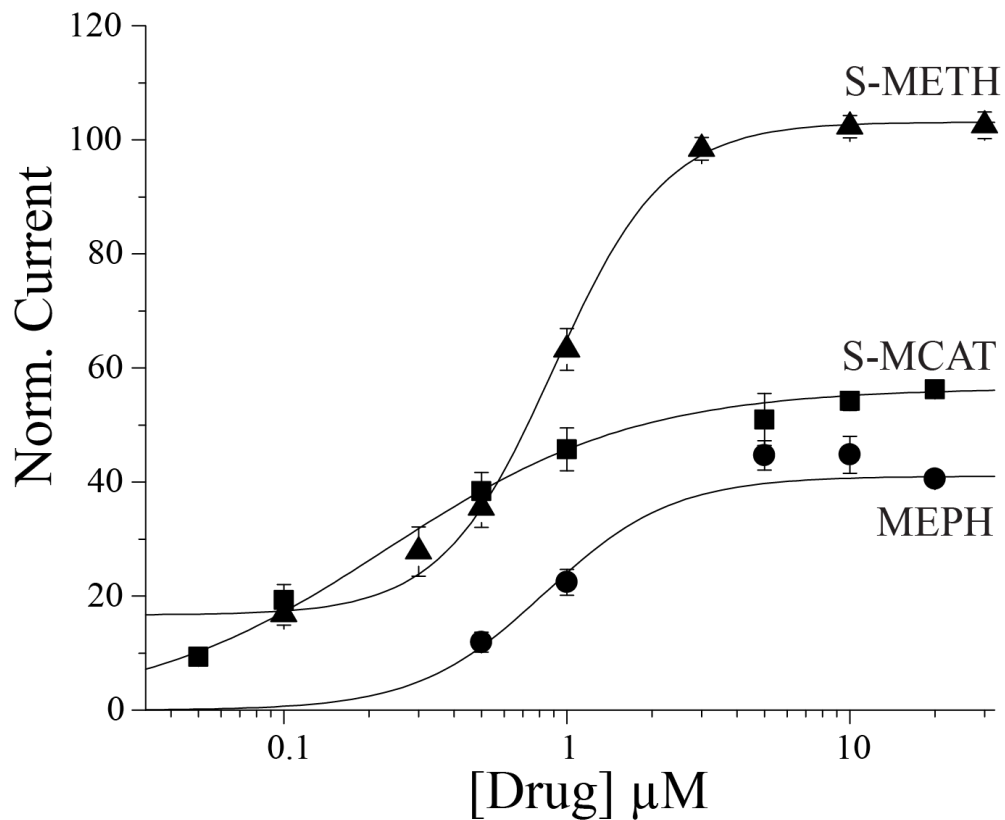


Figure 7: Dose-response curves of STPs (Figure adapted from [6]) Dose–response curves (\pm SEM) for S-METH, S-MCAT, and MEPH in hDAT expressing *Xenopus* oocytes at -60 mV. Data points were obtained by exposing hDAT-expressing oocytes to different concentrations of drug for 1 min and normalizing peak currents to a 10 μM DA pre-pulse ($n \geq 5$).

3.1.4. Difference in efficacy but not potency of MDPV and COC to inhibit constitutive hDAT current

As seen in Figure 6, unlike other tested cathinone analogues MDPV did not produce an inward peak current. In contrast, MDPV induced an outward current similar to that observed with COC, which indicated that MDPV is not transported but, rather, it is a reuptake inhibitor. Compared with COC, we observed a larger outward current upon application of MDPV and constructed a full dose-response curve for hDAT constitutive leak inhibition for both (Figure 8). MDPV was more efficacious than COC in inhibiting hDAT's constitutive leak current (32.9 ± 1.9 and 24.6 ± 0.5 % of DA pre-pulse respectively, $n=5$). Interestingly, both compounds had similar potency (0.33 ± 0.07 μM and 0.30 ± 0.04 μM respectively, $n=5$) to inhibit hDAT's endogenous leak, I_L . Because these reuptake inhibitors inhibit different magnitude of leak currents, we may think of them as full or partial inverse agonists when discussing hDAT-induced currents.

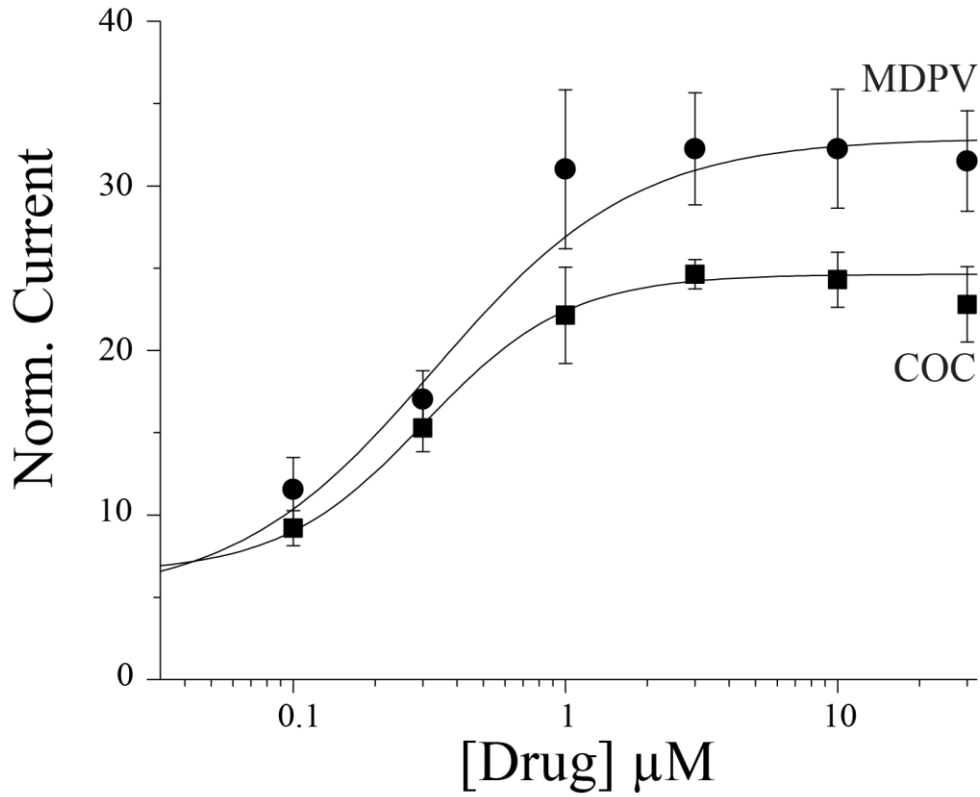


Figure 8: COC and MDPV dose-response curves (Figure adapted from [6]). Different concentrations of MDPV or COC were applied to hDAT-expressing *Xenopus* oocytes voltage clamped at -60 mV ($n=5$ for each concentration). Drug responses are normalized to a $10 \mu\text{M}$ DA pre-pulse.

3.2. Action of reuptake inhibitors at hDAT

3.2.1. Reuptake inhibitors block different levels of hDAT's constitutive leak current

In Figure 6 and Figure 8 we see the synthetic cathinone MDPV induces a larger upward current deflection than COC. As mentioned previously, reuptake inhibitors do not produce a net outflow of positive charge at -60 mV; rather, they decrease the net inward current through hDAT. Because a larger outward deflection occurs upon blockade by MDPV, we conclude that COC does not block all of the constitutive leak. To eliminate possibility of endogenous oocyte conductance inhibition by the blockers, both COC and MDPV were applied to uninjected oocytes: no deflection from original baseline current level was observed in either case (data not shown).

3.2.2. MDPV has the electrophysiological signature of a tight binding reuptake inhibitor

To compare the potency of COC and MDPV to inhibit I_{DA} , we competed 5 μ M DA with various concentrations of the two compounds (Figure 9A and 9B, respectively). Both compounds either reduced or eliminated the dopamine-induced current. Interestingly, while COC application inhibited I_{DA} within 15-30 s., MDPV blockade of the dopamine-induced inward current never reached a steady state within the timeframe of the experiment which made it impossible to obtain an IC_{50} value for MDPV. For the high concentrations (10 μ M), steady state was achieved within 15 s. Lower concentrations of MDPV (0.5 μ M) reached steady state at 5 min post application (see slow inhibition of DA-induced current in panel B).

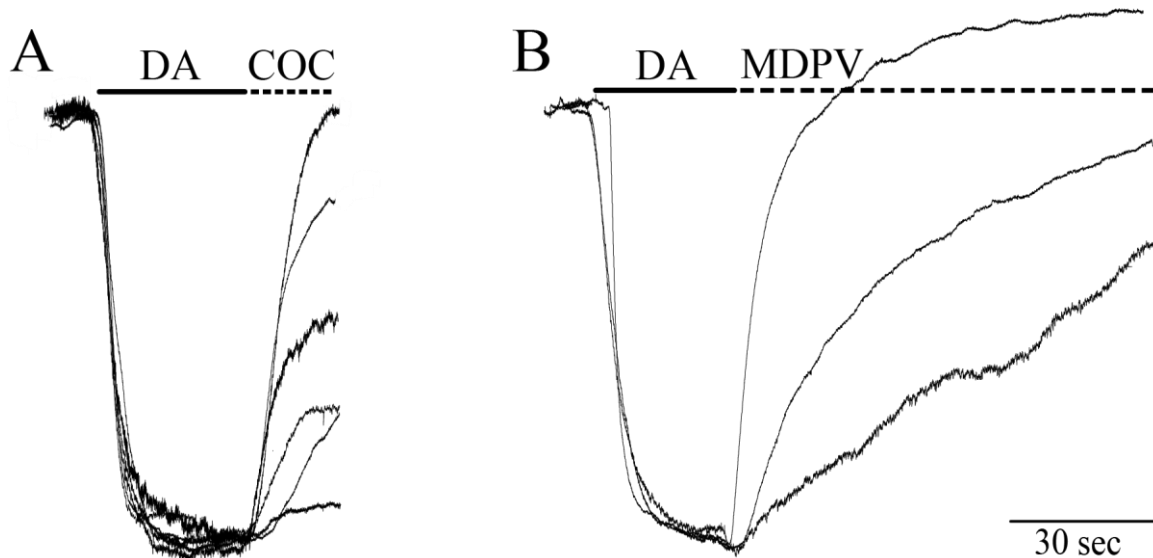


Figure 9: COC and MDPV blockade. (Adapted from [6]) *Xenopus* oocytes voltage clamped to -60 mV A) Raw traces for cocaine (COC) dose-inhibition curve: 5 μ M dopamine (DA) applied for 30 s (solid line) followed by perfusion of 5 μ M DA plus various concentrations of COC (dashed line). B) Raw traces for MDPV dose-inhibition under the same conditions as A. Unlike COC, MDPV inhibition did not reach a steady state level within 1 min. The inhibitory effect at all MDPV concentrations persisted until maximum inhibition was reached (for the lowest concentrations, 0.5 μ M, it takes more than 5 min to reach steady state; in contrast, the highest concentration of MDPV (10 μ M) reaches the steady state in 15 s).

3.2.3. Time course of COC and MDPV block in oocytes

In Figure 10A, 10 μM MDPV was applied during 10 μM MEPH-induced I_{PC} . After MDPV was removed, the baseline remained elevated (block of hDAT's constitutive leak) for an extended period of time. Under the same conditions, 10 μM COC caused a block of hDAT currents only for the duration of its application (Figure 10B). To better characterize the differences between these two reuptake inhibitors, we designed a protocol to quantify DAT's recovery after exposure to the blocker. We applied a 30 s DA pre-pulse to estimate DAT's expression level. Next, we applied either COC or MDPV for 1 min to block the constitutive leak current. Finally, to monitor recovery after block, we measured the DA-induced current at 1, 5, 10, 15, 20, 25, and 30 min following blockade. To account for transporter down-regulation due to numerous substrate applications, we did a control measurement without blocker and applied DA pulses at the same time points as in the experiment shown in Figure 10C-D. The observed decrease in the I_{DA} control was used to normalize the results in the blocker-applied measurements. Raw traces for each blocker are shown in Figure 10C. Each experiment was repeated three times at each concentration. The summary plot shown in Figure 10D illustrates the dramatic differences in the time course of inhibition of MDPV compared with COC. Whereas all MDPV concentrations tested caused at most 10% recovery of hDAT currents 1 min post blocker application, all COC concentrations tested showed immediate recovery at equivalent time points. MDPV's action was difficult to wash off on this time scale and even 30 min after inhibition, only 40% recovery occurred following blockade at lower concentrations (1 and 3 μM) and only 20% recovery occurred after 10 μM MDPV. Although modest recovery from MDPV begins at 10 min, we cannot distinguish between hDAT recovery and new copies of hDAT inserted into the membrane. Because uptake inhibitors up-regulate

hDAT, the recovery after MDPV block may be due to new hDATs inserted into the membrane, which correlates with recovery after COC block.

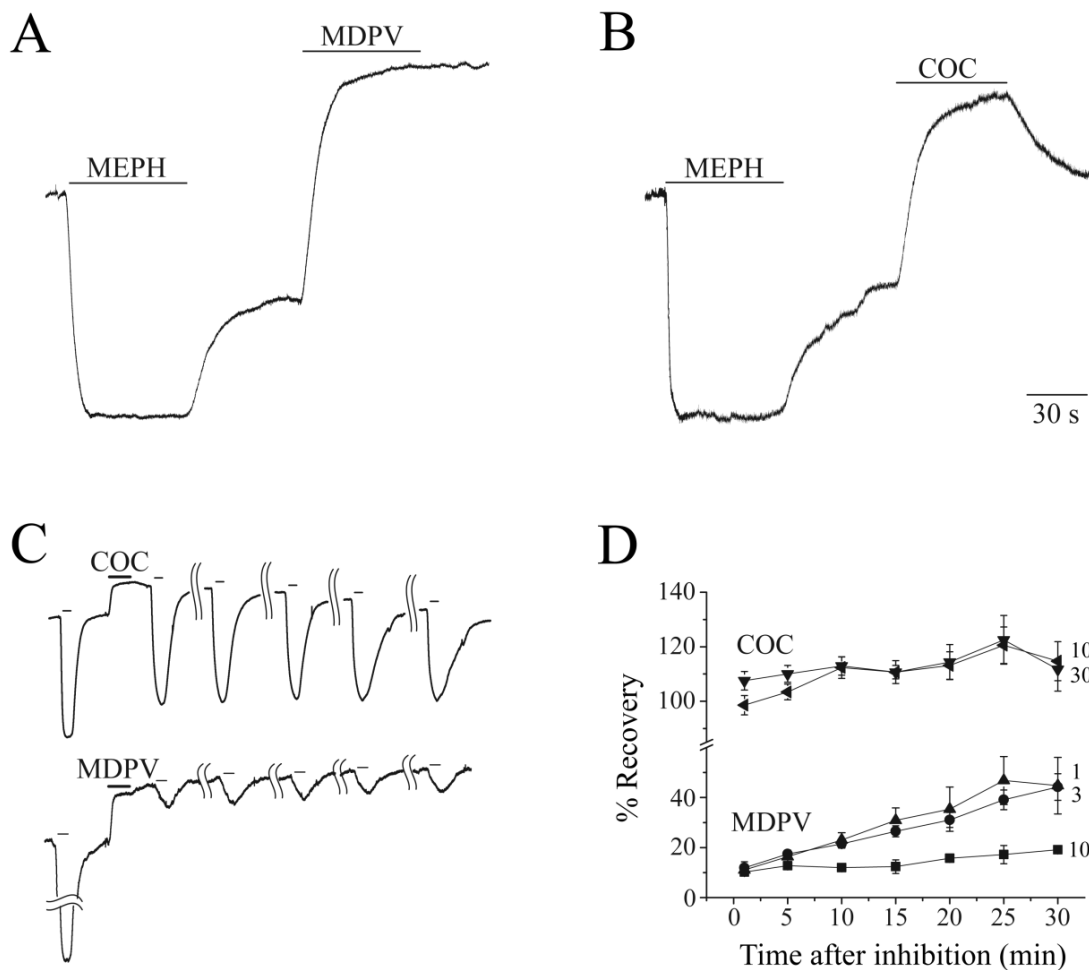


Figure 10: MDPV and COC blockade reversibility. (Adapted from [1]) Panels A) and B) show raw traces of 60 s blocker application (MDPV or COC, 10 μ M) during I_{PC} induced by 60 s MEPH external application (10 μ M) at $V = -60$ mV C) At $V = -60$ mV, 30 s exposure of 10 μ M DA is followed by 60 s application of 10 μ M COC (top) or MDPV (bottom). 30 s pulses of DA follow the block at time in min: 1, 5, 10, 15, 20, 25, 30 (25 and 30 min not shown) D) Cumulative data from C), $n = 3$. Recovery of I_{DA} after block is plotted on the y-axis. One minute after COC treatment (10 and 30 μ M), the DA-induced current recovers completely. One minute after MDPV treatment (1, 3, 10 μ M), the DA-induced current recovers only 10% of its initial value. At 30 min, recovery from MDPV is 50, 50 and 20%, respectively.

3.2.4. MDPV reversibility in mammalian expression system

We tested MDPV's long lasting effect at hDAT expressed in HEK 293 cell at physiological temperature ($T= 37^{\circ}\text{C}$) using fluorescent microscopy. First, $2\ \mu\text{M APP}^+$ was applied for 3 min to establish a stable rate of uptake. Next, either $10\ \mu\text{M DA}$ (black trace) or MDPV (red trace) was applied to compete the APP^+ uptake (flat portion of Figure 11A). Lastly, $2\ \mu\text{M APP}^+$ was reapplied to monitor the off rates of DA and MDPV. We define full recovery as rate of uptake after block being equal to the pre- DA and pre-MDPV rate of uptake. For times greater than 400 s, the two traces in Figure 11B have different shapes, illustrating the differences in off rates of each compound. Since we cannot determine the exact recovery point, we show the same data in 11A but converting APP^+ uptake into rate of uptake by taking the 1st derivative of the two traces. Figure 11B compares the rates of APP^+ uptake following DA and MDPV application. Arrowheads emphasize rate differences between the two drugs. This distance between the arrowheads indicate 300 s or 5 min; that is, it takes 5 min for hDAT to recover after MDPV block vs. 30 s after DA inhibition of APP^+ uptake. The inhibitory effect in oocytes is at least 6 times longer than in HEK 293 cells. However, there are a few differences that can account for the differences. First, we have different expression systems with difference in membrane and protein composition. In addition, the perfusion in oocytes is at room temperature while the HEK 293 cells is at 35°C . Furthermore, in oocytes, we measure I_{DA} to determine hDAT function recovery at $-60\ \text{mV}$, while in HEK 293 cells we monitor the ability of hDAT to transport fluorescent substrate APP^+ without voltage clamp.

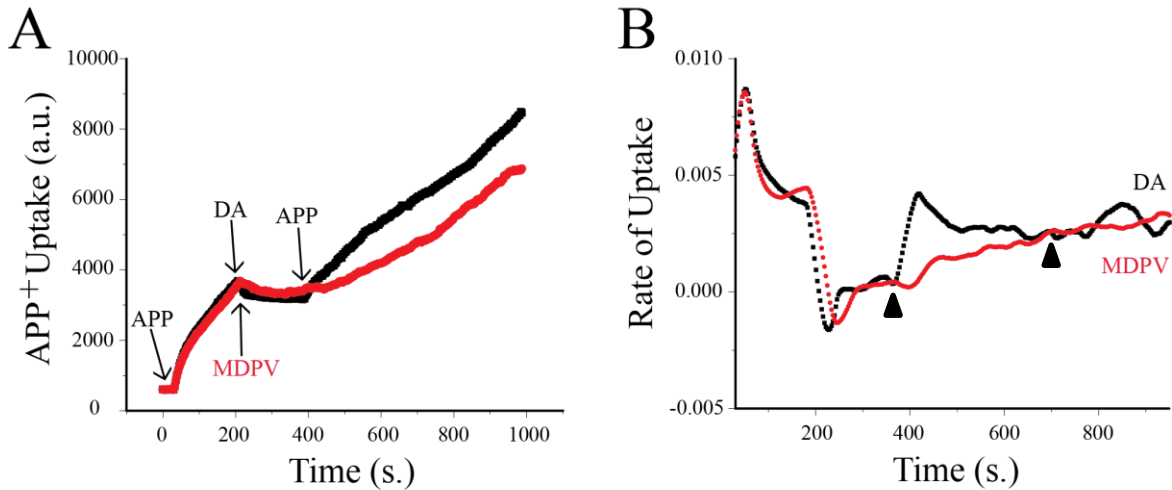


Figure 11: MDPV long action in hDAT expressing HEK 293 cells A) 2 μM APP⁺ is applied for 3min to hDAT expressing HEK 293 cells, T= 37°C to establish a stable uptake rate. Either 10 μM DA (black trace) or MDPV (red trace) is then applied with 2 μM APP⁺ to observe the competitive inhibition of the fluorescent substrate. Following the inhibition, APP⁺ was reapplied for 10 min to observe the off kinetics of DA and MDPV B) To quantify the difference of off kinetics of DA and MDPV, rate of uptake (1st derivative) of APP⁺ uptake was plotted against experiment progress in time.

3.2.5. Action of *bath salts* mixture

In the past few years, a number of synthetic cathinones have invaded the clandestine market [83] under the name *bath salts*. In most samples a mixture of several compounds was identified, including cathinone analogues, cocaine, caffeine, THC, and other compounds [83]. MEPH and MDPV are among the more popular ingredients (Fig. 1) and were placed on Schedule I in October 2011 [89]. *Bath salts* are easily obtainable in head shops and on the Internet in packages clearly mislabeled as: “bath salts not for human consumption”, “research chemicals” or “plant food” [75, 77, 116]. We investigated the effect of MEPH and MDPV together, as might be expected for *bath salts* samples. Figure 12 shows currents in hDAT-expressing oocytes voltage clamped at -60 mV. Different ratios of MEPH/MDPV were continuously perfused for the entire duration of the experiment. From top to bottom the ratios of MEPH/MDPV (in μM) are 1/19, 5/15, and 15/5. In mixtures composed predominantly of MEPH (lowest trace), we observed initial large size inward current that eventually reversed as the comparatively lower concentration MDPV blocked hDAT. In mixtures composed predominantly of MDPV (top trace), the effect is essentially a long-lasting inhibitory current. The kinetics of MEPH are more rapid than the kinetics of MDPV in terms of their ability to either elicit or block current through hDAT. We hypothesize that *in vivo*, assuming equal concentrations of both compounds in the brain, there could be a reinforcement of DA for *bath salts* abusers caused by: 1) exocytotic release due to MEPH-induced transient depolarization, and 2) retention of DA in the synapse due to long-lasting MDPV block of hDAT.

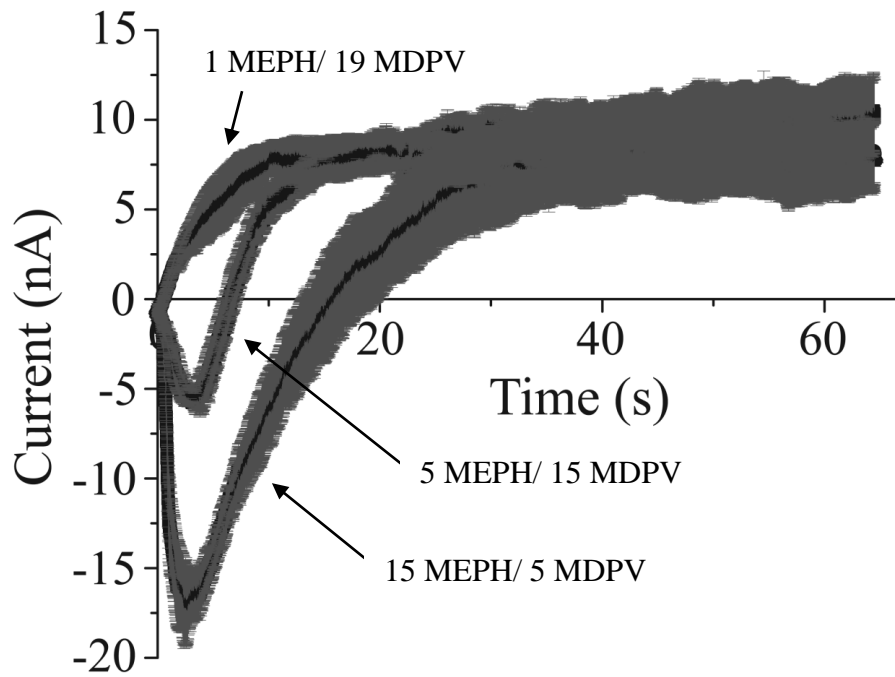


Figure 12: Bath salts currents hDAT currents induced by continuous exposure of different proportions of bath salts components in hDAT expressing oocytes, $V = -60$ mV: MEPH/MDPV (substrate/blocker) (in mM): 1/19, 5/15 and 15/5 ($n = 3$, grey color represent SEM).

3.3. STP-induced persistent current at hDAT

3.3.1. I_{PC} is dependent on intracellular STP concentration

In Figure 13A we see raw traces from hDAT expressing oocytes voltage clamped at -60 mV. External 10 μ M S-AMPH perfusion induced an I_{STP} that returned to baseline after 30 s application. However, longer exposures to S-AMPH caused a persistent current after drug removal. The longer duration of S-AMPH application, the greater the amplitude of I_{PC} suggesting that internal accumulation of S-AMPH might be impairing normal hDAT function and not allowing it to close; hence, we named S-AMPH action a ‘molecular stent’ within the transporter. I_{PC} does not only depend on the duration of STP application but also on its concentration (Figure 13B). Exposure to 10 μ M S-AMPH for 20 s did not produce I_{PC} in Figure 13B, while 20 s. exposure of 30 μ M S-AMPH induce a pronounced persistent current. This suggests again that I_{PC} is due to S-AMPH accumulation, and it acts at an intracellular site. To directly test our ‘internal action’ hypothesis, we titrated various concentrations and/or volumes of S-AMPH into hDAT expressing oocytes voltage clamped to -60 mV. DA-induced hDAT current swiftly and consistently returned to the original baseline prior to STP exposure (Figure 13C, left trace). Prior to injection of S-AMPH inside of the oocyte, DA external application produced I_{DA} ; however, after injection of S-AMPH a persistent current was observed after DA wash-out. We were able to affect the I_{PC} magnitude by either repeated injections of the same concentration or by using a single higher concentration injection of S-AMPH, therefore confirming the involvement of internal S-AMPH in the I_{PC} phenomenon [2].

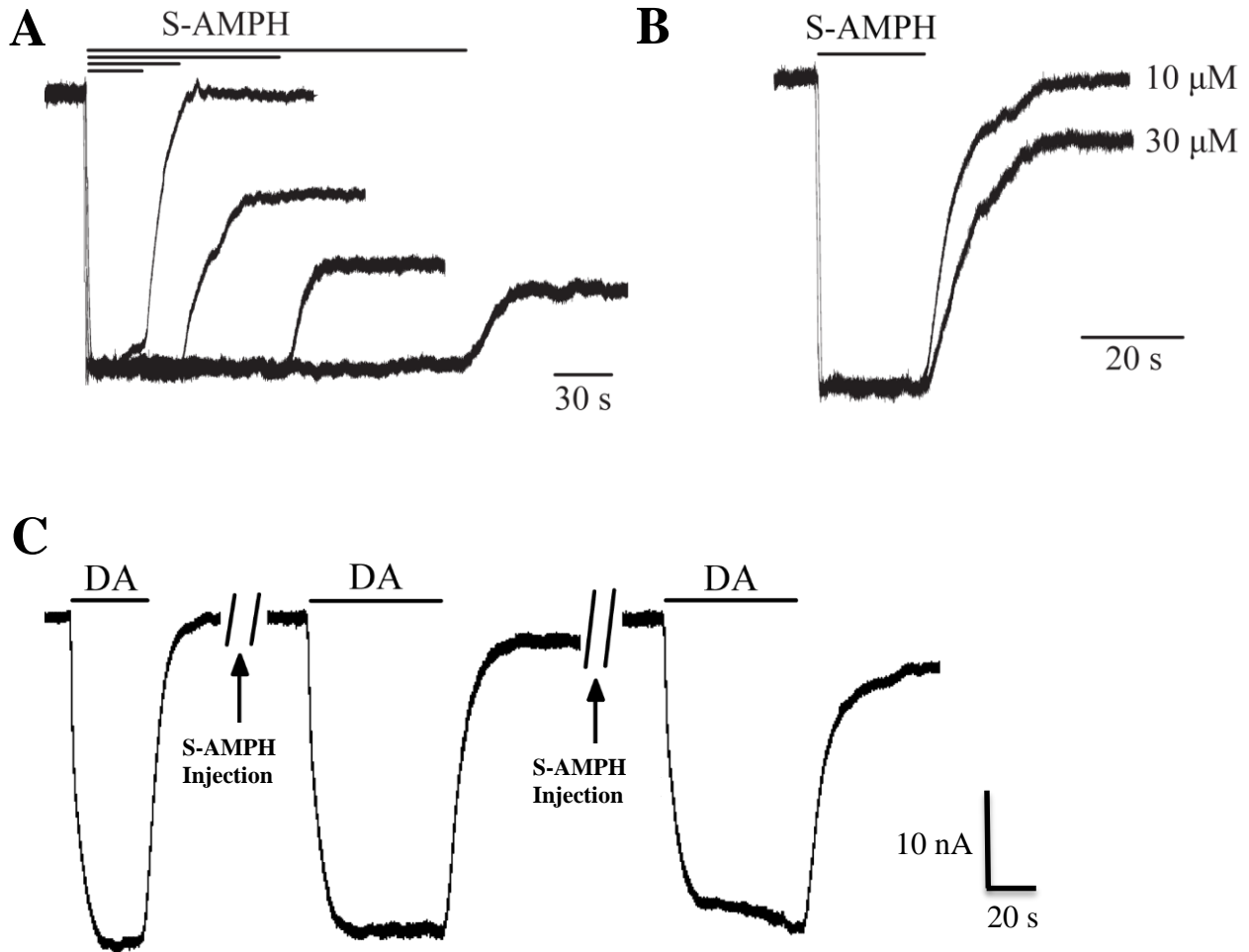


Figure 13: I_{PC} is time and concentration dependent and is induced by internal STP (Figure adapted from [2]) A) S-AMPH ($10\ \mu\text{M}$) induced inward peak current for exposures less than 30 s; however, for longer exposure times, a current that we term I_{PC} remained long after S-AMPH had been removed, and the amplitude of I_{PC} was proportional to the exposure duration. S-AMPH peak currents were normalized to the briefest exposure time. B) A relatively brief and initial exposure to S-AMPH (20 s), which ordinarily would not produce a persistent current, did so if the concentration of S-AMPH was increased from 10 to $30\ \mu\text{M}$. C) Dopamine, which ordinarily would not produce I_{PC} (left trace), induced a persistent current after $25\ \mu\text{M}$ internal injection of S-AMPH (middle trace). Doubling the internal S-AMPH concentration (second injection) resulted in the generation of a larger I_{PC} (right trace).

3.3.2. I_{PC} does not depend on the lipophilicity of STPs

Amphetamine is lipophilic and can partition through the membrane. It was suggested that certain drugs produce long lasting depolarizing currents through hDAT due to accumulation of these lipophilic compounds in the oocyte [119]. According to the lipophilicity model of I_{PC} , when drugs are washed away, passive diffusion and partitioning of accumulated drugs to the outside will activate hDAT externally [119]. Figure 14 plots the magnitude of the persistent current measured 60 seconds after removal of compounds (10 μ M) against the lipophilicity represented using logP. logP is the octanol/water partition coefficient expressed in logarithm form. Its values were obtained from chemicalize.org. High logP values represent more lipophilic molecules that would more easily penetrate lipid membranes and reach molecular targets such as ion channels, receptors, and in this case DAT. Figure 14 shows that S-AMPH and R-AMPH, which have the same logP, differ in their ability to generate a persistent current: S-AMPH induced I_{PC} , while R-AMPH did not. Considering that both enantiomers of AMPH are equipotent in inducing I_{STP} in hDAT-expressing oocytes (1.31 \pm 0.22 for R-AMPH and 1.25 \pm 0.14 for S-AMPH, data not shown), lipophilicity cannot explain the differences observed in their ability to produce I_{PC} . In addition, S-AMPH and S-METH have different logP values, yet the two compounds have approximately the same amplitude I_{PC} . Finally, S-MCAT has the highest persistent current of the group we studied, but is not the most lipophilic providing additional evidence that lipophilicity is uncorrelated with the ability of STPs to produce a persistent current.

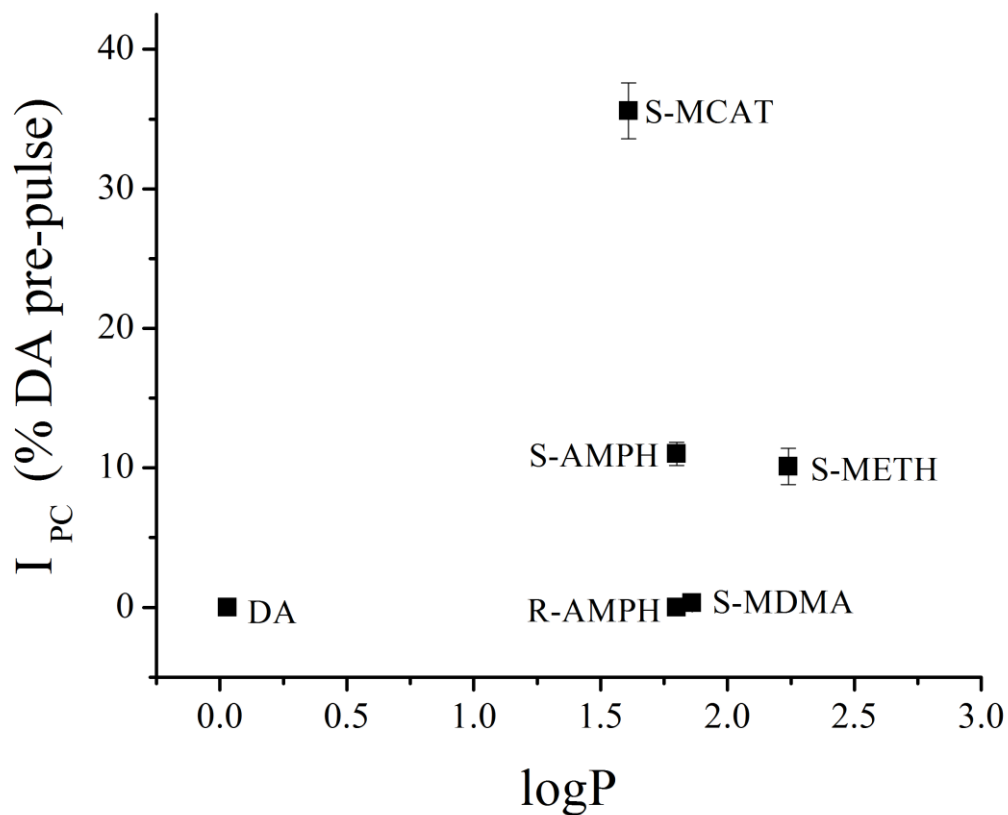


Figure 14: I_{PC} vs. lipophilicity. (Figure adapted from [5]). hDAT expressing oocytes, V= -60 mV, room temperature. All drugs are applied for 60 s and at 10 μ M in concentration. The persistent current is given as a fraction of the DA-induced current for each oocyte to normalize for expression levels from cell to cell. The logP values were obtained from chemicalize.org. Mean +/- SEM (n \geq 5).

3.3.3. I_{PC} is induced by a unique conductance state of hDAT

In order to definitively state that I_{PC} is caused by a unique conduction state of hDAT, we compared the current-voltage relationships, $I(V)$, of S-AMPH-induced I_{STP} and I_{PC} in Figure 15. All $I(V)$ curves are buffer-subtracted to show only the drug-induced changes in conductance. The $I(V)$ for I_{DA} has a negligible slope at more positive potentials, interpreted as a blockade of endogenous conductance by DA [23]. Unlike DA, the S-AMPH-induced I_{STP} $I(V)$ curve shifted to the left and has a reversal potential of approximately 0 mV. The S-AMPH I_{PC} $I(V)$ was further shifted to the left compared with STP and had a $V_{rev} = -20$ mV. This is the reported reversal potential of Cl^- in oocytes and is further in agreement with previous publications of Cl^- involvement in substrate-induced currents [24, 25].

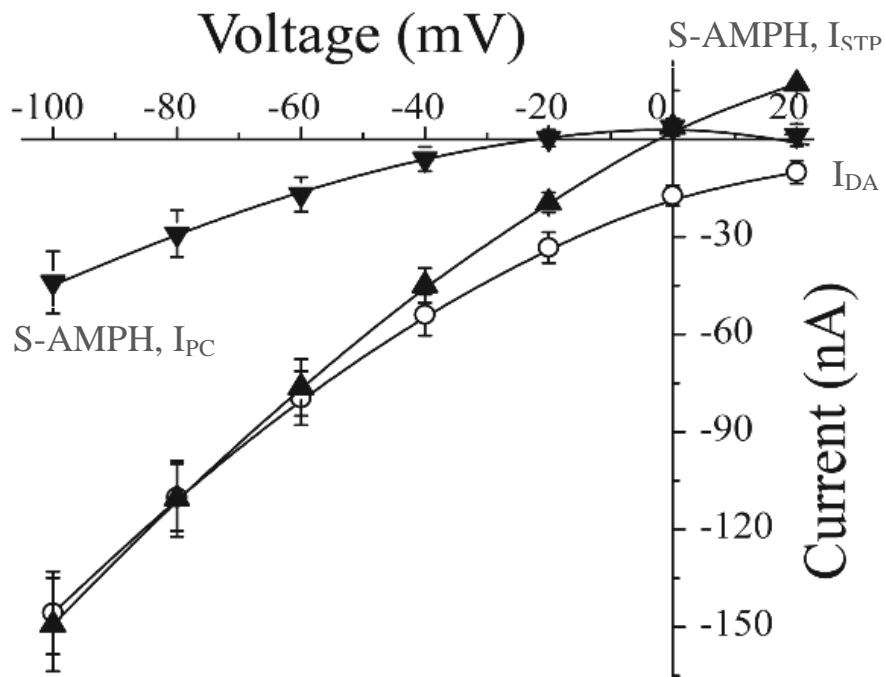


Figure 15: Current-voltage relationship of I_{DA} , I_{STP} , and I_{PC} (Figure adapted from [2]). Baseline subtracted I(V) curves for DA, S-AMPH peak (I_{STP}) and S-AMPH persistent current (I_{PC}). The S-AMPH I_{STP} I(V) is shifted to the left above -60 mV compared with the DA peak and reversed at 0 mV. The S-AMPH I_{PC} I(V) is further shifted to the left and V_{rev} was at -20 mV suggesting the flow of Cl^- ions.

3.3.4. I_{PC} causes a dysfunctional DAT state

As seen in Figure 13B, high concentrations of externally applied S-AMPH lead to more pronounced I_{PC} . In Figure 16, we applied 100 μM S-METH to produce a large persistent current. Allowing some time for S-METH wash, substrates (10 μM DA and 100 μM S-METH) were pulsed to interrogate the conduction state of DAT. Surprisingly, neither DA nor S-METH were able to stimulate DAT currents from the I_{PC} state, albeit the partial current recovery during the wash. It appears that S-METH locks hDAT in a conformation that is unable to interact with its substrates or induce currents upon external substrate application. To discriminate between transporter dysfunctional and transporter internalization (research shows DAT down-regulation in response to substrate exposure [120]), we designed a functional experiment to test transporter presence at the membrane.

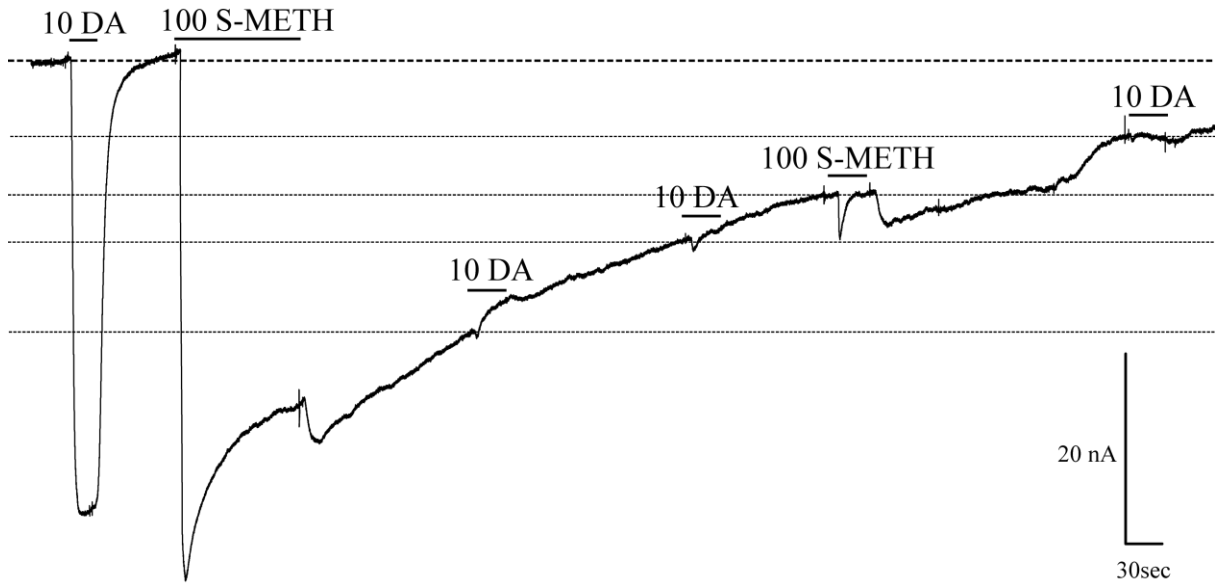


Figure 16: S-METH induced dysfunctional hDAT hDAT expressing oocytes, $V = -60$ mV. 100 s application of 100 μ M S-METH induces a large I_{pc} . 30 s pulses of 10 μ M DA at 2, 4, and 10 min after wash out cannot stimulate hDAT to elicit currents. 30 s pulse of 100 μ M S-METH at 5.5 min was also unable to stimulate the transporter to elicit currents.

3.3.5. DAT's dysfunctional state can be reversed using reuptake inhibitor

In Figure 17 we took advantage of COC's inhibitory action at hDAT to test if the transporter was unresponsive to substrates due to an I_{PC} -induced dysfunctional state, or due to change in surface expression of hDAT. COC eliminated or reduced all hDAT-mediated currents reflected in the upward deflection of current that levels off above the original baseline (Figures 4, 6, 9, and 10). In this experiment a 10 μM DA pre-pulse was followed by 100 s exposure to 60 μM S-METH. A large I_{PC} was induced upon wash out of S-METH. One minute following removal of S-METH, 10 μM COC was perfused. As seen in Figure 17, COC was able to block both the I_{PC} and I_L . This demonstrates that the unresponsiveness of hDAT is due to a conformational change of the transporter upon interaction with internal S-METH, not due to its down-regulation. Additionally, a DA stimulus was delivered following COC block and an inward current with similar amplitude was observed, indicating that S-METH locks hDAT in a conduction mode not responsive to external stimulus, possibly due to a new conformational state that cannot form interactions with substrates that are necessary for eliciting substrate-induced currents. When DA was removed, the current did not return to the original baseline but I_{PC} was maintained, likely due to internal S-METH accumulation. To test the effect of Na^+ on I_{PC} , the cell was perfused for 30 s with Na^+ -free, NMDG containing Ringer buffer. NMDG induced a pronounced upward shift in the current due to the inhibition of Na^+ conduction through hDAT and possibly other oocyte endogenous Na^+ pathways, which are inward at -60 mV [2, 23]. When Na^+ was reintroduced during the subsequent DA application, I_{DA} was generated and I_{PC} ensued after the wash, likely due to the presence of internal S-METH.

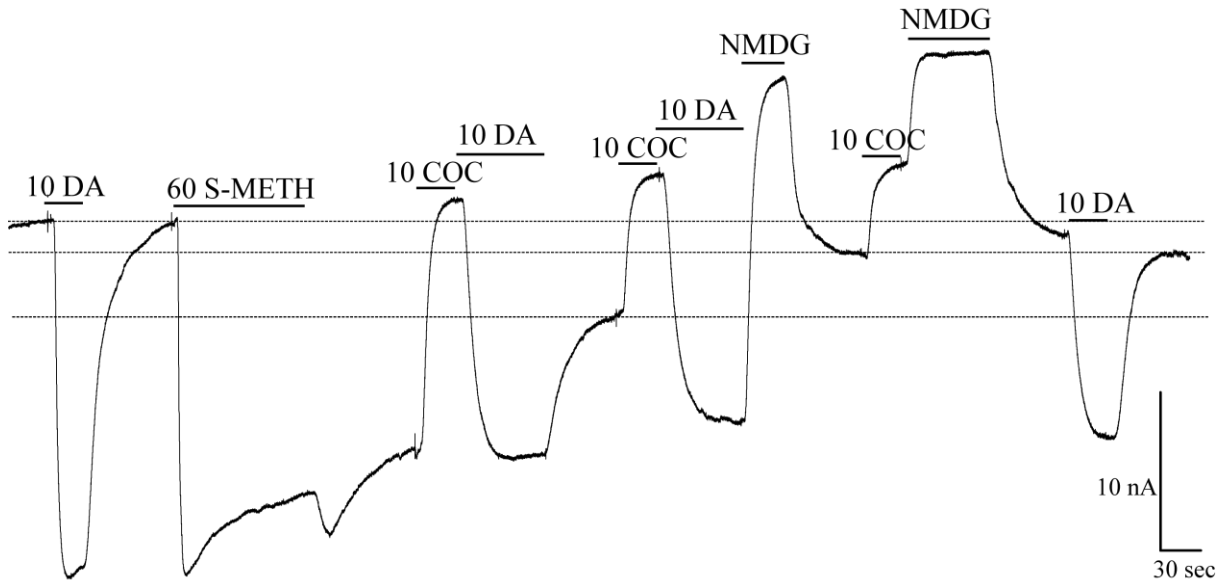


Figure 17: COC recovers hDAT from substrate-insensitive state hDAT expressing oocytes, $V = -60$ mV. 90 s. application of 60 μ M S-METH induces large I_{PC} . 10 μ M COC eliminates both I_{PC} and I_L . Following the block, 10 μ M DA pulse is able to illicit I_{DA} ; nevertheless, I_{PC} is observed upon DA wash out. 10 μ M COC blocks hDAT current. Second DA pulse elicits I_{DA} of the same magnitude as the 1st pulse. 30 s removal of Na^+ (substitution with equimolar NMDG) eliminates hDAT and oocyte endogenous conductances. Upon introduction of Na^+ the new baseline is still more depolarized compared to the original. Addition of 10 μ M COC reduces hDAT's constitutive leak and removal of Na^+ for 1 min now is able to eliminate hDAT's I_{PC} . However, activation of hDAT with a 30 s DA pulse is able to again incur I_{PC} .

3.4. hDAT expression in mammalian cells

To investigate the implications of hDAT currents in more complex systems, we first assayed DA and STP effects in Flp_{hDAT} cells; a stable inducible cell line. Immunostaining in conjunction with confocal microscopy showed membrane localization of hDAT in Flp_{hDAT} cells three days after doxycycline induction (Figure 18), whereas the parental Flp-In T-rex 293 cells showed no hDAT expression (data not shown). In addition, hDAT protein levels were also visualized using Western immunoblotting. As seen in Figure 18 right, hDAT was absent in parental Flp-In cells and present in doxycycline induced Flp_{hDAT} cells. Equal amounts of protein loaded were confirmed using antibody against GAPDH.

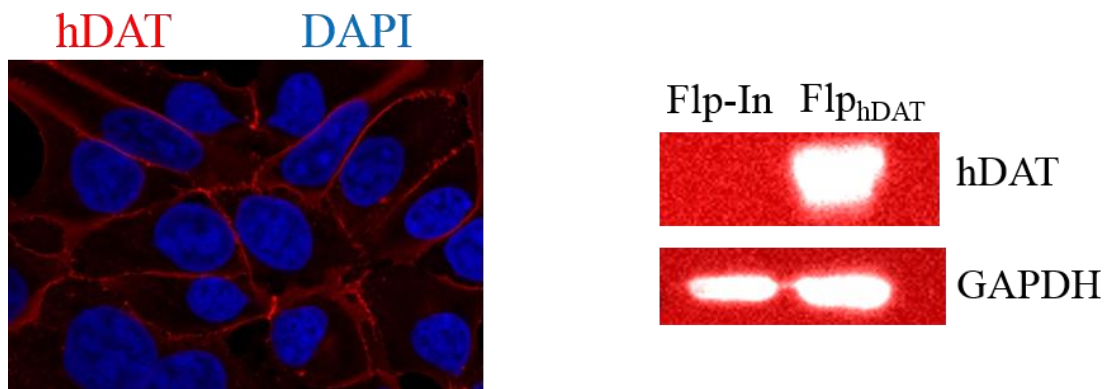


Figure 18: Expression of hDAT in Flp-In T-Rex mammalian cells (left) Confocal image shows hDAT expression in Flp_{hDAT} cells (red stain concentrated at the membrane). DAPI nuclear staining appears in blue. (right) Parental Flp-In and Flp_{hDAT} were cultured and lysed to confirm expression of hDAT using Western immunoblotting. Antibodies against human hDAT and GAPDH were used as listed in “Methods”.

3.4.1. hDAT currents in HEK 293 cells

In Figure 19 we compare the hDAT current elicited by DA and S-AMPH application under voltage clamp at $V = -60$ mV and physiological temperature. The currents are obtained from hDAT transiently transfected HEK 293 cells. 10 μ M DA induces an inward current that returns to baseline when DA is removed. 30 s of 10 μ M S-AMPH induces a similar inward peak current; however, the return of current upon wash out of S-AMPH is slower and persists tens of seconds for up to one minute. DA and S-AMPH are overlaid for better comparison of kinetics. Using a mono-exponential function, the time constants for the current decay were obtained: $\tau_{DA} = 1.3$ s, $\tau_{S-AMPH} = 5.1$ s, $\tau_{S-AMPH}/\tau_{DA} = 3.8$ [5]. The results agree with a study conducted by Sandtner et al. comparing serotonin (5-HT), p-chloroamphetamine (pCA), and methylenedioxymethamphetamine (MDMA) responses in hSERT-expressing *Xenopus laevis* oocytes and HEK 293 cells [119]. In oocytes, pCA-induced hSERT currents decayed 4 times more slowly than 5-HT with a half-life of 20 s and 5 s, respectively. In HEK 293 cells, the pCA-induced current decayed 5 times more slowly than 5-HT, 2.5 s vs. 0.5 s respectively. Thus for Sandtner et al. the persistence ratio for drug to substrate was comparable in oocytes and HEK cells. Reviewing the τ of both this study and Sandtner et. al. published results, we see: 1) the absolute value of the off kinetics between oocytes and mammalian cells are 10 fold different with mammalian kinetics being faster, and 2) the ratio of the off kinetics of psychostimulant to control (endogenous substrate) is comparable in both expression system, approximately 4-5 fold difference.

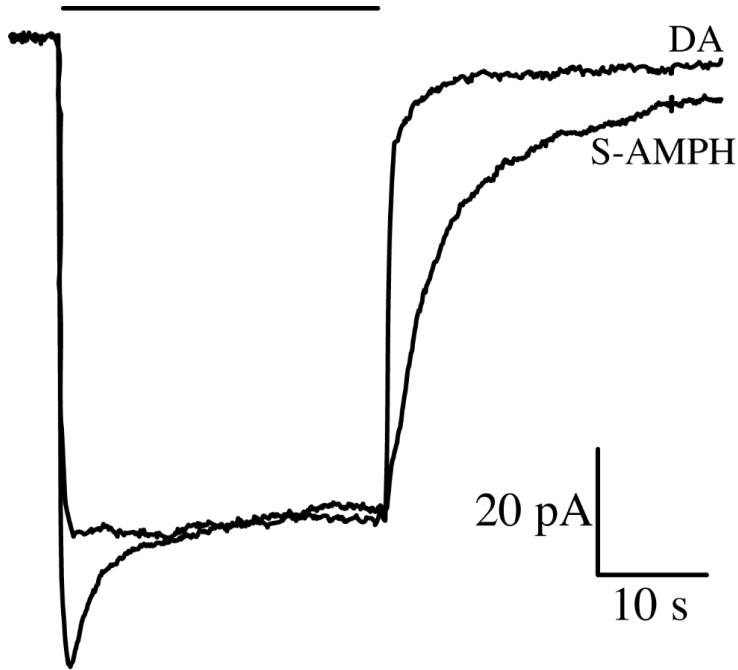


Figure 19: Persistent current in hDAT transfected HEK cells Current through hDAT transiently transfected HEK 293 cells. $V = -60$ mV, $T = 37^\circ\text{C}$. 30 s of $10\ \mu\text{M}$ DA induces an inward current that returns to baseline when DA is removed. 30 s of $10\ \mu\text{M}$ S-AMPH induces a similar inward peak current; however, the return of current upon wash-out of S-AMPH is slower and persists tens of seconds for up to one minute. DA and S-AMPH are overlaid for better comparison of kinetics. Using a mono-exponential function, the time constants for the current decays were determined: $\tau_{\text{DA}} = 1.3$ s, $\tau_{\text{S-AMPH}} = 5.1$ s, $\tau_{\text{S-AMPH}}/\tau_{\text{DA}} = 3.8$. Figure adapted from [5].

3.4.2. Potency of S- and R- AMPH differs in mammalian cells

In Figure 20 we explore hDAT currents in Flp_{hDAT} cells, voltage clamped to -60 mV using whole cell voltage clamp technique. We compare the currents elicited by various concentrations of DA, S-AMPH, and R-AMPH following a 30 μM DA pre-pulse. S-AMPH-induced inward currents with higher potency than DA and R-AMPH. Dose response curves were fit to Hill equation using Origin 8:

$$y = START + (END - START) \frac{x^n}{k^n + x^n}$$

where x is the concentration of the tested compound, y is the response measured, START is min response and END is the maximal response, k is the concentration that yield half-maximal response, and n is the Hill slope parameter. EC₅₀ = 1.50 ± 0.29 μM, 0.31 ± 0.04 μM, and 0.63 ± 0.27 μM for DA, S-AMPH, and R-AMPH respectively. The efficacy of DA and S-AMPH was comparable (99 % and 101 %) while R-AMPH appears less efficacious similar to oocyte results (85 %) [50, 121]. A 2.4-fold potency difference appears between S- and R-AMPH in mammalian cells, which is not present in oocytes (equipotent in oocyte expression system). A 6.3-fold potency difference exists between the S- and R-AMPH enantiomers, was reported by Sitte et al. in HEK 293 cells stably expressing hDAT [50]. Possible reasons behind the potency variation between expressions systems and studies will be examined later in the Discussion.

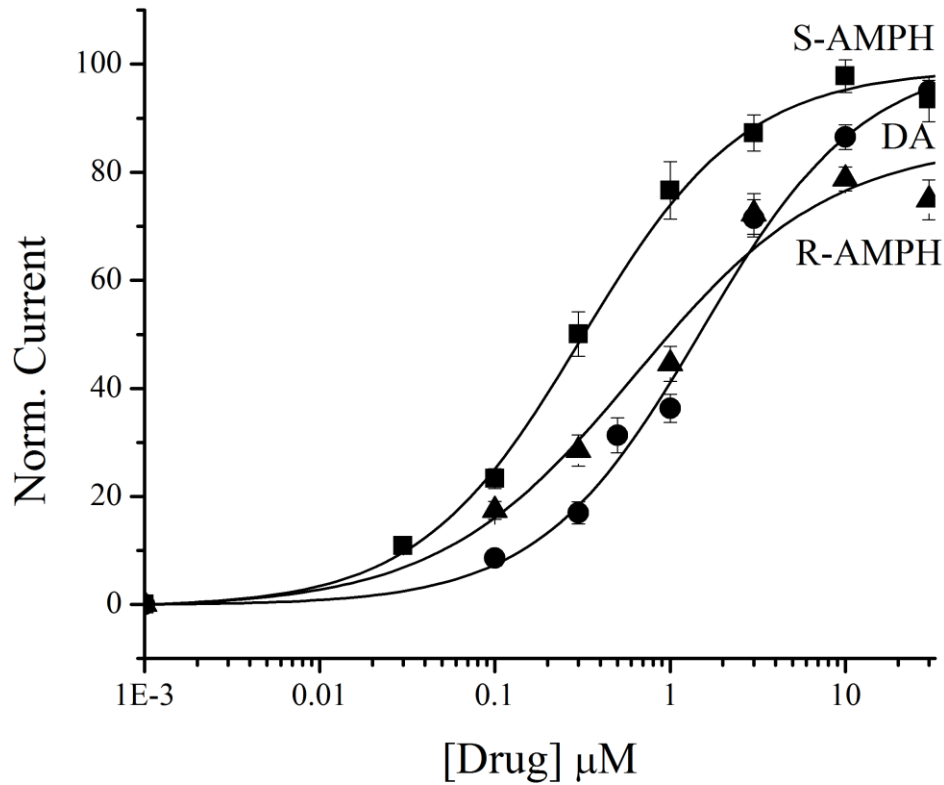


Figure 20: Dose-response curves for DA and AMPH enantiomers in mammalian cells Flp_{hDAT} cells clamped at -60 mV were exposed to a constant DA pre-pulse and a variable pulse of DA, S-AMPH, and R-AMPH. The full dose-response curves were fit to Hill1 equation and yield the following fitting parameters: $EC_{50} = 1.50 \pm 0.29 \mu\text{M}$, $0.31 \pm 0.04 \mu\text{M}$, and $0.63 \pm 0.27 \mu\text{M}$ and Hill Slope = 1.6 ± 0.1 , 0.93 ± 0.1 , and 0.78 ± 0.2 for DA, S-AMPH, and R-AMPH respectively. Each point shows mean \pm SEM, $n \geq 5$.

3.4.3. hDAT-induced currents are electrically coupled to voltage-gated Ca²⁺ channels

To study the possible electrical coupling of hDAT and voltage gated Ca²⁺ channels, the voltage dependence of Cav1.2, Cav1.3, and Cav2.2 was determined in transiently transfected HEK 293T cells. Figure 21 shows the I(V) relationship of the Ca²⁺ currents measured under whole-cell voltage clamp. The voltage dependence of the currents was fit to the following equation:

$$I_{Ca}(V) = \frac{G_{\max}(V - V_r)}{1 + \exp\left(\frac{V_{1/2} - V}{k}\right)}$$

where G_{\max} is the maximal conductance, V is the test potential, $V_{1/2}$ is the potential at which $G=1/2 G_{\max}$, k represent a slope parameter, and V_r is the reversal potential.

Using this equation the test potential that yielded half of the maximal conductance ($V_{1/2}$) was -25.6 ± 1.0 mV ($n=8$), -3.2 ± 0.8 mV ($n=7$) and $+5.5 \pm 1.0$ mV ($n=8$) for Cav1.3, Cav1.2 and Cav2.2, respectively. The 30 mV range of $V_{1/2}$ the three channels under investigation illustrates the variability in high-voltage activated Cav_s. It is easy to imagine that depending on the expression levels of specific type Cav, similar amounts of depolarization may have or not an effect on excitability and neurotransmitter release.

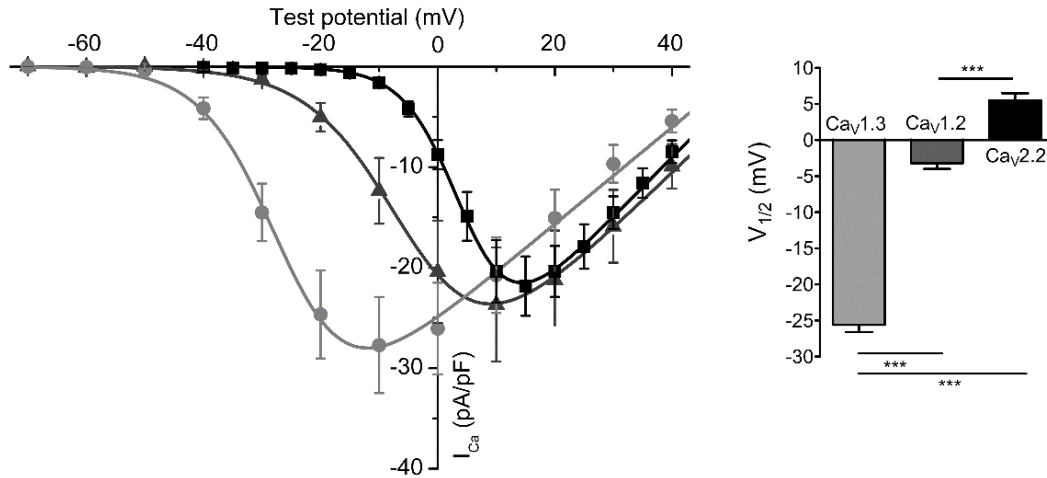


Figure 21: Voltage dependence of Cav1.3, Cav1.2, and Cav2.2 Voltage dependence of Cav1.2, Cav1.3 and Cav2.2-mediated Ca²⁺ currents: HEK 293T cells were co-transfected with β_3 , $\alpha_2\delta$, and EGFP expression plasmids plus alternatively Cav1.3, Cav1.2 or Cav2.2 plasmids. Recordings were carried out at room temperature under constant perfusion. Test pulses in 5 mV steps for Cav2.2 or 10 mV steps for Cav1.2 and Cav1.3 were applied from a holding potential of -80 mV. Representative responses are shown for Cav1.3 (light grey circle), Cav1.2 (dark grey triangle) and Cav2.2 (black square) and the magnitude of the test potentials are indicated in mV. $V_{1/2} = -25.6 \pm 1.0$, -3.2 ± 0.8 and 5.5 ± 1.0 mV, Cav1.3 (n=8), Cav1.2 (n=7) and Cav2.2 (n=8), respectively. Figure adapted from Cameron, Solis, Ruchala, De Felice, and Eltit, submitted for publication.

To determine if depolarization by S-AMPH- or DA-induced hDAT currents is sufficient to activate voltage-gated Ca^{2+} channels, Ca^{2+} signals were measured using the Ca^{2+} sensitive dye Fura-2AM in Flp_{hDAT} cells transfected with Cav1.2, Cav1.3, or Cav2.2 (Figure 22). Both, 5 s application at 35 °C of saturating concentrations of 10 μM DA (upper panel) or 5 μM S-AMPH (lower panel), produced Ca^{2+} signals in Flp_{hDAT} cells expressing Cav1.3 or Cav1.2. The S-AMPH and DA stimulated increase in Ca^{2+} signal was blocked by 2 μM isradipine, a potent L-type Ca^{2+} channel blocker. Conversely, under the same conditions, the intracellular Ca^{2+} concentration did not change in Flp_{hDAT} cells expressing Cav2.2 (right trace). As seen in Figure 21 Cav2.2 requires the highest amount of depolarization to activate: + 5 mV. Depolarization induced by a sequential exposure to high K^+ external solution (right trace, top and bottom) yielded a convincing Ca^{2+} transient demonstrating adequate expression of Cav2.2 in the cells, hence, insufficient hDAT-induced depolarization to activate this type of channels.

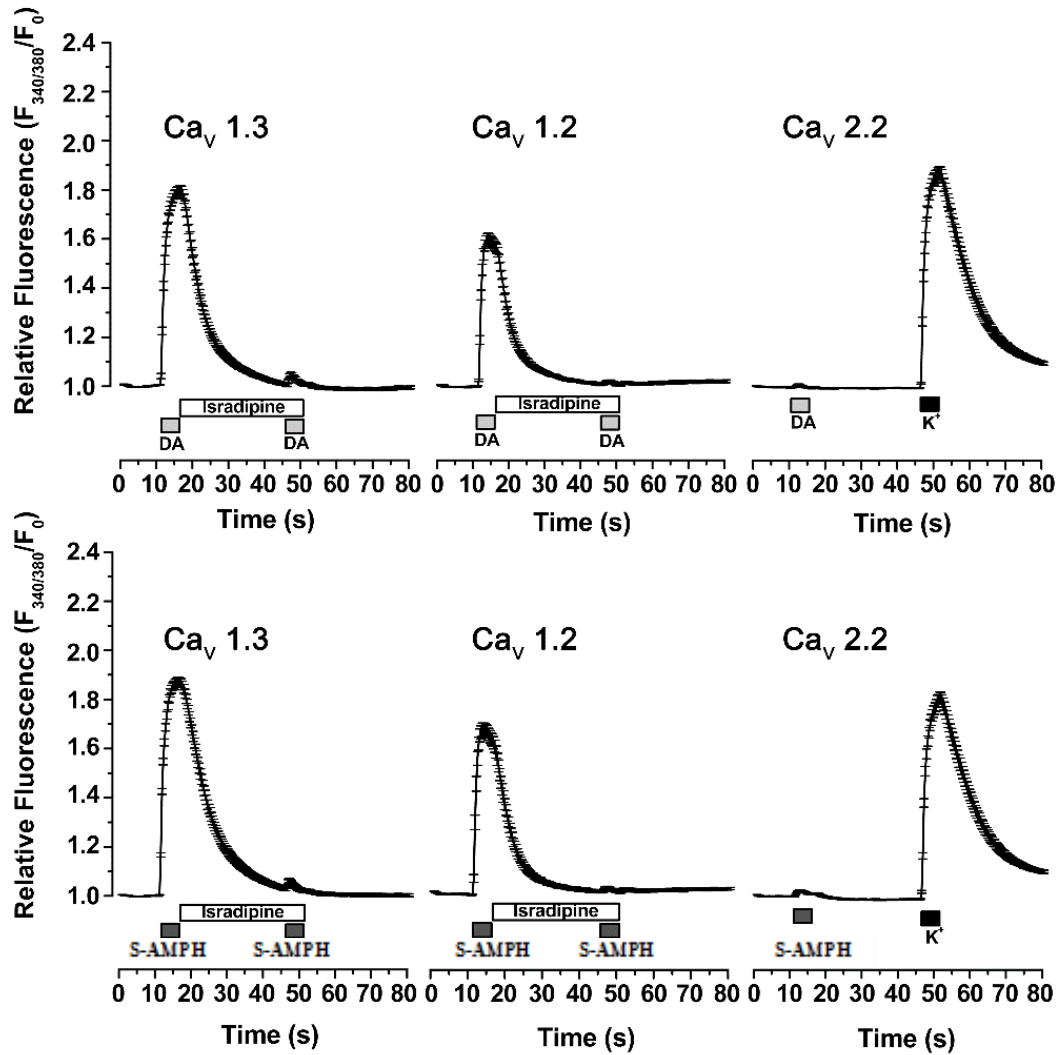


Figure 22. S-AMPH- and DA-induced hDAT currents activate Cav1.2 and Cav1.3, but not Cav2.2. Intracellular Ca^{2+} determinations in Fura-2AM loaded Flp-hDAT cells evaluated by fluorescence microscopy, under constant perfusion and at 35°C. Flp-hDAT cells were co-transfected with Cav1.3, Cav1.2 or Cav2.2 plus β_3 , $\alpha_2\delta$ and EGFP plasmids. Transfected cells were identified by their EGFP signal and then briefly exposed to 10 μ M DA, 5 μ M S-AMPH, or 130 mM K^+ as indicated in the timeline of each panel. 2 μ M isradipine eliminates Ca^{2+} signals induced by both hDAT substrates. Each trace shows the mean \pm SEM, $n \geq 81$. Figure adapted from Cameron, Solis, Ruchala, De Felice, and Eltit, submitted for publication.

In Figure 22 we saw that both DA and S-AMPH application can activate Cav1.3 and Cav1.2. To rule out a direct activation of Cav channels by DA or S-AMPH, intracellular Ca²⁺ was determined in the presence of a potent hDAT blocker, MDPV [1, 6]. This reuptake inhibitor, as described earlier, blocks current and uptake with extremely high potency. Figure 23 shows perfusion of 1 μM MDPV eliminates both DA and S-AMPH-induced Ca²⁺ transients in Flp_{hDAT} cells expressing either Cav1.2 or Cav1.3. A control showing that MDPV does not directly interact with CaVs, hDAT-independent depolarization was induced by high K⁺ produced Ca²⁺ signals refractory to MDPV treatment.

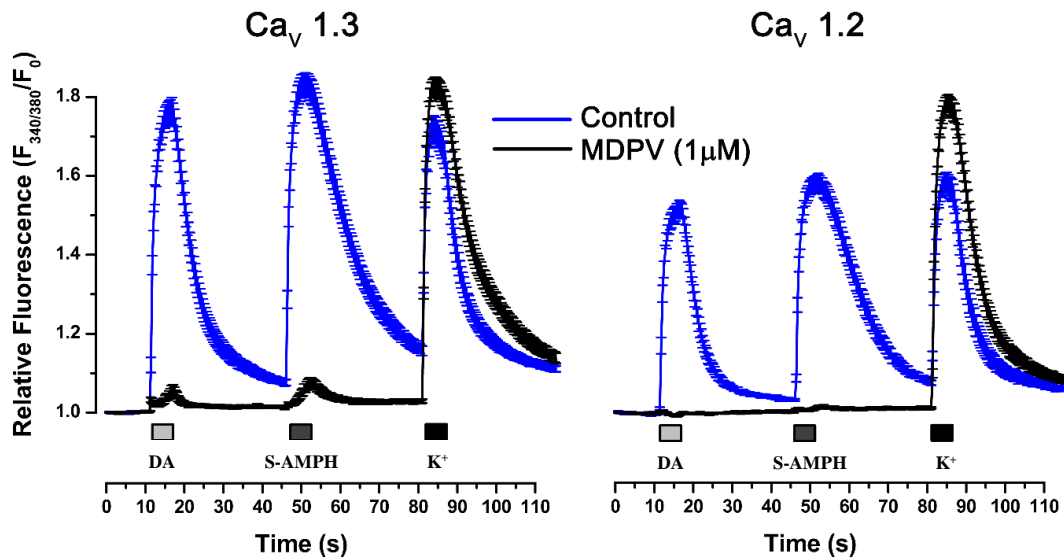


Figure 23: hDAT blockade prevents L-type Ca^{2+} channel activation in Flp_{hDAT} cells
 Intracellular Ca^{2+} concentration was determined by fluorescence microscopy in Flp-hDAT cells co-transfected with Cav1.3 or Cav1.2 plus β_3 , $\alpha_2\delta$ and EGFP plasmids, using the Ca^{2+} sensitive dye Fura-2AM. The experiments were carried out under constant perfusion at 35°C . The transfected cells were identified by their EGFP signal and then were briefly exposed to $10\mu\text{M}$ DA, $5\mu\text{M}$ S-AMPH or 130 mM K^+ as indicated in each panel. hDAT blocker MDPV ($1\mu\text{M}$) prevented Ca^{2+} signals induced by substrate-induced hDAT currents. Each trace shows the mean \pm SEM, $n \geq 60$. Figure adapted from Cameron, Solis, Ruchala, De Felice, and Eltit, submitted for publication.

The depolarization induced by DA- or S-AMPH- hDAT interactions activates both L-type Ca_v s: $\text{Ca}_v1.2$ and $\text{Ca}_v1.3$. Dose –response effects measuring Ca^{2+} signals and hDAT current elicited by DA and S-AMPH in Flp_{hDAT} are shown in Figure 24. S-AMPH appears more potent in activating the two L-type Ca^{2+} channels (top panel) with EC_{50} of 144 ± 11 nM and 102 ± 16 nM for $\text{Ca}_v1.2$ and $\text{Ca}_v1.3$ respectively, while the less potent DA has EC_{50} values of 916 ± 54 nM and 693 ± 25 nM, respectively.

To better understand the electrical coupling between hDAT and the L-type Ca^{2+} channels, dose-response curves for DA- and S-AMPH-induced hDAT currents were generated (Figure 24, bottom left). Although the EC_{50} values were 5-fold different, 1.44 ± 0.24 μM and 0.28 ± 0.04 μM for DA and S-AMPH respectively, the efficacy were not different under the experimental conditions used.

Lastly to see the coupling of hDAT currents and Ca_v s activation, we plotted Ca^{2+} signals fits vs. hDAT current fits (Figure 24, bottom right). These curves show that S-AMPH, compared to DA, generates a relatively larger Ca^{2+} transient in response to smaller hDAT inward currents. With both DA and S-AMPH, $\text{Ca}_v1.3$ activated more than $\text{Ca}_v1.2$, confirming that it requires less hDAT-induced depolarization to open. From this plot we see that small amplitude S-AMPH-induced hDAT currents were coupled tighter than DA to both Ca_v s activation.

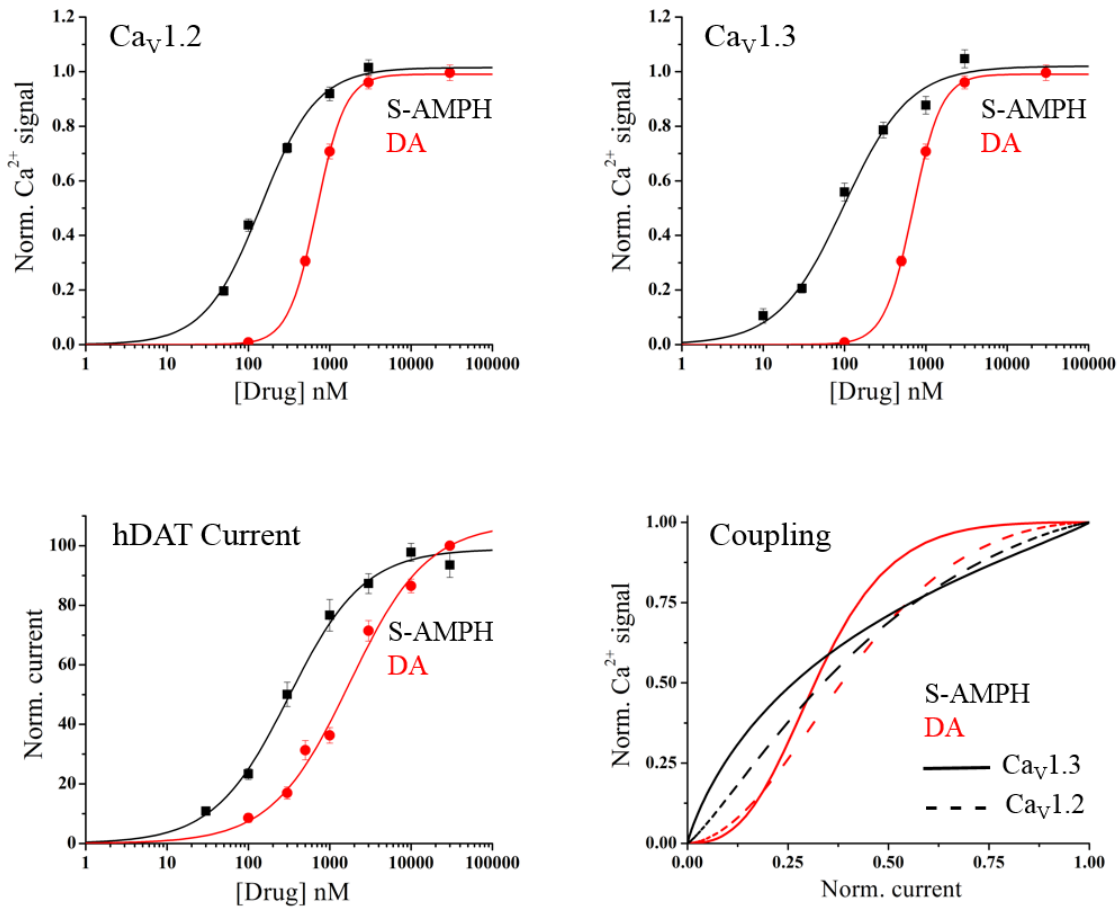


Figure 24: S-AMPH is more potent in producing Ca^{2+} signals, hDAT currents, and hDAT- Ca_v coupling Intracellular Ca^{2+} concentration was determined by fluorescence microscopy in Flp-hDAT cells co-transfected with $Ca_v1.3$ or $Ca_v1.2$ plus β_3 , $\alpha_2\delta$ and EGFP plasmids, using the Ca^{2+} sensitive dye Fura-2AM. (top) Dose-response curves were generated for DA and S-AMPH activation of $Ca_v1.2$ or $Ca_v1.3$ through hDAT-induced depolarization. EC_{50} values in $Ca_v1.2$: 916 ± 54 nM and 144 ± 11 nM for DA and S-AMPH respectively. EC_{50} values in $Ca_v1.3$: 693 ± 25 nM and 102 ± 16 nM for DA and S-AMPH respectively. (bottom left) hDAT currents were measured using whole-cell voltage clamp, $V = -60$ mV, $T = 35^\circ C$. $EC_{50} = 1.44 \pm 0.24$ μM and 0.28 ± 0.04 μM for DA and S-AMPH respectively. (bottom right) The Ca^{2+} signal fits of both $Ca_v1.2$ and $Ca_v1.3$ are plotted against the normalized current fit to represent hDAT- Ca_v coupling. Figure adapted from Cameron, Solis, Ruchala, De Felice, and Eltit, submitted for publication.

3.5. hDAT current effect in neurons

3.5.1. LUHMES selection

To investigate the importance of hDAT currents on cellular excitability we chose a human mesencephalic neuronal cell line, LUHMES. The line is subcloned of a source material derived from eight-week-old human ventral mesencephalic tissue [122]. The committed neural precursor cells were transformed with *myc* oncogenes for continuous proliferation [123]. Addition of low tetracycline concentration abolishes the *v-myc* expression. DA phenotype is confirmed in many studies [114, 122, 124]. In addition, the use of dbcAMP during differentiation, leads to TH production; therefore, LUHMES synthesize and release DA [123]. To determine the optimal conditions for our study with the highest expression of both dopaminergic and neuronal marker we explored different time courses of differentiation. As seen in Figure 25, the cells undergo dramatic morphological changes upon differentiation induction. Using inverted microscopy with 10x magnification we see undifferentiated cells at day 0 (left panel) have relatively large somas and cell neurites are absent. Using 20x magnification, 5 days post differentiation the cells appear to have short neurite network and the somas appear smaller and more round. At 10 days post differentiation (20x magnification) the cells have long, dense network of projections and a small, round cell body.

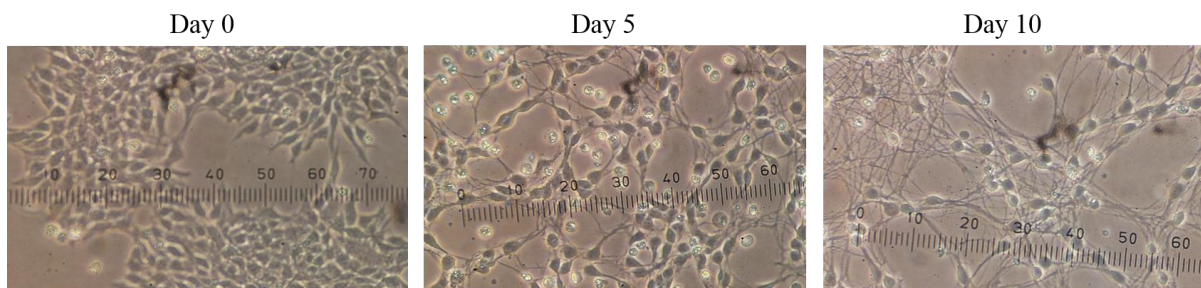


Figure 25: Conversion of LUHMES from proliferating to post-mitotic neurons LUHMES were differentiated for 10 days in presence of tetracycline, GDNF, and dbcAMP. Images of undifferentiated (Day 0) and differentiated (Day 5 and 10) cells are shown. Cells undergo morphological changes and appear as mature neurons at Day 10 with dense network of projections and smaller and rounded cell bodies. Cells were examined using inverted microscope using 20x magnification for day 0 and 40x magnification for days 5 and 10.

3.5.2. Differentiation changes

Immunostaining in conjunction with confocal microscopy showed modest expression of hDAT at 7 and 10 days of differentiation respectively. Figure 26, left panel, shows membrane localized hDAT (red stain) at cell body and processes 10 days post differentiation. Staining for all voltage-gated Na⁺ channels (Navs, green stain- Pan antibody with epitope present in all Navs in vertebrates) appears at cell body and processes and partial co-localization with hDAT is observed (not shown). DAPI nuclear staining appears in blue.

In attempt to boost hDAT's expression level, the use of retroviral transduction of hDAT in the parental LUHMES cell line was employed. To evaluate the expression level of hDAT in parental and transduced LUHMES (LUHMES_{hDAT}), we used Western immunoblotting of undifferentiated and Day 7 of differentiation cells (Figure 26, right). Day 0 parental LUHMES have no detectable levels of hDAT, while the transduced LUHMES_{hDAT} show hDAT expression. After 7 days of differentiation, parental LUHMES show a significant level of hDAT expression (larger than transduced at Day 0), whereas LUHMES_{hDAT} shows complete lack of hDAT. The control GAPDH shows equal amount of protein is loaded for the comparison. Optimum hDAT condition appears to be 7 days of differentiation of parental LUHMES.

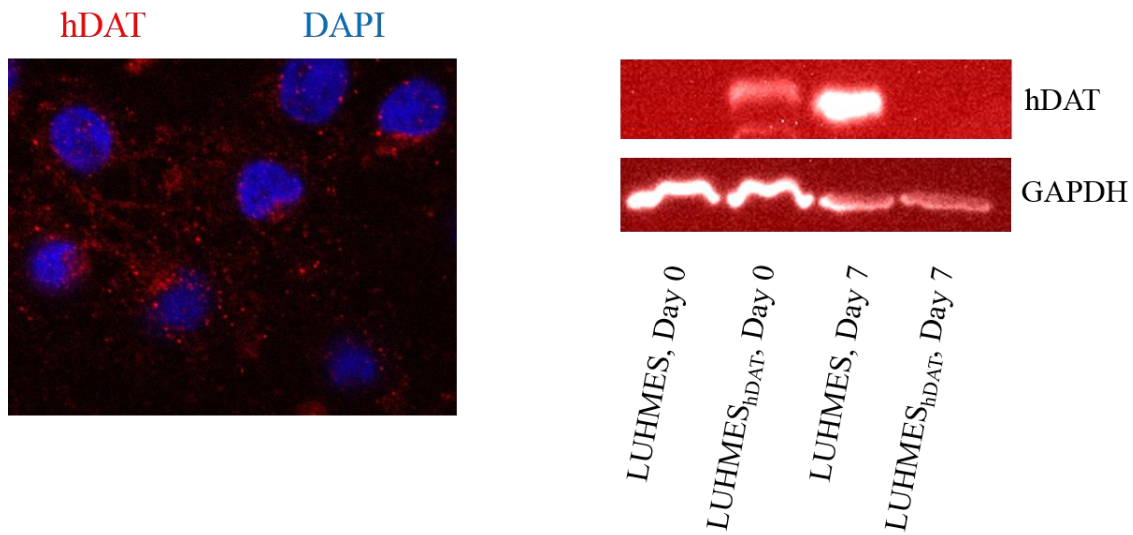


Figure 26: hDAT expression in Lund derived human mesencephalic cells (LUHMES) (left) Confocal image shows hDAT (red stain) expression in LUHMES cells at 10 days of differentiation. DAPI nuclear staining appears in blue. (right) LUHMES and hDAT transduced LUHMES (LUHMES_{hDAT}) were cultured and lysed before or 7 days post differentiation to assay the expression of hDAT using Western immunoblotting. Antibodies against human hDAT and GAPDH were used as listed in “Methods”.

In order to better characterize the differentiation, in Figure 27 we analyzed the parental LUHMES (top) and LUHMES_{hDAT} (bottom) for seven genes of importance for neural and dopaminergic phenotype using qPCR (quantitative polymerase chain reaction). To find the peak for dopaminergic markers we chose to monitor mRNA levels for DAT, tyrosine hydroxylase (TH), and dopamine receptor 2 (D₂R). In addition, we were interested in finding the peak electrical activity time point since we investigate activation of voltage-gated channels related to AP generation; therefore, we chose to monitor endogenous dopaminergic channels: Cav1.3, Cav1.2, Nav1.2, and G-protein-regulated inward-rectifier potassium channel 2 (GIRK2). Results were normalized to the expression of GAPDH mRNA (control gene encoding glyceraldehyde phosphate dehydrogenase) and are presented as fold difference relative to expression in undifferentiated parental LUHMES (day 0).

Parental LUHMES displays an increase in mRNA levels of all genes in day 5 as compared to day 0 with TH and Cav1.3 being absent at day 0 but in detectable amounts at day 5. The mRNA levels of hDAT, both Cav_s, and Nav continued to increase, revealed in day 10. For D₂R, GIRK2, and TH, the mRNA levels were lower at day 10 compared to day 5.

LUHMES_{hDAT} appears in some ways similar to parental LUHMES: mRNA for TH and Cav1.3 were undetectable at day 0 but present at day 5. All other genes of interested, except for hDAT, were detectable at day 0 in equal amounts to the parental line. All genes of interest showed increasing mRNA levels at day 5. hDAT appeared strongly upregulated at day 0 of transduced LUHMES, 755-fold increase compared to parental line, and as expected it increased at day 5. The levels of hDAT mRNA in LUHMES_{hDAT} at day 5 were much higher than parental line (1538-fold vs. 28-fold); however, this was the peak level observed in LUHMES_{hDAT} and the peak in parental line at 10 days was higher (1960-fold vs. 1538-fold). At day 10, the transduced line only showed

increase in mRNA levels of Cav1.2 and Nav1.2. All other genes appeared to have decreasing amount of mRNA, especially out target hDAT and TH was not detectable. As a result of the findings we picked LUHMES differentiation of 7-9 days for further studies.

qPCR LUHMES

Ca_v1.3 <i>CACNA1D</i>	Ca_v1.2 <i>CACNA1C</i>	hDAT <i>SLC6A3</i>	D₂R <i>DRD2</i>	GIRK2 <i>KCNJ6</i>	Na_v1.2 <i>SCN2A</i>	TH <i>TH</i>	Days of differentiation
0	1	1	1	1	1	0	day 0
1	83	28	1734	1348	687	1	day 5
6	234	1960	963	1008	5315	0.1	day 10

qPCR LUHMES_{hDAT}

Ca_v1.3 <i>CACNA1D</i>	Ca_v1.2 <i>CACNA1C</i>	hDAT <i>SLC6A3</i>	D₂R <i>DRD2</i>	GIRK2 <i>KCNJ6</i>	Na_v1.2 <i>SCN2A</i>	TH <i>TH</i>	Days of differentiation
0	1	755	1	1	1	0	day 0
10	96	1538	1141	1631	631	0.3	day 5
5	253	154	552	583	4094	0	day 10

Figure 27: Quantitative PCR analysis of dopaminergic and neuronal mRNA in LUHMES and LUHMES_{hDAT} Data from day 0, 5, and 10 of differentiation. Results are normalized to the expression of GAPDH mRNA (control gene encoding glyceraldehyde phosphate dehydrogenase) and are presented as fold difference relative to expression in undifferentiated LUHMES (day 0). (top) Both neuronal and dopaminergic markers increase with days of differentiation. Cav1.3 and TH are not detected before differentiation therefore data is normalized to Day 5. (bottom) LUHMES_{hDAT} values show initial high mRNA levels of hDAT at day 0 which decline at day 10. Cav1.3 and TH are not detected before differentiation.

3.5.3. STP effect on LUHMES excitability

LUHMES cells were differentiated for 9 days. Intracellular Ca^{2+} concentration was determined by fluorescence microscopy using the Ca^{2+} sensitive dye Fura-2AM. The experiments were carried out under constant perfusion at 35 °C. A 5 min perfusion protocol was designed to monitor the change in excitability (transient Ca^{2+} increase in the cell soma due to Cav opening, no increase from cellular stores).

While exploring for best imaging conditions, we discovered that the UV light used for signal acquisition affects profoundly the cells. As a result, all measurements were acquired under 11% light intensity and 200x gain. Two recordings per set of cells were done. First, pictures were taken under physiological imaging solution (IS-control set). The same set of cells is then exposed to the test condition. During the course of investigation, we observed vastly different results in cellular activity between different wells seeded with same number of cells. While some cells had very little activity in both imaging solution and test condition, others appear to be dramatically stimulated with the test condition. Upon further control testing (consecutive IS applications) we determined that certain cells increase their activity yet again due to UV light used for signal acquisition.

To eliminate the variability induced by the prolonged light exposure (2x 5 min), we used only one 5 min Ca^{2+} measurement per set of cells. In Figure 28, three test conditions were used: buffer solution showing background activity, 2 μM S-METH, and 2 μM S-METH in Ca^{2+} free buffer. Due to difficulty of identifying and selecting active projections from single cell (very dense and complex network) data were only collected from the cell somas. All cells within the imaging frame were selected and data were exported and manually reviewed for Ca^{2+} increases indicative of cell excitability. To compare between control (IS) and test conditions (2 μM S-METH and 2

μM S-METH in Ca^{2+} free buffer), % excitable cells was calculated for each frame which equates # cells with Ca^{2+} signal increase above 0.5 / total # of cells in that frame * 100. As many as 11 frames were acquired and used for the calculation of the final mean. The results are expressed as mean \pm SEM. In comparing control buffer (IS) condition to S-METH we saw an increase in cell excitability; however, the difference was not statistically different. Due to the high variability between cells, additional recordings could be beneficial in decreasing the error and possibly turning the increasing trend to being statistically different.

The second test condition tested was S-METH application in Ca^{2+} free buffer. This experimental condition was used to determine if the Ca^{2+} increase comes from outside source through the activation of Cav_s similar to our finding in Figures 22 and 23, or from internal store release. The % excitable cells decreased significantly ($p < 0.05$) in Ca^{2+} free conditions.

In the course of the study using LUHMES it was established that this cell line shows low spontaneous activity and due to the requirement for highly confluent cells, voltage clamp and current-clamp experiments were not within our reach. This cell line would be best for performing biochemical analyses which require a large number of cells.

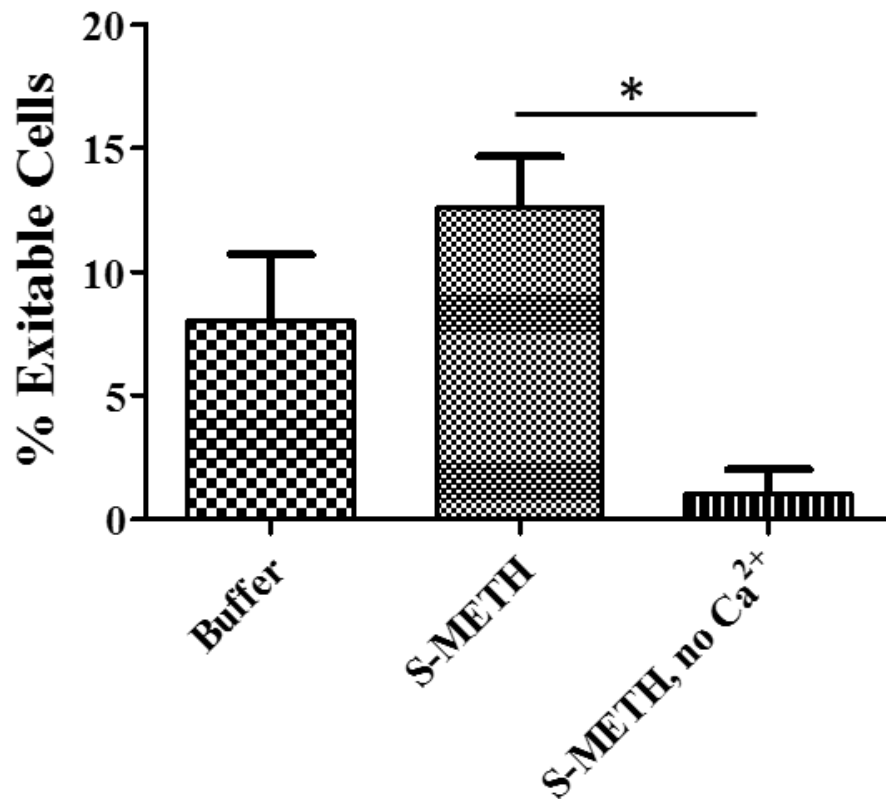


Figure 28: Excitability of LUHMES LUHMES cells were differentiated for 9 days. Intracellular Ca²⁺ concentration was determined by fluorescence microscopy using the Ca²⁺ sensitive dye Fura-2AM. The experiments were carried out under constant perfusion at 35°C. The cells were exposed to 2 μM S-METH or 2 μM S-METH in Ca²⁺ free buffer. The % of excitable cells was calculated as # cells with increased intracellular Ca²⁺ above 0.5 / total # cells *100. Each bar represent mean ± SEM, n ≥ 200.

Chapter 4 DISCUSSION

In this work, we present novel results for the action of S-enantiomers of STPs on hDAT, in particular, the effect of STPs on transporter currents that modulate voltage-gated channels involved in dopaminergic excitability. DAT currents are much larger than the predictions of fixed stoichiometry transport: 1DA, 2 Na⁺, and 1 Cl⁻ which would produce only 0.16 pA current if 1 million transporters would be active simultaneously. Relatively large DAT currents are measured not only in over-expression systems but also in dopaminergic neurons [1, 2, 6, 25, 47, 125]. The role of DAT currents is not clear at this time; however, because the current is relatively small in amplitude and it can persist after stimulation is removed, we hypothesize that it would have an influence on neuronal excitability.

Our results suggest when an STP is transported into the cell through hDAT, it accumulates inside the cell and interacts with an internal site on hDAT, since a persistent current is observed after STP removal. This interaction interferes with transporter's swift closure upon STP removal resulting in a long-lasting depolarization after external STP exhaustion (longer than would persist with DA). The presence of a persistent depolarization in a neuron may have an effect on neuronal excitability, a probability of neurotransmitter release, and could potentially be toxic. Furthermore, we showed that once S-AMPH or S-METH accumulates inside the cell, hDAT has an altered response towards its endogenous substrate, DA (DA stimulation now produces I_{PC}), and in the

Xenopus oocyte expression system, S-METH induces a dysfunctional state of the transporter that does not respond to subsequent substrate exposure (i.e., does not elicit additional currents). This dysfunctional state was reversed by COC, a DAT reuptake inhibitor. A subsequent DA pulse elicits I_{PC} after wash out since S-METH has built up in concentration inside of the oocyte. This experiment in addition to the internal S-AMPH injections illustrates the long term effects that I_{PC} exerts on DAT function.

We found that in oocytes the persistent current is pronounced, with a clear shift in baseline in addition to slowing the off-kinetics. When we performed equivalent experiment in mammalian HEK 293 cells we saw a prominent difference in DA and S-AMPH off-kinetics; however, the current does not establish a new baseline which is the case in oocytes. Although there are dissimilar effects in the STP-induced DAT currents in the two expression systems, the ratio of STP/DA time off is ~ 4 . I.e., although HEK cells have faster kinetics than oocytes, this is true for DA as well as for the STPs resulting in the same ratio. In both expression systems, the ratio of STP/DA time off is ~ 4 . Similar results are reported in SERT expressed in both oocytes and HEK 293 cells upon exposure to pCA and 5-HT [119]. The off ratio of pCA/ 5-HT was determined to be $\sim 4-5$ [5, 119].

In addition to a no baseline shift in HEK 293 cells, we saw no effect of STPs on DAT activity, in contrast to the effect observed in oocytes (data not shown). No matter the concentration of the STP delivered (inside the cell through the patch pipette, or outside through perfusion) the I_{PC} remained unaltered or produced relatively minor shifts in the off-kinetics. A possible explanation for the variable observations between oocyte and HEK 293 cell recordings could be the difference in techniques employed. In TEVC used for the oocyte recordings, the inside of the cell is not dialyzed which is the case in whole-cell patch-clamp employed with HEK cell measurements. If there is a requirement for an important soluble component to observe I_{PC} ,

perforated patch clamp techniques should eliminate the inconsistencies. Additionally, differences in lipid composition, temperature of solutions (room T vs. 35 °C), and secondary protein interactions could account for the discrepancies.

A further suggestion that secondary factors exist that affect hDAT function in the two expression systems is the finding that S- and R-AMPH, that appear equipotent in oocytes have a 2-fold potency difference in mammalian cells [2, 121]. Even more striking is the difference in potency of the enantiomers to elicit hDAT currents under whole-cell patch clamp at physiological temperature, with the only difference in the results coming from stable vs. transient transfection of hDAT (data from Figure 21 and reference# [50]). Here we show 2-fold difference in EC₅₀ values of S-AMPH and R-AMPH, while Sitte et. al. report ~7-fold difference [50].

How do we explain the persistent current? Since we observe I_{PC} after washout of the STP, an internal site of STP action at the transporter is hypothesized. I_{PC} is STP concentration- and time-dependent supporting the hypothesis that STPs act at an internal site on DAT. Direct injection of a STP inside the cell does not elicit any current; however, when an external stimulus is applied to activate hDAT currents, I_{PC} is observed. This finding suggests that the internal interaction must be in a place that is not accessible in the closed state of hDAT; rather a specific conformation (conducting state) is required for the STP to access a site and establish interactions that then interferes with the swift closure of the transporter. One possible site for this interaction would be near the internal transporter gate. A potential interaction at this location with residues forming the gate or residues interacting with the gate would affect the proper closure of the transporter. Further studies including molecular simulations and mutagenesis are warranted to answer this question.

Knowing the electrophysiological signature of the enantiomers of AMPH, we proceeded to investigate the mechanism of action of components of *bath salts*. *Bath salts* consist of

heterogeneous mixtures of various psychoactive substances, primarily synthetic cathinones. Drug sample analyses reveal that *bath salts* can contain a complex mixture of compounds such as cathinones (MEPH, MDPV, methylone, butylone, flephedrone, etc.), other abused substances (AMPH, MDMA, COC), and caffeine [75, 89]. Due to the wide range of compounds and compound combinations found in *bath salts* it is important to identify their mechanisms of action alone and in combination. Since MEPH and MDPV appear to be most prevalent on the market, we explored those two compounds in greatest detail, individually and together in varying proportions [1].

Our findings show that similar to AMPH and METH, MEPH is an hDAT substrate because it produces an inward current at physiological membrane potentials under voltage clamp. Its maximal current amplitude or efficacy is approximately 50% of I_{DA} ; however, MEPH induces a large persistent current that is approximately twice in absolute value size of S-AMPH and S-METH-induced I_{PC} under the same conditions, which would enhance its DA releasing capacity in neurons [1, 6]. MEPH-induced I_{PC} is 2nd largest after S-MCAT which may change if only the more potent enantiomer is used. Other studies in synaptosomes report that MEPH inhibits dopamine uptake in agreement with our findings that it has dopaminergic effects similar to the STPs [126]. This agrees with numerous other studies, presenting that both *in vitro* and *in vivo* MEPH appears as a mixed, nonselective releaser of not only DA but also of 5-HT [3, 78]; hence, it resembles the action of MDMA. Although MEPH is self-administered, *in vivo* studies on motor stimulation show a modest increase, much lower compared to METH, pointing again toward dual dopaminergic and serotonergic action [82].

3,4-methylenedioxypyrovalerone (MDPV) is a common *bath salts* component that we discovered is not a substrate for hDAT [1, 6, 78, 127]. MDPV behaves similar to a cocaine-like

dopamine reuptake inhibitor. Like COC, MDPV produces an outward current at hDAT and can inhibit both I_{STP} and I_{PC} when applied in succession to STP. Simmler et al. showed that MDPV has a very high affinity for DAT [78]. MDPV is 20-30-fold more potent than COC in DAT transport inhibition [1, 78]. In our electrophysiological assays, MDPV produced more outward hDAT current than COC in oocytes voltage-clamped to -60 mV. This is a strong indication that COC inhibits only partially hDAT's endogenous leak current while MDPV inhibits more, or potentially all, leak current. Under voltage clamp, MDPV produced a long-lasting outward current deflection, while COC blockade of the endogenous DAT current was short-lived under the same conditions. An *in vivo* rat ICSS study showed similarly a long-lasting effect of MDPV (Figure 29) [1, 3]. Bonano et. al show that MDPV produced ICSS facilitation that was significant after 300 min (upward triangle, Figure 29), with facilitation still present 24 h after drug administration [3]. The recovery of hDAT current following MDPV inhibition was investigated first in oocytes and compared to DAT current recovery following COC block. There was 100% recovery of DA-induced hDAT current 1 min after COC blockade, whereas 1 min after MDPV block there was 11% recovery I_{DA} and 30 min later there was only 45% recovery which we hypothesize may be partially due to hDAT up-regulation induced by reuptake inhibitors.

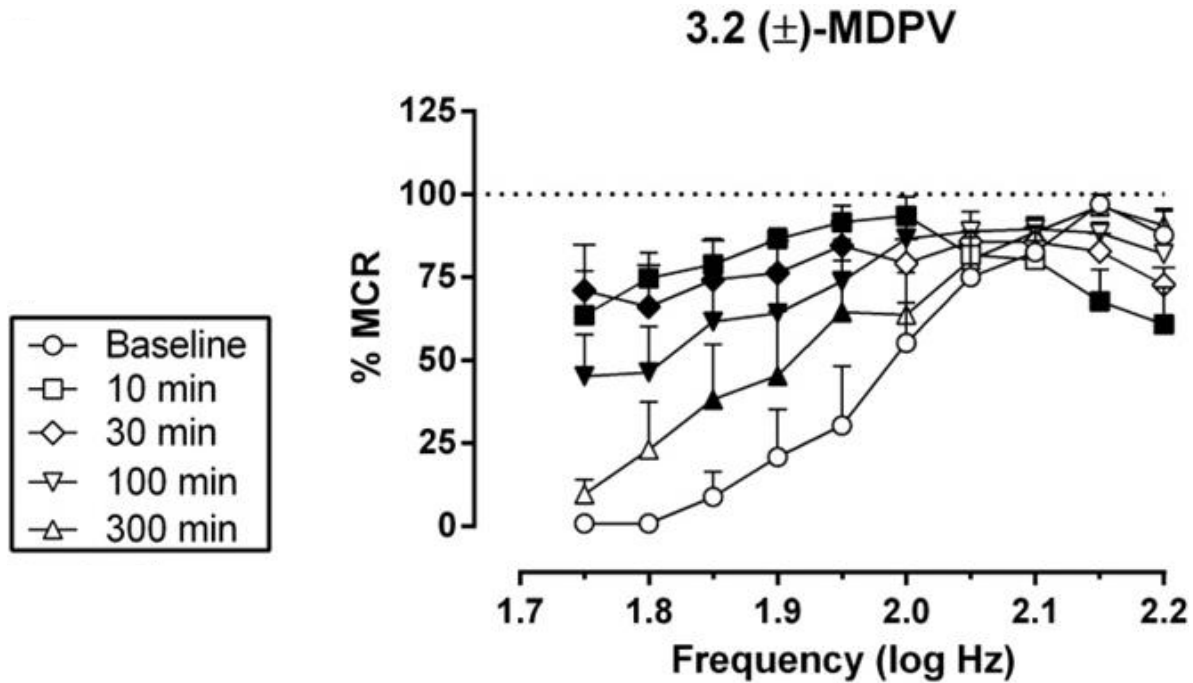


Figure 29: Time courses (±)-MDPV effects on full ICSS frequency– rate curves. Drug effect of 3.2 mg/kg (±)-MDPV. Abscissae: frequency of electrical brain stimulation in log Hz. Ordinates: percent maximum control reinforcement rate (%MCR). Filled points represent frequencies at which reinforcement rates were statistically different from vehicle rates as determined by two-way ANOVA followed by Holm– Sidak post hoc test, $p < 0.05$. All data show mean \pm SEM for six rats. Figure adapted from [3].

To test if MDPV has also a long-lasting inhibitory effect on hDAT uptake, its action was tested in HEK 293 cells under no voltage clamp. In this case we tested not the ability of hDAT to elicit DA currents, but rather the transport process itself. We took advantage of an hDAT fluorescent substrate (APP⁺ [111]) and showed that after MDPV block, it took 5 min for the transporters to completely recover their rate of transport as compared to immediate recovery after COC block. We may speculate that either MDPV is still present and available after external removal (e.g. due to high lipophilicity [78]), or MDPV induces a long-lived conformational state in hDAT.

An interesting finding about I_{PC} was revealed while testing the COC and MDPV block of hDAT currents. When COC and MDPV were applied to baseline current levels (before DA or STP exposure), both compounds elicited long lasting inhibitory effects (reflected in a stable outward current deflection for minutes). However, when COC and MDPV were applied during a persistent current state of the transporter, the outward current (above baseline level) was long-lasting only in the case of MDPV whereas COC's block reversed to I_{PC} as soon as the compound was washed out. These findings suggest that the I_{PC} is a distinct conduction state of the transporter rather than an exaggerated I_L.

It is known that both MEPH and MDPV enhance DA neurotransmission [3]. Whereas *bath salts* are not well defined as a mixture, samples include MEPH, MDPV, methylone and other compounds [83]. So far, most studies report exposure to single cathinone analogue; therefore we explored how two synthetic cathinones act together when applied simultaneously to hDAT. We observed a two-component response separated by a few seconds: first, an inward current induced by the substrate MEPH ensued followed by the outward current induced by MDPV [1]. The magnitude and duration of the inward current depended on the concentration balance of the two

compounds. These results suggest DA release could precede DA uptake blockade in a mixture of *bath salts* containing MEPH and MDPV. Furthermore, the blockade of hDAT by MDPV is longer lasting than the blockade by COC, hence, a long-lasting neurochemical, physiological, and behavioral effects would be observed [3]. Although *in vitro* experiments are far removed from the *in vivo* conditions of drug abuse, this synergistic combination may be especially dangerous to the user for whom the combined action of releasing drugs and blocking drugs is greater than the sum of their individual effects.

Studies in dopaminergic neurons report increased excitability (firing rate) caused by substrate-induced DAT currents [24, 25, 59, 125]. The reports show that DAT-dependent increases in neuronal excitability display results during drug application (i.e., I_{STP} and I_{DA}). Moreover, some reports highlight that only low concentrations of STPs enhance neuron firing and neurotransmission, whereas high concentrations of substrate inhibit firing as a result of D_2 autoreceptor activation [125]. In our studies we explored possible cross-talk of hDAT and specific L- ($Cav1.2$ and $Cav1.3$) and N-type ($Cav2.2$) $Cavs$ co-expressed in mammalian Flp-In T-rex 293 cells. These voltage-gated Ca^{2+} channels are, reportedly, involved in dopaminergic neuron excitability (L-type) and vesicular fusion (N-type). Our results demonstrate that DA- and S-AMPH-induced hDAT currents are sufficient to depolarize the cells enough to activate both L-type Ca^{2+} channels ($Cav1.2$ and $Cav1.3$) but not N-type ($Cav2.2$). This is not a surprising finding as a broad range of voltage sensitivity is observed among Ca^{2+} channels. $Cav1.2$ and $Cav2.2$ have a ~ 20 mV and ~ 30 mV right shifted voltage dependence compared to $Cav1.3$ respectively. These results indicate that the hDAT-mediated depolarization is in the range of the activation threshold of some $Cavs$: L-type ($Cav1.2$ and $Cav1.3$) but not N-type ($Cav2.2$) $Cavs$ are within the activation range of hDAT-mediated depolarization under our experimental conditions. The results also

suggest that S-AMPH- and DA-induced currents through hDAT are qualitatively different, with S-AMPH producing greater L-type channel activation. One explanation for the difference could be the different ionic composition of I_{DA} and I_{STP} as reported by Rodriguez-Menchaca et. al. (different reversal potentials with DA and S-AMPH I(V)s crossing at -80 mV) [2]. Another possible explanation for the S-AMPH superiority in activating Ca_v s at low transporter steady-state current levels is the existence of transient peak current that can be resolved under piezoelectric rapid solution exchange [47]. This transient peak current which is several folds larger than the I_{STP} decays rapidly to form the steady state peak current which we name I_{STP} . Although I_{STP} it is also present with DA, it is reported to be significantly larger in AMPH [47].

To understand better the coupling of I_{DA} or I_{STP} to Ca^{2+} channel activation, we looked at the Ca^{2+} signal to hDAT current relationships of DA and S-AMPH at $Ca_v1.2$ and $Ca_v1.3$. The results were consistent with the voltage-dependence of the channels: $Ca_v1.3$ which displays the lowest voltage dependence had greater coupling strength for S-AMPH and DA as compared to $Ca_v1.2$. The initial high coupling strength values at low I_{DA} and I_{STP} may activate a small percentage of the lowest threshold $Ca_v1.3$ whose Ca^{2+} conductance may favor further depolarization which would recruit more $Ca_v1.3$ thus potentiating the coupling-strength. At higher I_{DA} and I_{STP} , increase in internal Ca^{2+} may induce channel saturation and inactivation, thus decreasing the coupling-strength. Furthermore, in dopaminergic neurons the increase in intracellular Ca^{2+} causes Ca^{2+} activated K channels to open and re-polarize the cells.

In this study we show that hDAT is electrically coupled to L type Ca_v s important in cell excitability. We have also presented that in addition to the peak current, STPs generate a persistent current (I_{PC}) through hDAT. We hypothesize that I_{PC} would prolong depolarization induced by STP after washout and although in the synapse the voltage is not clamped but rather dynamic, the

effect of the internal STP could be elicited after either tonic or phasic DA release upon uptake. Moreover, cell depolarization is shown to impair DA uptake [10, 11, 128], therefore, I_{PC} may contribute through several different mechanisms to extracellular DA augmentation associated with drug addiction. Interestingly and in addition to the increased excitability due to hDAT conductance, at high STP concentrations several reports show that instead of enhancement of dopamine neurotransmission and dopamine neuron firing, the opposite is observed [24, 125]. Autoinhibitory D_2 receptors are activated by the released DA and neuronal firing is decreased [125]. The caveat again is that under hyperpolarized conditions, DAT exhibit a more efficient uptake, so more STP or DA would enter the cell and as $I(V)$ s show, at hyperpolarizing potentials I_{DA} and I_{STP} are larger [2, 10, 11, 128]. Hence, we designed experiments to test our hypothesis on increased neuronal excitability due to hDAT currents: I_{STP} and I_{PC} . For this purpose we selected a neuronal cell line from human mesencephalon, LUHMES, which has been immortalized for continuous proliferation and continuous formation of committed dopaminergic neuronal precursor cells. Upon completion of biochemical analyses to determine the best conditions for expression of both dopaminergic and neuronal markers, we identified a few potential problems that affected our future work. The cells have a low hDAT expression. After 7 days of differentiation we did not detect hDAT-specific uptake using the fluorescent substrate APP^+ (data not shown). Furthermore, only approximately 10 % of cells appeared spontaneously active, and even transduction with hDAT aimed at increasing hDAT's levels was unsuccessful in producing larger effects, apparently due to early down-regulation or degradation of transporters during the differentiation process. In addition to these challenges, the cells undergo dramatic morphological changes during differentiation, grow long and dense network of projections while the soma becomes small and round making it technically difficult to voltage-clamp or current-clamp the cells. To overcome

those obstacles, we took a different approach to monitor the cellular excitability: we measured Ca^{2+} signals as we did with Flp_{hDAT} . The Ca^{2+} dye acts almost as a voltage sensor since we show that Ca_{vS} activation require certain amount of depolarization. In addition, we can confirm that increases in internal Ca^{2+} are due to voltage-gated channel activation rather than release from internal stores since we can easily manipulate extracellular Ca^{2+} as in our experiment. We faced further hurdles with the Fura-2 Ca^{2+} signals measurements due to UV light-stimulated LUHMES activity. Although we decreased the UV light to only 11% intensity, we could still see increase in Ca^{2+} signals with some cells during our 10 min experimental protocol (5 min buffer/control, 5 min test condition). Finally we acquired 5 min signal for single condition and increased the number of measurements to get a reliable mean value. The results from our study suggest that additional image acquisitions will be necessary. Nevertheless, an increasing trend in excitability occurred by this measure between control/buffer and S-METH application; however, due to the large statistical error we saw no significant difference in the values. On the other hand, there was a significant decrease in excitability when the external Ca^{2+} was removed, confirming the importance of Ca_{vS} in dopaminergic neuronal excitability [94, 101].

In summary, this investigation on the conduction states of the dopamine transporter reveals: 1) reuptake inhibitors could exert only partial block of hDAT's endogenous leak current as seen with COC and MDPV, 2) substrate type psychostimulants (STPs) induce a steady-state peak (I_{STP}) and a persistent current (I_{PC}) through hDAT, 3) DA and STP induced currents (I_{DA} and I_{STP}) may activate L-type voltage-gated Ca^{2+} channels, 4) L-type Ca_{vS} activation increases dopaminergic excitability and removal of external Ca^{2+} abolishes neuronal firing. Additional studies are required to investigate the possible effects of I_{PC} on neuronal excitability and DA release, i.e. compare the excitability induced by S- and R- enantiomers of STPs. As discussed earlier, depolarization by the

STPs would cause exocytotic DA release, and the uptake of DA would be interfered by not only STP competition for transport but also by depolarization-induced DAT uptake slowing down, and D₂ receptors hyperpolarization. That however, would cause DAT uptake to become more efficient and STPs would once again elicit larger currents. Understanding this complex mechanism of action of drugs at hDAT is of great importance since a number of synthetic cathinones have invaded the clandestine market and we have shown that some act through DAT and produce large persistent currents with physiological effects after their removal [1, 6].

REFERENCES

1. Cameron, K.N., et al., *Bath salts components mephedrone and methylenedioxypyrovalerone (MDPV) act synergistically at the human dopamine transporter*. Br J Pharmacol, 2013. **168**(7): p. 1750-7.
2. Rodriguez-Menchaca, A.A., et al., *S(+)-amphetamine induces a persistent leak in the human dopamine transporter: molecular stent hypothesis*. Br J Pharmacol, 2012. **165**(8): p. 2749-57.
3. Bonano, J.S., et al., *Abuse-related and abuse-limiting effects of methcathinone and the synthetic "bath salts" cathinone analogs methylenedioxypyrovalerone (MDPV), methylone and mephedrone on intracranial self-stimulation in rats*. Psychopharmacology (Berl), 2014. **231**(1): p. 199-207.
4. Pramod, A.B., et al., *SLC6 transporters: structure, function, regulation, disease association and therapeutics*. Mol Aspects Med, 2013. **34**(2-3): p. 197-219.
5. De Felice, L.J. and K.N. Cameron, *Comments on "A Quantitative Model of Amphetamine Action on the Serotonin Transporter, by Sandtner et al. (2013)*. Br J Pharmacol, 2014.
6. Cameron, K., et al., *Mephedrone and methylenedioxypyrovalerone (MDPV), major constituents of "bath salts," produce opposite effects at the human dopamine transporter*. Psychopharmacology (Berl), 2013. **227**(3): p. 493-9.
7. Torres, G.E., R.R. Gainetdinov, and M.G. Caron, *Plasma membrane monoamine transporters: structure, regulation and function*. Nat Rev Neurosci, 2003. **4**(1): p. 13-25.
8. Bozzi, Y. and E. Borrelli, *Dopamine in neurotoxicity and neuroprotection: what do D2 receptors have to do with it?* Trends Neurosci, 2006. **29**(3): p. 167-74.
9. Sulzer, D., *How addictive drugs disrupt presynaptic dopamine neurotransmission*. Neuron. **69**(4): p. 628-49.
10. Krueger, B.K., *Kinetics and block of dopamine uptake in synaptosomes from rat caudate nucleus*. J Neurochem, 1990. **55**(1): p. 260-7.
11. McElvain, J.S. and J.O. Schenk, *A multisubstrate mechanism of striatal dopamine uptake and its inhibition by cocaine*. Biochem Pharmacol, 1992. **43**(10): p. 2189-99.
12. Erickson, J.D., L.E. Eiden, and B.J. Hoffman, *Expression cloning of a reserpine-sensitive vesicular monoamine transporter*. Proc Natl Acad Sci U S A, 1992. **89**(22): p. 10993-7.
13. Hoffman, B.J., et al., *Localization and dynamic regulation of biogenic amine transporters in the mammalian central nervous system*. Front Neuroendocrinol, 1998. **19**(3): p. 187-231.
14. Di Chiara, G. and A. Imperato, *Drugs abused by humans preferentially increase synaptic dopamine concentrations in the mesolimbic system of freely moving rats*. Proc Natl Acad Sci U S A, 1988. **85**(14): p. 5274-8.
15. Mogenson, G.J., D.L. Jones, and C.Y. Yim, *From motivation to action: functional interface between the limbic system and the motor system*. Prog Neurobiol, 1980. **14**(2-3): p. 69-97.
16. Tammimaki, A. and P.T. Mannisto, *Effect of genetic modifications in the synaptic dopamine clearance systems on addiction-like behaviour in mice*. Basic Clin Pharmacol Toxicol. **108**(1): p. 2-8.
17. Ritz, M.C., et al., *Cocaine receptors on dopamine transporters are related to self-administration of cocaine*. Science, 1987. **237**(4819): p. 1219-23.
18. Jones, S.R., et al., *Mechanisms of amphetamine action revealed in mice lacking the dopamine transporter*. J Neurosci, 1998. **18**(6): p. 1979-86.

19. Donovan, D.M., et al., *Cocaine reward and MPTP toxicity: alteration by regional variant dopamine transporter overexpression*. Brain Res Mol Brain Res, 1999. **73**(1-2): p. 37-49.
20. Salahpour, A., et al., *Increased amphetamine-induced hyperactivity and reward in mice overexpressing the dopamine transporter*. Proc Natl Acad Sci U S A, 2008. **105**(11): p. 4405-10.
21. Jardetzky, O., *Simple allosteric model for membrane pumps*. Nature, 1966. **211**(5052): p. 969-70.
22. Povlock, S.L. and J.O. Schenk, *A multisubstrate kinetic mechanism of dopamine transport in the nucleus accumbens and its inhibition by cocaine*. J Neurochem, 1997. **69**(3): p. 1093-105.
23. Sonders, M.S., et al., *Multiple ionic conductances of the human dopamine transporter: the actions of dopamine and psychostimulants*. J Neurosci, 1997. **17**(3): p. 960-74.
24. Ingram, S.L., B.M. Prasad, and S.G. Amara, *Dopamine transporter-mediated conductances increase excitability of midbrain dopamine neurons*. Nat Neurosci, 2002. **5**(10): p. 971-8.
25. Carvelli, L., et al., *Dopamine transporters depolarize neurons by a channel mechanism*. Proc Natl Acad Sci U S A, 2004. **101**(45): p. 16046-51.
26. Kolanos, R., et al., *"Deconstruction" of the abused synthetic cathinone methylenedioxypyrovalerone (MDPV) and an examination of effects at the human dopamine transporter*. ACS Chem Neurosci, 2013. **4**(12): p. 1524-9.
27. Li, L.B., et al., *The role of N-glycosylation in function and surface trafficking of the human dopamine transporter*. J Biol Chem, 2004. **279**(20): p. 21012-20.
28. Schmitt, K.C. and M.E. Reith, *Regulation of the dopamine transporter: aspects relevant to psychostimulant drugs of abuse*. Ann N Y Acad Sci, 2010. **1187**: p. 316-40.
29. Ramamoorthy, S., T.S. Shippenberg, and L.D. Jayanthi, *Regulation of monoamine transporters: Role of transporter phosphorylation*. Pharmacol Ther, 2011. **129**(2): p. 220-38.
30. Khoshbouei, H., et al., *N-terminal phosphorylation of the dopamine transporter is required for amphetamine-induced efflux*. PLoS Biol, 2004. **2**(3): p. E78.
31. Granas, C., et al., *N-terminal truncation of the dopamine transporter abolishes phorbol ester- and substance P receptor-stimulated phosphorylation without impairing transporter internalization*. J Biol Chem, 2003. **278**(7): p. 4990-5000.
32. Fog, J.U., et al., *Calmodulin kinase II interacts with the dopamine transporter C terminus to regulate amphetamine-induced reverse transport*. Neuron, 2006. **51**(4): p. 417-29.
33. Steinkellner, T., et al., *Ca(2+)/calmodulin-dependent protein kinase IIalpha (alphaCaMKII) controls the activity of the dopamine transporter: implications for Angelman syndrome*. J Biol Chem, 2012. **287**(35): p. 29627-35.
34. Holton, K.L., M.K. Loder, and H.E. Melikian, *Nonclassical, distinct endocytic signals dictate constitutive and PKC-regulated neurotransmitter transporter internalization*. Nat Neurosci, 2005. **8**(7): p. 881-8.
35. Hamilton, P.J., et al., *PIP2 regulates psychostimulant behaviors through its interaction with a membrane protein*. Nat Chem Biol, 2014. **10**(7): p. 582-9.
36. Saunders, C., et al., *Amphetamine-induced loss of human dopamine transporter activity: an internalization-dependent and cocaine-sensitive mechanism*. Proc Natl Acad Sci U S A, 2000. **97**(12): p. 6850-5.

37. Johnson, L.A., et al., *Regulation of amphetamine-stimulated dopamine efflux by protein kinase C beta*. J Biol Chem, 2005. **280**(12): p. 10914-9.
38. Kahlig, K.M., J.A. Javitch, and A. Galli, *Amphetamine regulation of dopamine transport. Combined measurements of transporter currents and transporter imaging support the endocytosis of an active carrier*. J Biol Chem, 2004. **279**(10): p. 8966-75.
39. Staley, J.K., et al., *High affinity cocaine recognition sites on the dopamine transporter are elevated in fatal cocaine overdose victims*. J Pharmacol Exp Ther, 1994. **271**(3): p. 1678-85.
40. Mash, D.C., et al., *Dopamine transport function is elevated in cocaine users*. J Neurochem, 2002. **81**(2): p. 292-300.
41. Penmatsa, A., K.H. Wang, and E. Gouaux, *X-ray structure of dopamine transporter elucidates antidepressant mechanism*. Nature, 2013. **503**(7474): p. 85-90.
42. Leviel, V., *Dopamine release mediated by the dopamine transporter, facts and consequences*. J Neurochem, 2011. **118**(4): p. 475-89.
43. Howell, L.L. and H.L. Kimmel, *Monoamine transporters and psychostimulant addiction*. Biochem Pharmacol, 2008. **75**(1): p. 196-217.
44. Ramsson, E.S., et al., *High doses of amphetamine augment, rather than disrupt, exocytotic dopamine release in the dorsal and ventral striatum of the anesthetized rat*. J Neurochem. **119**(6): p. 1162-72.
45. Jackson, D.M., N.E. Anden, and A. Dahlstrom, *A functional effect of dopamine in the nucleus accumbens and in some other dopamine-rich parts of the rat brain*. Psychopharmacologia, 1975. **45**(2): p. 139-49.
46. Rothman, R.B. and M.H. Baumann, *Therapeutic potential of monoamine transporter substrates*. Curr Top Med Chem, 2006. **6**(17): p. 1845-59.
47. Erreger, K., et al., *Currents in response to rapid concentration jumps of amphetamine uncover novel aspects of human dopamine transporter function*. J Neurosci, 2008. **28**(4): p. 976-89.
48. Sitges, M., A. Reyes, and L.M. Chiu, *Dopamine transporter mediated release of dopamine: role of chloride*. J Neurosci Res, 1994. **39**(1): p. 11-22.
49. Parker, E.M. and L.X. Cubeddu, *Comparative effects of amphetamine, phenylethylamine and related drugs on dopamine efflux, dopamine uptake and mazindol binding*. J Pharmacol Exp Ther, 1988. **245**(1): p. 199-210.
50. Sitte, H.H., et al., *Carrier-mediated release, transport rates, and charge transfer induced by amphetamine, tyramine, and dopamine in mammalian cells transfected with the human dopamine transporter*. J Neurochem, 1998. **71**(3): p. 1289-97.
51. Glaser, P.E., et al., *Differential effects of amphetamine isomers on dopamine release in the rat striatum and nucleus accumbens core*. Psychopharmacology (Berl), 2005. **178**(2-3): p. 250-8.
52. Butcher, S.P., et al., *Amphetamine-induced dopamine release in the rat striatum: an in vivo microdialysis study*. J Neurochem, 1988. **50**(2): p. 346-55.
53. Carboni, E., et al., *Amphetamine, cocaine, phencyclidine and nomifensine increase extracellular dopamine concentrations preferentially in the nucleus accumbens of freely moving rats*. Neuroscience, 1989. **28**(3): p. 653-61.
54. Daberkow, D.P., et al., *Amphetamine paradoxically augments exocytotic dopamine release and phasic dopamine signals*. J Neurosci. **33**(2): p. 452-63.

55. Fischer, J.F. and A.K. Cho, *Chemical release of dopamine from striatal homogenates: evidence for an exchange diffusion model*. J Pharmacol Exp Ther, 1979. **208**(2): p. 203-9.
56. Sulzer, D., N.T. Maidment, and S. Rayport, *Amphetamine and other weak bases act to promote reverse transport of dopamine in ventral midbrain neurons*. J Neurochem, 1993. **60**(2): p. 527-35.
57. Sulzer, D., et al., *Amphetamine redistributes dopamine from synaptic vesicles to the cytosol and promotes reverse transport*. J Neurosci, 1995. **15**(5 Pt 2): p. 4102-8.
58. Kahlig, K.M., et al., *Amphetamine induces dopamine efflux through a dopamine transporter channel*. Proc Natl Acad Sci U S A, 2005. **102**(9): p. 3495-500.
59. Saha, K., et al., *Intracellular Methamphetamine Prevents the Dopamine-induced Enhancement of Neuronal Firing*. J Biol Chem, 2014. **289**(32): p. 22246-57.
60. Bauer, C.T., et al., *Use of intracranial self-stimulation to evaluate abuse-related and abuse-limiting effects of monoamine releasers in rats*. Br J Pharmacol, 2013. **168**(4): p. 850-62.
61. Negus, S.S., et al., *Selective suppression of cocaine- versus food-maintained responding by monoamine releasers in rhesus monkeys: benzylpiperazine, (+)phenmetrazine, and 4-benzylpiperidine*. J Pharmacol Exp Ther, 2009. **329**(1): p. 272-81.
62. Badiani, A., et al., *Opiate versus psychostimulant addiction: the differences do matter*. Nat Rev Neurosci, 2011. **12**(11): p. 685-700.
63. Svensson, T.H., *Functional and biochemical effects of d- and l-amphetamine on central catecholamine neurons*. Naunyn Schmiedebergs Arch Pharmacol, 1971. **271**(2): p. 170-80.
64. Sharp, T., et al., *A direct comparison of amphetamine-induced behaviours and regional brain dopamine release in the rat using intracerebral dialysis*. Brain Res, 1987. **401**(2): p. 322-30.
65. Mechner, F. and M. Latranyi, *Behavioral effects of caffeine, methamphetamine, and methylphenidate in the rat*. J Exp Anal Behav, 1963. **6**: p. 331-42.
66. Yamanaka, Y., T. Yamamoto, and T. Egashira, *Methamphetamine-induced behavioral effects and releases of brain catecholamines and brain concentrations of methamphetamine in mice*. Jpn J Pharmacol, 1983. **33**(1): p. 33-40.
67. Carpenter, A.C., T.P. Saborido, and G.D. Stanwood, *Development of hyperactivity and anxiety responses in dopamine transporter-deficient mice*. Dev Neurosci, 2012. **34**(2-3): p. 250-7.
68. Spielewoy, C., et al., *Hypolocomotor effects of acute and daily d-amphetamine in mice lacking the dopamine transporter*. Psychopharmacology (Berl), 2001. **159**(1): p. 2-9.
69. Rocha, B.A., et al., *Cocaine self-administration in dopamine-transporter knockout mice*. Nat Neurosci, 1998. **1**(2): p. 132-7.
70. Giros, B., et al., *Hyperlocomotion and indifference to cocaine and amphetamine in mice lacking the dopamine transporter*. Nature, 1996. **379**(6566): p. 606-12.
71. Snyder, S.H., et al., *Drugs, neurotransmitters, and schizophrenia*. Science, 1974. **184**(4143): p. 1243-53.
72. Najib, J., *The efficacy and safety profile of lisdexamfetamine dimesylate, a prodrug of d-amphetamine, for the treatment of attention-deficit/hyperactivity disorder in children and adults*. Clin Ther, 2009. **31**(1): p. 142-76.
73. Nishino, S., *Clinical and neurobiological aspects of narcolepsy*. Sleep Med, 2007. **8**(4): p. 373-99.

74. Bray, G.A., *Use and abuse of appetite-suppressant drugs in the treatment of obesity*. Ann Intern Med, 1993. **119**(7 Pt 2): p. 707-13.
75. Kelly, J.P., *Cathinone derivatives: a review of their chemistry, pharmacology and toxicology*. Drug Test Anal, 2011. **3**(7-8): p. 439-53.
76. Durham, M., *Ivory wave: the next mephedrone?* Emerg Med J, 2011. **28**(12): p. 1059-60.
77. Prosser, J.M. and L.S. Nelson, *The toxicology of bath salts: a review of synthetic cathinones*. J Med Toxicol, 2012. **8**(1): p. 33-42.
78. Simmler, L.D., et al., *Monoamine transporter and receptor interaction profiles of a new series of designer cathinones*. Neuropharmacology, 2014. **79**: p. 152-60.
79. Glennon, R.A., et al., *Methcathinone: a new and potent amphetamine-like agent*. Pharmacol Biochem Behav, 1987. **26**(3): p. 547-51.
80. Young, R. and R.A. Glennon, *Discriminative stimulus effects of S(-)-methcathinone (CAT): a potent stimulant drug of abuse*. Psychopharmacology (Berl), 1998. **140**(3): p. 250-6.
81. Kalix, P. and R.A. Glennon, *Further evidence for an amphetamine-like mechanism of action of the alkaloid cathinone*. Biochem Pharmacol, 1986. **35**(18): p. 3015-9.
82. Motbey, C.P., et al., *Mephedrone (4-methylmethcathinone, 'meow'): acute behavioural effects and distribution of Fos expression in adolescent rats*. Addict Biol, 2012. **17**(2): p. 409-22.
83. Spiller, H.A., et al., *Clinical experience with and analytical confirmation of "bath salts" and "legal highs" (synthetic cathinones) in the United States*. Clin Toxicol (Phila), 2011. **49**(6): p. 499-505.
84. Baumann, M.H., et al., *The designer methcathinone analogs, mephedrone and methylone, are substrates for monoamine transporters in brain tissue*. Neuropsychopharmacology, 2012. **37**(5): p. 1192-203.
85. Beuming, T., et al., *The binding sites for cocaine and dopamine in the dopamine transporter overlap*. Nat Neurosci, 2008. **11**(7): p. 780-9.
86. Crumb, W.J., Jr. and C.W. Clarkson, *Characterization of cocaine-induced block of cardiac sodium channels*. Biophys J, 1990. **57**(3): p. 589-99.
87. Robinson, T.E. and B. Kolb, *Structural plasticity associated with exposure to drugs of abuse*. Neuropharmacology, 2004. **47 Suppl 1**: p. 33-46.
88. Daws, L.C., et al., *Cocaine increases dopamine uptake and cell surface expression of dopamine transporters*. Biochem Biophys Res Commun, 2002. **290**(5): p. 1545-50.
89. Register, F., *Schedules of controlled substances: temporary placement of three synthetic cathinones into Schedule I*. Fed Regist, 2011. **76**: p. 65371-65375.
90. Fantegrossi, W.E., et al., *In vivo effects of abused 'bath salt' constituent 3,4-methylenedioxypyrovalerone (MDPV) in mice: drug discrimination, thermoregulation, and locomotor activity*. Neuropsychopharmacology, 2013. **38**(4): p. 563-73.
91. Murray, B.L., C.M. Murphy, and M.C. Beuhler, *Death following recreational use of designer drug "bath salts" containing 3,4-Methylenedioxypyrovalerone (MDPV)*. J Med Toxicol, 2012. **8**(1): p. 69-75.
92. Grace, A.A. and B.S. Bunney, *Intracellular and extracellular electrophysiology of nigral dopaminergic neurons--I. Identification and characterization*. Neuroscience, 1983. **10**(2): p. 301-15.
93. Wanat, M.J., et al., *Phasic dopamine release in appetitive behaviors and drug addiction*. Curr Drug Abuse Rev, 2009. **2**(2): p. 195-213.

94. Cardozo, D.L. and B.P. Bean, *Voltage-dependent calcium channels in rat midbrain dopamine neurons: modulation by dopamine and GABAB receptors*. J Neurophysiol, 1995. **74**(3): p. 1137-48.
95. Steinberg, E.E., et al., *A causal link between prediction errors, dopamine neurons and learning*. Nat Neurosci, 2013. **16**(7): p. 966-73.
96. Ungless, M.A., P.J. Magill, and J.P. Bolam, *Uniform inhibition of dopamine neurons in the ventral tegmental area by aversive stimuli*. Science, 2004. **303**(5666): p. 2040-2.
97. Banks, M.L., et al., *Abuse-related effects of dual dopamine/serotonin releasers with varying potency to release norepinephrine in male rats and rhesus monkeys*. Exp Clin Psychopharmacol, 2014. **22**(3): p. 274-84.
98. Banks, M.L., B.E. Blough, and S.S. Negus, *Effects of monoamine releasers with varying selectivity for releasing dopamine/norepinephrine versus serotonin on choice between cocaine and food in rhesus monkeys*. Behav Pharmacol, 2011. **22**(8): p. 824-36.
99. Negus, S.S., et al., *Monoamine releasers with varying selectivity for dopamine/norepinephrine versus serotonin release as candidate "agonist" medications for cocaine dependence: studies in assays of cocaine discrimination and cocaine self-administration in rhesus monkeys*. J Pharmacol Exp Ther, 2007. **320**(2): p. 627-36.
100. Clapham, D.E., *Calcium signaling*. Cell, 2007. **131**(6): p. 1047-58.
101. Comunanza, V., et al., *CaV1.3 as pacemaker channels in adrenal chromaffin cells: specific role on exo- and endocytosis?* Channels (Austin), 2010. **4**(6): p. 440-6.
102. Simms, B.A. and G.W. Zamponi, *Neuronal voltage-gated calcium channels: structure, function, and dysfunction*. Neuron, 2014. **82**(1): p. 24-45.
103. Tsien, R.W., et al., *Multiple types of neuronal calcium channels and their selective modulation*. Trends Neurosci, 1988. **11**(10): p. 431-8.
104. Takahashi, T. and A. Momiyama, *Different types of calcium channels mediate central synaptic transmission*. Nature, 1993. **366**(6451): p. 156-8.
105. Catterall, W.A., *Voltage-gated calcium channels*. Cold Spring Harb Perspect Biol, 2011. **3**(8): p. a003947.
106. Liu, Y., et al., *Cav1.2 and Cav1.3 L-type calcium channels regulate dopaminergic firing activity in the mouse ventral tegmental area*. J Neurophysiol, 2014. **112**(5): p. 1119-30.
107. Marcantoni, A., et al., *Loss of Cav1.3 channels reveals the critical role of L-type and BK channel coupling in pacemaking mouse adrenal chromaffin cells*. J Neurosci, 2010. **30**(2): p. 491-504.
108. Ferrari, D.C., et al., *Midbrain dopaminergic neurons generate calcium and sodium currents and release dopamine in the striatum of pups*. Front Cell Neurosci, 2012. **6**: p. 7.
109. Ruchala, I., et al., *Electrical coupling between the human serotonin transporter and voltage-gated Ca(2+) channels*. Cell calcium, 2014. **56**(1): p. 25-33.
110. Machaca, K. and H.C. Hartzell, *Asymmetrical distribution of Ca-activated Cl channels in Xenopus oocytes*. Biophys J, 1998. **74**(3): p. 1286-95.
111. Solis, E., Jr., et al., *4-(4-(dimethylamino)phenyl)-1-methylpyridinium (APP+) is a fluorescent substrate for the human serotonin transporter*. J Biol Chem. **287**(12): p. 8852-63.
112. Ruchala, I., et al., *Electrical coupling between the human serotonin transporter and voltage-gated Ca channels*. Cell Calcium, 2014.
113. Eltit, J.M., et al., *Orthograde dihydropyridine receptor signal regulates ryanodine receptor passive leak*. Proc Natl Acad Sci U S A, 2011. **108**(17): p. 7046-51.

114. Lotharius, J., et al., *Progressive degeneration of human mesencephalic neuron-derived cells triggered by dopamine-dependent oxidative stress is dependent on the mixed-lineage kinase pathway*. J Neurosci, 2005. **25**(27): p. 6329-42.
115. Harikumar, K.B., et al., *K63-linked polyubiquitination of transcription factor IRF1 is essential for IL-1-induced production of chemokines CXCL10 and CCL5*. Nat Immunol, 2014. **15**(3): p. 231-8.
116. Ramoz, L., et al., *Mephedrone ("bath salt") pharmacology: insights from invertebrates*. Neuroscience, 2012. **208**: p. 79-84.
117. Joyce, B.M., P.E. Glaser, and G.A. Gerhardt, *Adderall produces increased striatal dopamine release and a prolonged time course compared to amphetamine isomers*. Psychopharmacology (Berl), 2007. **191**(3): p. 669-77.
118. Glennon, R.A., et al., *Methcathione ("cat"): an enantiomeric potency comparison*. Pharmacol Biochem Behav, 1995. **50**(4): p. 601-6.
119. Sandtner, W., et al., *A Quantitative Model of Amphetamine Action on the Serotonin Transporter*. Br J Pharmacol, 2013.
120. Chen, R., et al., *Protein kinase Cbeta is a critical regulator of dopamine transporter trafficking and regulates the behavioral response to amphetamine in mice*. J Pharmacol Exp Ther, 2009. **328**(3): p. 912-20.
121. Tang, Q., et al., *Structural Analysis of Dopamine- and Amphetamine-induced Depolarization Currents in the Human Dopamine Transporter*. ACS Chem Neurosci, 2015.
122. Lotharius, J., et al., *Effect of mutant alpha-synuclein on dopamine homeostasis in a new human mesencephalic cell line*. J Biol Chem, 2002. **277**(41): p. 38884-94.
123. Scholz, D., et al., *Rapid, complete and large-scale generation of post-mitotic neurons from the human LUHMES cell line*. J Neurochem, 2011. **119**(5): p. 957-71.
124. Ilieva, M., et al., *Tracking neuronal marker expression inside living differentiating cells using molecular beacons*. Front Cell Neurosci, 2013. **7**: p. 266.
125. Branch, S.Y. and M.J. Beckstead, *Methamphetamine produces bidirectional, concentration-dependent effects on dopamine neuron excitability and dopamine-mediated synaptic currents*. J Neurophysiol, 2012. **108**(3): p. 802-9.
126. Martinez-Clemente, J., et al., *Interaction of mephedrone with dopamine and serotonin targets in rats*. Eur Neuropsychopharmacol, 2012. **22**(3): p. 231-6.
127. Baumann, M.H., et al., *Powerful cocaine-like actions of 3,4-methylenedioxypyrovalerone (MDPV), a principal constituent of psychoactive 'bath salts' products*. Neuropsychopharmacology, 2013. **38**(4): p. 552-62.
128. Holz R.W., C.J.T., *The effects of various salts, temperature, and the alkaloids veratridine and batrachotoxin on the uptake of [3H] dopamine into synaptosomes from rat striatum*. . Mol. Pharmacol., 1974. **10**: p. 13.

Curriculum Vitae

Krasnodara Nikolaeva Cameron

E-mail: stoychevakn@vcu.edu

EDUCATION:

- **Graduate:** Virginia Commonwealth University (Ph.D. Candidate, 2010- 2015)
 - Mentor: Dr. Louis J De Felice, Department of Physiology and Biophysics
 - Dissertation Title: Drug-induced conduction states of the human dopamine transporter
- **Undergraduate:** Virginia Union University (Bachelor of Science, summa cum laude, May 2005)
 - Major: Chemistry
 - Minor: Physics

POSITIONS AND EMPLOYMENT:

- PhD Candidate in Physiology and Biophysics (Virginia Commonwealth University, 2010- 2015)
- Teaching Assistant (Virginia Commonwealth University, 2012-2013)
- Biochemistry Research Assistant (University of Richmond, 2008-2010)
- Chemistry/ Ecology Teacher (Richmond Public Schools, 2006-2008)
- Material Chemistry Research Fellow (Virginia Union University, 2003-2005)
- Theoretical Physics Research Fellow (Hampton University, 2002)

HONORS AND AWARDS:

- Erice Course on Biophysics of Channels and Transporters Bursary (2014)
- Graduate School Travel Award (2014)
- Hibbs/Waller Scholarship for academic excellence of a female graduate student (2012)
- Travel Fellowship for the Tenth International Catecholamine Symposium (2012)
- Garnett Ryland Prize in Chemistry (2005)

- Panther 100 Club Scholarship for academic and athletic excellence (2004)
- Virginia Union University Fellow (05/03 – 05/05)
- Hampton University Fellow (05/02 – 07/02)
- Virginia Union University Presidential Scholar (2001-2005)

PUBLICATIONS:

- 1. Comments on “A Quantitative Model of Amphetamine Action on the Serotonin Transporter”, by Sandtner et al. (2013) Louis J De Felice and Krasnodara Cameron. *Br J Pharmacol*. 2014, May 13. doi: 10.1111/bph.12767.**
- 2. Mephedrone and Methylenedioxypropylamphetamine, major constituents of Bath Salts, differentially affect the dopamine transporter Krasnodara Cameron, Renata Kolanos, Rakesh Verkariya, Louis De Felice, and Richard A. Glennon *Psychopharmacology (Berl)*. 2013 Jun;227(3):493-9.**
- 3. The evolution and function of the Pax/Six regulatory network in sponges Rivera, A.; Winters, I.; Rued, A.; Ding, S.; Posfai, D.; Cieniewicz, B.; Cameron, K.; Gentile, L.; and Hill, A. *Evol Dev*. 2013 May;15(3):186-96.**
- 4. Bath salts components mephedrone and methylenedioxypropylamphetamine (MDPV) act synergistically at the human dopamine transporter Krasnodara Cameron, Renata Kolanos, Ernesto Solis, Jr., Richard A. Glennon and Louis De Felice *Br J Pharmacol*. 2013 Apr;168(7):1750-7.**
- 5. Neurosteroid binding to the amino terminal and glutamate binding domains of ionotropic glutamate receptors Cameron, K.; Bartle, E.; Roark, R.; Fanelli, D.; Pham, M.; Pollard, B.; Borkowski, B.; Rhoads, S.; Kim, J.; Rocha, M.; Kahlson, M.;Kangala, M.; and Gentile, L.N. *Steroids*. 2012 Jun;77(7):774-9.**
- 6. S(+)-Amphetamine Induces a Persistent Leak in the Human Dopamine Transporter: Molecular Stent Hypothesis Ernesto Solis, Jr., Aldo Rodriguez-Menchaca, Krasnodara N. Cameron, and Louis J. De Felice *Br. J. Pharmacol*. 2012 Apr;165(8):2749-57.**

SUBMITTED PUBLICATIONS:

- 1. Electrophysiological signature of methamphetamine and 3,4-methylenedioxymethamphetamine (MDMA) stereoisomers on the human dopamine and serotonin transporters: implications for drug effects Ernesto Solis, Jr., Krasnodara Cameron, Renata Kolanos, Richard A. Glennon and Louis De Felice Submitted to *Br J Pharmacol*.**
- 2. Amphetamine supports activation of Ca²⁺ channels through dopamine transporter-mediated depolarization Krasnodara N. Cameron, Ernesto Solis Jr., Iwona Ruchala, Louis J. De Felice, Jose M. Eltit Submitted to PNAS**

ABSTRACTS:

1. Cameron, K.; Eltit, JM.; De Felice, L.: **Internal S-AMPH induces a persistent current at hDAT.** Poster for Erice Course on Biophysics of Channels and Transporters, May 2014, Erice, Italy.
2. Cameron, K.; Eltit, JM.; De Felice, L.: **Amphetamine induced conduction states of the human dopamine transporter.** Poster for Annual CVCNS Symposium at VCU, March 2014, Richmond, VA.
3. Cameron, K.; Eltit, JM.; De Felice, L.: **Amphetamine induced conduction states of the human dopamine transporter.** Poster for 30th Annual Watts Research Symposium at VCU, October 2013, Richmond, VA.
4. Solis, E.; Cameron, K.; Kolanos, R.; Glennon, R.; and De Felice, L.: **Methylenedioxypyrovalerone (MDPV) is a potent inhibitor of hDAT and hNET.** Poster for Experimental Biology, March 2013, Boston, MA.
5. Solis, E.; Cameron, K.; Kolanos, R.; Glennon, R.; and De Felice, L.: **A Comparison of Persistent Leak Currents Induced by Methamphetamine and 3,4-Methylenedioxymethamphetamine in the Human Dopamine and Serotonin Transporters.** Poster for Society for Neuroscience Annual Meeting, November 2012, New Orleans, LA.
6. Cameron, K.; Kolanos, R.; Solis, E.; Vekariya, R.; Glennon, R.; De Felice, L.: **BATH SALTS Double Trouble at the Dopamine Transporter.** Poster for The Tenth International Catecholamine Symposium, September 2012, Pacific Grove, CA.
7. Cameron, K.; Solis, E.; Kolanos, R.; Vekariya, R.; Deitz, R.; Glennon, R.; De Felice, L.: **Persistent Leak Current at the Dopamine Transporter Caused by Psychoactive Stimulants.** Poster for 15th Annual Research Symposium of VCU Graduate Student Association, April 2012, Richmond, VA.
8. Cameron, K.; Kolanos, R.; Solis, E.; Vekariya, R.; Glennon, R.; De Felice, L.: **BATH SALTS' Double Action at the Dopamine Transporter.** Poster for The Central Virginia Chapter of the Society for Neuroscience Annual Symposium, March 2012, Richmond, VA.
9. Cameron, K.; Kolanos, R.; Solis, E.; Vekariya, R.; Glennon, R.; De Felice, L.: **Bath salts: A synthetic cathinone whose two major components act similar to methamphetamine and cocaine on the human dopamine transporter.** Platform presentation for Biophysical Society Annual Meeting, February 2012, San Diego, CA.
10. Cameron, K. and De Felice, LJ: **Dialogue between DA and AMPH as they travel through the human dopamine transporter.** Poster for Society for Neuroscience Annual Meeting, November 2011, Washington, DC.
11. Kolanos, R.; Cameron, K.; Vekariya, R.; De Felice, L.; Glennon, R.: **Bath salts: A doubling-up of methamphetamine plus cocaine?** Poster for ACS meeting, October 2011, Richmond, VA.
12. Solis, E.; Menchaca, A.; Cameron, K.; De Felice, L. **"S(+)"Amphetamine induces a persistent**

leak current in the human dopamine transporter; molecular stent hypothesis.” Poster for the International school of biophysics “Antonio Borsellino” 2011, Erice-Sicily, Italy

13. Cameron, K.; Fanelli, D.; Bartle, E.; Pollard, B.; and Gentile, L. “Understanding the inhibitory regulation of AMPA and NMDA iGluRs by sulfated neurosteroids.” Poster for the National Protein Society meeting, July 2010, San Diego, CA.

14. Cameron, K.; Rhodes, S.; and Gentile, L. “Understanding the potentiation of NMDA iGluRs by pregnenolone sulfate.” Poster for the National Protein Society meeting, July 2010, San Diego, CA.

15. Cameron, K.; Borkowski, B.; Kim, J.; Rhodes, S.; Cassada, G.; Rocha, M.; and Gentile, L. “Neurosteroid binding domains of the NMDA receptor NR2B and NR2D subunits.” Poster for the ASBMB national meeting, April 2010, Anaheim, CA.

16. Cameron, K.; Kim, J.; Cassada, G.; and Gentile, L. “Neurosteroid binding domains of the NMDA receptor NR2B subunit.” Poster for the National Protein Society meeting, July 2009, Boston, MA.

17. Cameron, K.; Kim, J.; Cassada, G.; and Gentile, L. “Neurosteroid binding domains of the NMDA receptor NR2B subunit.” Poster for Fall 2009, on campus HHMI science symposium, UR.

18. Borkowski, B.; Rocha, M.; Cameron, K.; and Gentile, L. “Determining the binding domain of the NR2D ionotropic glutamate receptor.” Poster for Spring 2009, A&S symposium, on campus, UR.